

WIS dies



This is to certify that the

dissertation entitled

DESIGN AND DEVELOPMENT OF A BEAM DEFLECTION TIME-OF-FLIGHT MASS SPECTROMETER: APPLICATIONS IN GAS CHROMATOGRAPHY/MASS SPECTROMETRY AND POTASSIUM ION IONIZATION OF DESORBED SPECIES presented by

Gary Allen Schultz

has been accepted towards fulfillment of the requirements for

Ph.D. degree in Chemistry

Major professor

Date_October 8, 1991

MSU is an Affirmative Action/Equal Opportunity Institution

LIBRARY Michigan State University

PLACE IN RETURN BOX to remove this checkout from your record. TO AVOID FINES return on or before date due.

DATE DUE	DATE DUE	DATE DUE
§1 260 ₁		

MSU is An Affirmative Action/Equal Opportunity Institution c;circidatedus.pm3-p.1

DESIGN AND DEVELOPMENT OF A BEAM DEFLECTION TIME-OF-FLIGHT MASS SPECTROMETER: APPLICATIONS IN GAS CHROMATOGRAPHY/MASS SPECTROMETRY AND POTASSIUM ION IONIZATION OF DESORBED SPECIES

By

Gary Allen Schultz

A DISSERTATION

Submitted to
Michigan State University
in partial fulfillment of the requirements
for the degree of

DOCTOR OF PHILOSOPHY

Department of Chemistry

1991

ABSTRACT

DESIGN AND DEVELOPMENT OF A BEAM DEFLECTION
TIME-OF-FLIGHT MASS SPECTROMETER:
APPLICATIONS IN GAS CHROMATOGRAPHY/MASS SPECTROMETRY
AND POTASSIUM ION IONIZATION OF DESORBED SPECIES

By

Gary Allen Schultz

A beam deflection time-of-flight mass spectrometer (BDTOF-MS) has been developed in conjunction with an integrating transient recorder (ITR) to provide time array detection (TAD). This beam defection system is the first to incorporate two pulses to form ion packets by applying a voltage pulse to each of two parallel deflection plates. The pulses are held at two different potentials, and by reversal of the potentials applied to each plate, an ion packet is produced at the time during which the electric field between the deflection plates is zero. This method of beam deflection produces a resolving power of m/\Delta m of 1400 at m/z 132 corresponding to the nominal atomic mass of xenon. The resolving power achieved by this procedure is better than unit resolution over the mass-to-charge ratio range of 20 to 749 u.

Gas Chromatography/Mass Spectrometry data were acquired during the analysis of a trimethylsilyl derivatized mixture of urinary organic acids at 1 and 10 scans-per-second to show improvements in the chromatographic information available from the reconstructed total ion current (RTIC) chromatograms generated at higher mass spectral acquisition rates. The RTIC chromatogram available from the mass spectral acquisition rate of 10 mass spectra/second is shown to be comparable to the profile obtained from a flame ionization detector in representing the chromatography performed under identical experimental parameters. The advantages of the higher mass spectral acquisition rate in representing the chromatographic profile and in allowing mass spectral data to be obtained for components in a complex mixture that are unresolved chromatographically are described.

The Desorption/Ionization technique, potassium ion ionization of desorbed species (K+IDS), developed in this laboratory, uses thermionic emitters as sources of alkali ions for attachment to thermally-desorbed analyte molecules and fragments. This technique produces analyte ion currents for periods of time ranging from one second to many seconds, with the mass spectral information available rapidly changing due to the temperature gradient produced by the heating of the sample by the "potassium glass". A preliminary investigation of K+IDS has been performed using the BDTOF mass spectrometer/ITR. Studies were performed to determine the effects of the accelerating voltage penetration into the ion volume of the ion source on the extent of conversion of gas phase K+ to gas phase (analyte + K+) by placing a wire grid across the ion volume exit slit. An increase in extent of conversion with the grid in the ion source is shown to be approximately a factor of 15.

This dissertation is dedicated to my family, especially my sister, Lori, who inspired me to achieve

ACKNOWLEDGMENTS

I would like to thank Dr. John Allison for taking me on as a graduate student. I am known as a stubborn person and know that advising me was challenging if not outright difficult at times. John is a person that I admire and respect as an advisor and a friend. Throughout this journey, he has made himself available to me whenever I needed help and advice, both professional and personal. I look forward to further interactions with him throughout my professional career and life.

Dr. Watson has also been instrumental in my development as a scientist and a person. He has opened my eyes to a greater understanding to what it takes to be a professional. He would always politely correct any errors in speech that I would utter, not to critize, but to make me aware of them so that I may better myself as a person. For this, I am very greatful.

This project would not have been successful without the help of a very good friend and colleague, Marty Rabb. Marty designed and built much of the intricate and complex electronics and pulsing circuitry for this project. I went to him with what appeared to be impossible requests and he always came through with what I needed. This department will be at a great loss when he retires. Over the years of close association with Marty, I have had the opportunity to get to know him as a friend. We have had numerous discussions about our experiences in life and I have learned much from this man. Marty, I will indeed miss you!

I would like to thank the staff at the Mass Spectrometry Facility for there help. Bev has been a friend and someone that I respect as a person. She is one of the most genuinely nice persons that I have ever met or expect to ever meet in my life and I will miss her. Mike has provided much assistance and humor along the way. Mel, Betty and Melinda have all been good friends. Kevin has been a friend and provided me with every program that I have requested. He alone has been the life support for the TOF group.

Of course, I cannot forget all of the friends that I have met here at Michigan State. My first two years here at MSU, living in the 'Chem House' on Spartan Ave, were anything but boring. Halloween parties at the Chem House were like no other. Jeff, Jim, Mike and I would be sitting around the Chem House talking, wondering what we were going to do for the evening and many times would end up at our favorite establishment at the time, Mac's. We were persuaded many times by Mark and Kris to make this trip. Here we met many friends, and for me, many good natured people. Of course, Mac's attracted all types. My times playing pool with Jeff T., singing every song on the jukebox, being excused from this fine establishment, etc. will remain with me always. My friendship with Dan has been close over the years. How two of the most stubborn people I know could remain friends like we have, I don't know. This is a friendship that will last a lifetime.

There are so many other friends that were gained in my later years, Judy, Karen, Jon, Dave G., Laura, Ron, Dave W., Ed, Jason, Kurt, and many, many more. All of them hold a special place in my heart and I will remember them always. Remember, the world is a very small place.

TABLE OF CONTENTS

LIST OF TABLESxi
LIST OF FIGURESxii
Chapter 1 - Introduction
Chapter 2 - Developments In Time-Of-Flight Mass Spectrometry 19
Chapter 3 - Design of BDTOF Mass Spectrometer
A. Ion Source
1. Dupont 21-491B ion source30
2. JEOL DM303 ion source31
B. Gas chromatography interface37
C. Beam Deflection Assembly37
1. Deflection Plate Geometries38
2. Beam Deflection Methods40
D. Detectors43
1. Galileo FTD-2003

a. Standard multichannel plates46
b. High output technology multichannel plates 46
2. Becton Dickinson MM-1-1SG electron multiplier47
E. Detector Slit Assembly48
F. Preamplifiers48
1. Comlinear49
2. "in-house"50
G. Ion Focus Assembly51
H. Vacuum System54
I. Integrating Transient Recorder
J. Comparison of BEDER-TOF and BDTOF Mass
Spectrometers57
Chapter 4 - Gas Chromatography/Beam Deflection Time-Of-Flight
Mass Spectrometry61
A. Grob programmed test mixture62
1. Experimental62
2. Reconstructed Total Ion Current Chromatograms6
a. Comparison of 1 and 20 scans/second63

b. Deconvolution of closely eluting components 64
c. Limits of Detection70
B. Complex mixture analysis of TMS-derivatized organic acids
of urine71
1. Background71
2. Experimental72
3. Chromatographic Profiles from the GC/FID and
GC/BDTOF mass spectrometer/ITR73
4. Mass Spectral Deconvolution79
5. Three-dimensional data presentation91
6. Conclusions93
Chapter 5 - Potassium Ion Ionization of Desorbed Species (K+IDS)95
A. Background95
B. Experimental103
1. K+IDS probe design10
2. Electronic circuit modifications102
B. K+IDS by TOF-MS103
1. Grided versus Gridless Ion Source

Experimental106
Results107
2. MK+ abundance versus pressure
B. K+IDS spectra116
1. Polyethylene Glycol (PEG) 600
2. PEG 750126
C. Current limitations of K+IDS by BDTOF-MS
Appendix I
Mass spectra of selected compounds using the BDTOF mass
spectrometer130
Appendix II
"Beam Deflection for Temporal Encoding in Time-of-Flight
Mass Spectrometry", Yefchak, G. E., Schultz, G. A., Allison,
J., Holland, J. F. and Enke, C. G., J. Am. Soc. Mass
Spectrom., 1, 440 (1990).
Appendix III
"Renaissance of gas chromatography-time-of-flight mass
spectrometry", Watson, J. T., Schultz, G. A., Tecklenburg, R.
E., Jr. and Allison, J., J. Chromatogr., 518, 283 (1990).

LIST OF TABLES

Table 3.1	Upper and lower electrical connections on Dupont ion source housing for JEOL DM303 ion source.	33
Table 3.2	Connector (amphenol) pin numbering for JEOL DM303 ion source voltages and ion source elements along with those of the original Old Hirose connector used by JEOL.	3 5
Table 3.3	Pin numbering on T-tube flange of flight tube for beam defection assembly and ion focussing assembly.	51
Table 4.1	Components in methylene chloride for the Grob programmed test mixture in the order of elution.	62
Table 4.2	TMS-derivatized urinary organic acids with a relative response greater than 2 $\mu\text{g/mg}$ creatinine.	7 6
Table 5.1	Average intensity of K^+ isotope at m/z 41 and (acetone + $K)^+$ at m/z 97 for various partial pressures of acetone in a gridless ion source.	112
Table 5.2	Average intensity of K^+ isotope peak at m/z 41 and (acetone + K) ⁺ at m/z 97 for various partial pressures of acetone in a grided ion source.	112
Table 5.3	Extent of conversion of palmitic acid versus background pressure of triethylamine.	115

LIST OF FIGURES

- Figure 1.1 The initial spatial distribution of neutrals upon ion formation gives rise to ions that acquire different final energies. Ions formed with some initial energy will attain final energies equal to their initial energy + accelerating potential. The turn-around time is a special aspect of the initial energy distribution where two isomass ions with the same initial energy, one with initial direction towards the detector and the other with direction away from the detector. Both will leave the ion source with the same final kinetic energy, but at different times.
- Figure 1.2 a) Schematic of beam deflection assembly located in the flight tube directly after the exit slit of the ion source. The beam deflection spacing and plate dimensions are also given. b) The repetition rate of mass spectral transient formation is 5kHz with pulse rise and fall times of 10ns. During time period 1, the ion beam is deflected downward. As the voltages applied to VA and VB change during time period 2, the beam is swept across the detector surface, resulting in a mass spectral transient available for acquisition. The continuous ion beam is deflected upward during time period 3.
- Figure 1.3 Mass spectrum of Xenon showing mass resolution with new beam deflection assembly of the BDTOF mass spectrometer.

13

Figure 1.4 The BDTOF mass spectrometer operates with a mass spectral transient generation rate of 5000s⁻¹. The summation of consecutive 5000 mass spectral transients by the ITR results in a mass spectral acquisition rate of 1 mass spectrum/second.

Figure 1.5	The BDTOF mass spectrometer operates with a mass spectral transient generation rate of 5000s ⁻¹ . The summation of consecutive 250 mass spectral transients by the ITR results in a mass spectral acquisition rate of 20 mass spectra/second.	17
Figure 2.1	Wiley-McLaren ion source showing two extraction fields, $\overrightarrow{E_s} + \overrightarrow{E_d}$.	21
Figure 2.2.	Plot showing ion flight times versus initial position of ion in region s of a Wiley-McLaren ion source for three isomass ions with different initial velocities. By waiting for a time τ , after ion formation and before ion extraction, the flight time of the two isomass ions with the same initial velocities but opposite direction can be made to arrive at the detector simultaneously.	23
Figure 3.1	Schematic diagram of GC/BDTOF mass spectrometer (not to scale). Shown are the ion source, flight tube, beam deflection assembly, ion focus plates, detector and integrating transient recorder.	29
Figure 3.2	Dupont 21-491B ion source.	31
Figure 3.3	JEOL DM303 ion source.	32
Figure 3.4	Electronic diagram of duplicate circuit for JEOL DM303 ion source.	34
Figure 3.5	Voltage divider for JEOL DM303 ion source. Provides V _A and First Focus 1 (left and right) voltages.	36
Figure 3.6	Electronic diagram of ±200V power supplies for DM303 ion source X-Y deflection plates.	3 6
Figure 3.7	Electronic diagram of beam deflection circuit. This circuit provides two output pulses that alternate between 0 and 63 V at 5 kHz. The rise and fall times for each pulse are adjustable as is the relative time at which each pulse changes potential with respect to the other.	42
Figure 3.8	Galileo FTD-2003 and Johnston MM-1 detector mounting flange for Bendix flight tube.	44
Figure 3.9	Voltage divider network for Galileo FTD-2003 channelplate detector.	45

Figure 3.10	Detector slit assembly for Bendix flight tube. Provides for adjustable ion beam widths up to 0.50". This assembly also contains necessary holes and mounting threads for the Allison-group beam visualizer.	49
Figure 3.11	Electronic circuit diagram for "in-house" preamplifier built around two CLC404 high-slew rate operational amplifiers. R_f = 501 Ω and R_g = 47 $\Omega.$	50
Figure 3.12	Electronic circuit diagram for ion focus assembly.	52
Figure 3.13	T-tube flange showing pin numbers. Table 3.1 contains a list of the electrical connections to this flange.	53
Figure 3.14	Five-pin Molex pin connector for quick disconnects to flight tube steering plates and ion lens.	54
Figure 3.15	Mass spectrum of perfluorotributylamine obtained on the BDTOF mass spectrometer. Also shown are the raw data points for the peaks at m/z 69 and at m/z 502.	58
Figure 3.16	Comparison of mass resolving power of the BEDER-TOF and BDTOF mass spectrometers for the major ions in the mass spectrum of perfluorotributylamine. The resolution is based upon Δm (or its equivalent, $2\Delta t$) being the full width of the peak at half its maximum height (FWHM). The BEDER-TOF data are from reference 13.	60
Figure 4.1	Reconstructed TIC chromatogram generated from the data base acquired at 1 scan/second of standard Grob test mixture.	67
Figure 4.2	a) Comparison of RTIC chromatograms reconstructed from the data bases acquired at 1 and 20 mass spectra/second over the region of the chromatogram between the arrows in Figure 4.1. b) RTIC chromatogram is shown along with the mass chromatograms of m/z 57 and m/z 122 available from the 20 mass spectra/second data base.	68
Figure 4.3	Mass spectrum in scan a) 192, b) 159, and c) 240.	æ
Figure 4.4	Complex mixture analysis of TMS-derivatized urinary organic acids. Comparison of a) GC-FID response to reconstructed total ion current chromatograms generated from mass spectral acquisition rates of b) 1 and c) 10 mass spectra/second.	74

- Figure 4.5 Selected region of RTIC chromatogram generated from mass spectral acquisition rates of a) 1 and b) 10 mass spectra/second showing improved representation of chromatographic profile at a higher mass spectral acquisition rate.
- Figure 4.6 Comparison of RTIC chromatograms at mass spectral acquisition rates of a) 1 and b) 10 mass spectra/second for a chromatographic doublet. c) mass chromatograms at m/z 180 and at m/z 227 identifying two components.

81

83

86

87

- Figure 4.7a shows the mass spectrum in scan 1197 that has mass spectral information for both of the components eluting over the peak profile shown in Figure 4.6c. Figure 4.7b shows the mass spectrum in scan 1220. The mass spectrum shown in Figure 4.7c is the result of subtracting 43 % of the ion currents in scan 1220 from the corresponding ones in scan 1197.
- Figure 4.8 Figure 4.8a is a region of the RTIC chromatogram generated from the 10 scans/second data base. Figure 4.8b shows the mass chromatograms at m/z 189 (solid line) and at m/z 210 (broken line). The difference in the maxima of the two peaks indicates the presence of two components.
- Figure 4.9 Comparison of mass spectral data (Figures 4.9a-c) in scans 1551, 1555, and 1557 over the peak profile in Figure 4.8. The changes in the relative intensities at m/z 189 and m/z 210 indicates the presence of more than one component. Figure 4.9d is the mass spectrum resulting from averaging scans 1560 to 1570. Figure 4.9e is the mass spectrum resulting from averaging scans 1540 to 1550.
- Figure 4.10 Figure 4.10a is a region of the RTIC chromatogram generated from the data base acquired at 10 scans/second. Figure 4.10b shows the mass chromatograms at m/z 174 (broken line) and at m/z 247 (solid line). The difference in the maxima of the two mass chromatograms indicates the presence of two components.

Figure 4.11	Comparison of mass spectral data (Figures a-c) in scans 1883, 1890, and 1899 over the peak profile in Figure 4.10. Comparison of the mass spectral data in each scan shown indicates that Figure 4.11a (scan 1883) represents the first component in the peak profile, Figure 4.11b (scan 1890) contains mass spectral data for both components, and Figure 4.11c (scan 1899) is the mass spectrum of the second component represented by the poorly resolved doublet in Figure 4.10b.	90
Figure 4.12	3-dimensional plot of scan range 1870 to 1910 of data base acquired at 10 mass spectra/second.	92
Figure 5.1	Previous K+IDS probe designs used on HP 5985 mass spectrometer. First design used by Bombick used the potassium emitter as a sample holder. Later design of Kassel used separate wire sample holder for better temporal overlap of potassium emission and sample desorption. A 30-fold improvement in detection limits result from the separation of the wire sample holder and potassium emitter.	96
Figure 5.2	Total ion current and desorption profiles at m/z 41 and m/z 295 for the K+IDS analysis of palmitic acid. Bead current was 2.7 A at a mass spectral acquisition rate of 10 mass spectra/second.	98
Figure 5.3	K+IDS mass spectrum of palmitic acid with MK+ at m/z 295. This mass spectrum is the sum of scans 42 to 47 from Figure 5.2. Bead current was 2.7 A with a mass spectral acquisition rate of 10 mass spectra/second.	99
Figure 5.4	K+IDS probe designed for HV ion source of BDTOF mass spectrometer.	102
Figure 5.5	SIMION model of Dupont ion source with a repeller voltage of 3005 V, ion volume exit slit voltage of 3000 V, and focus lens voltage of 1000 V. Each electric field line represents a change of 1 V. A penetration of 20 V into the ion volume of the ion source is evident.	106
Figure 5.6	Desorption profiles of $(M + K)^+$ at m/z 97 and K ⁺ isotope at m/z 41 for gridless ion source at 1.6 x 10^{-4} torr partial pressure of acetone and reconstructed from the data base acquired at 10 mass spectra/second.	108

Figure 5.7	Desorption profiles of $(M + K)^+$ at m/z 97 and K ⁺ isotope at m/z 41 for grided ion source at 1.2×10^{-4} torr partial pressure of acetone and reconstructed from the data base acquired at 10 mass spectra/second.	108
Figure 5.8	K+ CI mass spectrum of acetone in the gridless ion source at 1.6×10^{-4} torr and reconstructed from the data base acquired at 10 mass spectra/second. Bead current is 2.6A.	109
Figure 5.9	K ⁺ CI mass spectrum of acetone in the grided ion source at 1.2×10^{-4} torr and reconstructed from the data base acquired at 10 mass spectra/second. Bead current is $2.6A$.	110
Figure 5.10	Plot of adduct ion peak intensity versus partial pressure of acetone in the grided ion source. Shown is the intensity of the potassium isotope at m/z 41 along with the intensity of the acetone adduct ions at m/z 97, 155, 213 and the sum of the acetone adduct ion intensities.	113
Figure 5.11	Comparison of acetone adduct ion peak intensity to potassium isotope peak intensity at m/z 41 for the grided and gridless ion source. A factor of 15 improvement is adduct formation is gained by using a grid in the ion source.	114
Figure 5.12	Desorption profiles for oligomers with $n=5,8,11,13,16$ and 19 for PEG 600. The current was 2.7 A for the potassium carbonate support wire. The mass spectral acquisition rate was 10 mass spectra/second.	118
Figure 5.13	Mass spectrum of PEG 600 from the sum of scans 40 to 50. The current was 2.7 A for the potassium carbonate support wire. The mass spectral acquisition rate was 10 mass spectra/second.	119
Figure 5.14	Mass spectrum of PEG 600 from the sum of scans 50 to 60. The current was 2.7 A for the potassium carbonate support wire. The mass spectral acquisition rate was 10 mass spectra/second.	120
Figure 5.15	Mass spectrum of PEG 600 from the sum of scans 70 to 80. The current was 2.7 A for the potassium carbonate support wire. The mass spectral acquisition rate was 10 mass spectra/second.	12 1

Figure 5.16	Mass spectrum of PEG 600 from the sum of scans 40 to 80. The current was 2.7 A for the potassium carbonate support wire. The mass spectral acquisition rate was 10 mass spectra/second.	12 2
Figure 5.17	PEG 600 mass spectrum showing low mass ions. Scan rate is 10 mass spectra/second. Bead current is 2.6 A. Average of scans 20 to 100. Peaks are labeled based on Scheme I.	123
Figure 5.18	Raw data collected at 5ns time bins in flight time region of m/z 585 of PEG 600.	126
Figure 5.19	K+IDS mass spectrum of PEG 750 from average of scans 50 to 80. Bead current of 2.6 A was used at a mass spectral acquisition rate of 10 mass spectra/second.	127
Figure A.1	Mass spectrum of methyl stearate by GC/MS.	130
Figure A.2	EI mass spectrum of xenon with V_A of 1000 V. Beam deflection d spacing is 25 mm with no detector slit assembly.	131
Figure A.3	EI mass spectrum of xenon with V_A of 1500 V. Beam deflection d spacing is 25 mm with no detector slit assembly.	132
Figure A.4	EI mass spectrum of xenon with V_A of 2200 V. Beam deflection d spacing is 25 mm with no detector slit assembly.	13 3
Figure A.5	EI mass spectrum of xenon with V_A of 1000 V. Beam deflection d spacing is 25 mm with the detector slit assembly adjusted to 5 mm.	134
Figure A.6	EI mass spectrum of xenon with V_A of 1500 V. Beam deflection d spacing is 25 mm with the detector slit assembly adjusted to 5 mm.	135
Figure A.7	EI mass spectrum of xenon with V_A of 2200 V. Beam deflection d spacing is 25 mm with the detector slit assembly adjusted to 5 mm.	136
Figure A.8	K+IDS mass spectrum of the hexapeptide VGVAPG	197

Chapter 1 - Introduction

The coupling of a gas chromatograph to a mass spectrometer was first demonstrated by Gohlke¹ in 1959 using a time-of-flight (TOF) mass spectrometer. The mass spectrum for each of the compounds in a mixture was recorded by photographing the mass spectrum as it appeared on an oscilloscope connected to the detector of the mass spectrometer. Since the first demonstration of gas chromatography/mass spectrometry (GC/MS), this technique has been responsible for advancements in many fields of science. The analysis of mixtures by GC/MS can provide qualitative and quantitative information for each component. GC/MS has contributed greatly to structural determinations of classes of compounds by the method of electron ionization (EI), which provides reproducible fragmentation patterns.

Column technology has advanced over the years where, today, GC columns are available that can provide hundreds of thousands of theoretical plates. Peak widths of components eluting from these high efficiency capillary columns are typically 2 seconds or less in duration, allowing for the analysis of complex mixtures containing hundreds of components in less than an hour. The successful application of this new technology to GC/MS is directly related to the mass spectral acquisition rate of the mass spectrometer. Chromatographic profiles are reconstructed by summing the ion current at each m/z value acquired in each scan by the

mass spectrometer data system. The temporal profile of the intensity of this summed ion current (the total ion current) is an indication as to the amount of sample in the ion source during the acquisition of the mass spectrum. A plot of the total ion current for each scan versus scan number displays a reconstructed total ion current (RTIC) chromatogram that can be used to identify the retention times for each of the components in a mixture. The greater the mass spectral acquisition rate, the more accurately the "true" chromatographic profile can be represented by the RTIC chromatogram. With the chromatographic peak widths ever decreasing in width due to increased capillary column performance, the mass spectrometers currently used for GC/MS may limit the usefulness of this new technology.

In the early 1980s, a review was written on mass spectral acquisition rates² available with mass spectrometers commonly used in GC/MS, namely, quadrupole and magnetic sector mass spectrometers. At that time, the fastest mass spectral acquisition rate for a quadrupole was 4-8 Hz. Scan rates for quadrupole mass spectrometers are restricted by the transit time of the ions through the quadrupole filter. The rf and d.c. voltages for a given m/z value cannot change significantly during the ion's transit time through the quadrupole without serious degradation of the ion transmission efficiency and mass resolution. This will always be the ultimate limit on the scan rate of a quadrupole mass spectrometer. For a magnetic sector mass spectral acquisition rates are limited by the rate at which the magnetic field can be swept to focus each m/z value at the detector. Scan rates for a magnetic sector mass spectrometers were limited

to 0.1s/decade with 0.2s to reset the magnetic field, thus limiting the rates to 3-4 Hz.

Recently, improvements in quadrupole and magnetic mass spectrometers have led to the development of mass spectrometers that can attain mass spectral acquisition rates as high as 10 scans/second.³ The Hewlett-Packard 5970B GC/Mass Selective Detector (HP 5970B GC/MSD) is the state-of-the-art in quadrupole mass spectrometers used for GC/MS. This mass spectrometer provides scanning rates up to 1500 u/second⁴ with a maximum scan rate of 8 Hz and a mass-to-charge ratio (m/z) range of 1 to 800 u. Typically, mass spectral acquisition rates for these devices are 1 to 2 scans-per-second due to low signal intensity at higher scan rates.

In many GC/MS analyses, mass spectral acquisition rates of 1 to 2 mass spectra-per-second are sufficient. However, for the analysis of complex mixtures where there are regions of the chromatogram that have unresolved components, these relatively slow mass spectral acquisition rates are not sufficient to accurately represent the chromatography available from the gas chromatograph and also provide useful mass spectra for each component. An additional limitation resulting from these typical mass spectral acquisition rates for quadrupole and magnetic sector mass spectrometers is a misrepresentation of the relative ion currents at m/z values due to changes in partial pressure of the analyte during the time necessary to acquire a mass spectrum. The resulting mass spectra show a skewing of the relative mass spectral peak intensities, making mass spectral interpretation and library searches difficult.

The ion trap mass spectrometer has recently been introduced to the GC/MS market as a fast scanning, highly sensitive mass spectrometer. The ion trap is based on the Quadrupole Ion Storage Device (QUISTOR) consisting of a hyperbolic ring electrode and two end caps. By applying an rf potential to the central ring, ions once formed are stored in the device. Ions are formed by pulsing electrons into this region. Increasing the rf potential applied to the central ring destabilizes ion trajectories in the device from low to high m/z. Detection of the destabilized ions produces a mass spectrum. The pulsed nature of ion formation and subsequent storage of all ions until detection in the ion trap eliminates mass spectral skew.

Varian⁵ has introduced the Saturn II GC/MS based on this technology. This ion trap scans at a constant rate of 5600 u/second up to 650 u with a maximum scan rate of 9 scans-per-second from 30 to 650 u. The Saturn II averages 3 "micro-scans" resulting in a scan rate of 3 useable mass spectra/second. This scan rate can be increased by decreasing the mass range to be scanned. A comparison of mass spectral skew between the Saturn II and a benchtop quadrupole mass spectrometer was made using a capillary column and collecting 8 scans over the chromatographic peak of decafluorotriphenylphosphine (DFTPP).⁶ Each of the mass spectrometers was scanned from 50 to 450 u. The ratio of two major ions of DFTPP, m/z 198 and m/z 442 was compared for each of the 8 scans acquired across the chromatographic peak. The quadrupole had a variation of the ratio of m/z 198/442 of 50% (from 80% to 30%) indicating the presence of mass spectral skew in the data. The ion trap had a variation of the ratio of m/z 198/442 of 15% due to random noise in the mass spectra.

Time-of-flight mass spectrometry (TOF-MS) is another viable alternative for GC/MS because the mass spectral generation rate of TOF mass spectrometers can be as high as 25 kHz¹. Ions are typically formed in a TOF ion source by collision with electrons of energies up to 70 electron volts (eV) and then application of an extraction potential, pushing or pulling the ions out of the source. The ions are commonly accelerated to a given energy and have flight times, t, defined by the following equation:

flight time,
$$t = L\sqrt{\frac{m}{2zeV}}$$

where L = the length of the flight tube(meters), m = the mass of the ion in kg, $e = 1.609 \times 10^{-19}$ C, and V = the accelerating potential (volts). The flight time for a given ion is related to the square root of its m/z value. A transient mass spectrum is defined as the resulting ion currents at each m/z value that reach the detector after a single extraction pulse.

Collection of a mass spectrum from a TOF mass spectrometer has historically been accomplished by time-slice detection (TSD). TSD is accomplished by incrementing the delay time of a time window synchronized with the extraction pulse of the transient mass spectrum. In transients produced at 10 kHz, for unit mass resolution up to 500 u, this time window should be as narrow as 5 ns. Using TSD, acquisition of a complete mass spectrum can take from 1 to 2 seconds or longer. The major shortcoming in using TSD is that most of the available data from each

transient mass spectrum is ignored (only a single 5 ns time window is acquired from each transient mass spectrum).

A data collection system that utilizes all of the ion currents available in each transient mass spectrum would greatly improve the sensitivity of TOF-MS. This type of data collection has been termed time-array detection (TAD) and has been implemented at MSU. The development of the integrating transient recorder (ITR)⁷ that digitizes mass spectral data at 200-MHz, allows the continuous acquisition of the information in every one of the mass spectral transients generated, providing a data system that makes use of all of the available information afforded by TOF-MS. Figures 1.4 and 1.5 illustrate the capabilities of the ITR. The mass spectral acquisition rate of the TOF mass spectrometer is determined by the number of consecutive transient mass spectra integrated by successive summation. This mass spectral acquisition rate can be adjusted to meet the needs of the experiment.

Conventional TOF-MS, where ions are formed from gas phase molecules with a pulsed electron beam and a pulsed extraction voltage, suffers from poor mass resolving power. The initial spatial and energy distributions of the ions in the ion source upon formation result in a broad distribution of arrival times at the detector for isomass ion packets. Figure 1.1 is an illustration of the effects of each of these phenomena and their contribution to peak broadening. The initial spatial distribution gives rise to ions that are accelerated through different dimensions of an accelerating field resulting in a distribution of kinetic energies and ion flight times to the detector. Ions that are formed with some initial energy are going to maintain that energy distribution upon acceleration producing a

distribution of flight times. A special aspect of the initial energy distribution considers two ions with the same initial kinetic energy with one ion having its kinetic energy in the direction of the detector and the other ion having its kinetic energy directly away from the detector. Upon acceleration, both ions will leave the ion source with the same kinetic energy, but the ion with initial kinetic energy away from the detector will leave the ion source later in time. This has been termed the turn-around time and can be corrected by time-lag focussing for narrow m/z ranges, but is mass-dependent.

Conventional TOF-MS, with its mass-dependent focussing, has limited applicability with a time array detector, such as the ITR, because all of the ion current at each m/z value is not optimally focussed at the detector for each source extraction. TOF mass spectra of unit resolving power can be obtained using TSD in conjunction with time-lag focussing by synchronizing the time window with the time-lag optimized for that m/z value collected, but not at mass spectral acquisition rates suited for GC/MS. Erickson, et. al., determined that three different values of time-lag would be necessary to sufficiently represent the mass spectral information available over a mass range from m/z 50 to 575 u using a Wiley/McLarentype TOF mass spectrometer.

One of the primary research goals of the Michigan State University/National Institutes of Health Mass Spectrometry Facility is to take advantage of the high mass spectral acquisition rates available with TOF-MS and develop a GC/MS instrument based on a TOF mass spectrometer in conjunction with TAD. Improvements in the mass resolving power of TOF mass spectrometers would be necessary to provide

Phenomena limiting resolution in time-of-flight mass spectrometry

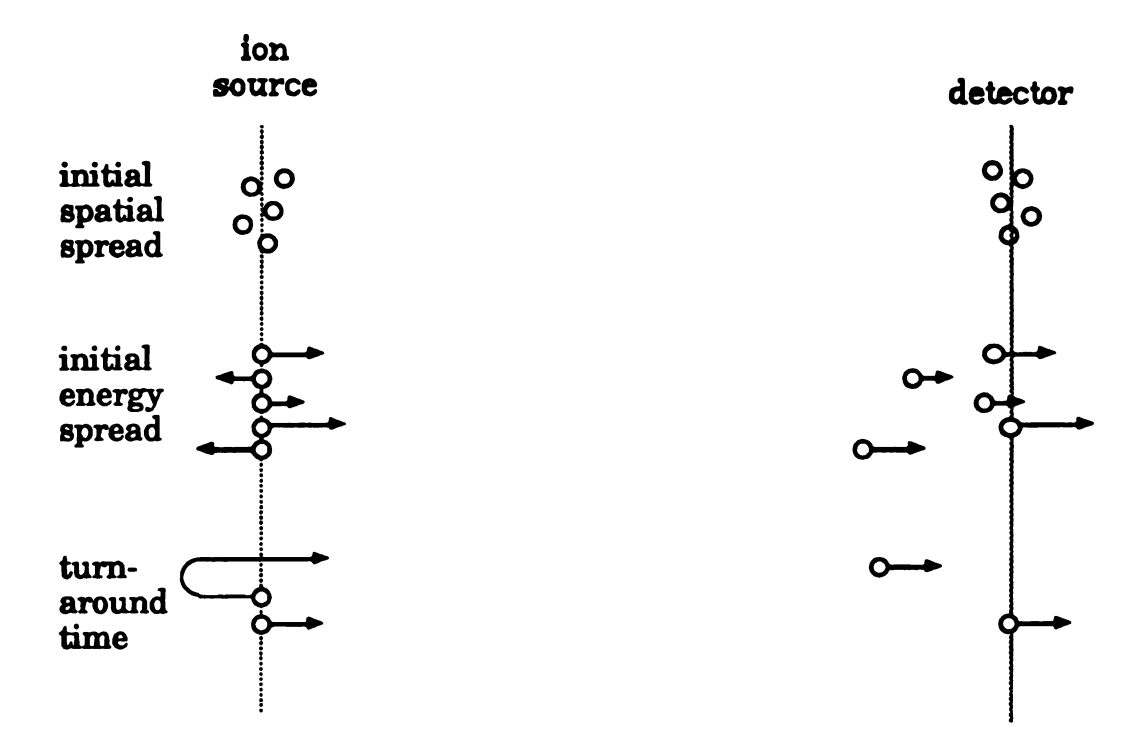


Figure 1.1 The initial spatial distribution of neutrals upon ion formation gives rise to ions that acquire different final energies. Ions formed with some initial energy will attain final energies equal to their initial energy + accelerating potential. The turn-around time is a special aspect of the initial energy distribution where two isomass ions with the same initial energy, one with initial direction towards the detector and the other with direction away from the detector. Both will leave the ion source with the same final kinetic energy, but at different times.

unit resolution over a mass range of m/z 20 to 600 u, for each transient mass spectrum. Another goal was to develop a TOF mass spectrometer capable of high pressure ionization techniques, in particular chemical ionization, which is commonly used to complement GC/MS data collected using EI. In order for high pressure ionization techniques to be successfully implemented, a mass spectrometer that did not require source extraction pulses to form transient mass spectra would be required due to low and diverse ion mobilities in the ion source under CI pressures.

The successful development of beam-modulation techniques by Bakker^{9,10} was the first demonstration of a TOF mass spectrometer that provided mass-independent resolution. This TOF mass spectrometer incorporates a continuous ion source for extraction of the ions.¹¹ A 'slice' of the continuous ion beam is selected by an electric gate to be mass analyzed. The turn-around time no longer limits the resolving power of the TOF mass spectrometer using beam-modulation techniques because the ion source is operated in a continuous ion extraction mode. The major contribution to mass spectral peak broadening in the beam modulation technique is the energy distribution of the isomass ions in the continuous ion beam and the temporal dimension of the excised slice.

Initial work towards the development of a beam modulation mass spectrometer at MSU led to the design and development of the BEam Deflection Energy-Resolved (BEDER) TOF mass spectrometer 12,13 by David Pinkston. This mass spectrometer incorporated an ion source with narrow slits and an electric sector to provide energy-resolved ion beams. The ion source was operated in a continuous ion extraction mode, which allowed the use of high pressure ionization techniques, such as chemical ionization

(CI), to be successfully implemented on a TOF mass spectrometer. The continuous ion beam passed through an energy filter that had an adjustable exit slit to control the energy distribution of the ion beam analyzed. The continuous ion beam was then time-encoded by beam deflection producing a mass spectrum of much improved resolving power compared to that of conventional source-pulsed TOF-MS, and having better than unit mass resolution for each m/z value in the mass range of 20 to 600 u. The BEDER-TOF mass spectrometer also showed the capability of MS/MS by time-resolved ion kinetic energy spectrometry (TRIKES)¹².

Other developments in TOF-MS at MSU involve the development of time-resolved ion momentum spectrometry (TRIMS)¹⁴. TRIMS originally combined a pulsed ion source and magnetic sector to disperse ions based on their momentum. Ions of a given momentum are selected to pass down a tube with a detector at the end. The simultaneous measurement of the magnetic field and flight time of an ion to the detector is used to determine its m/z value. TRIMS later implemented beam deflection for improved mass resolution.¹⁵ Mass spectrometry/mass spectrometry (MS/MS) is achieved by scanning the magnetic field and collecting ion flight times for each magnetic field setting.^{16,17}. This mass spectrometer was the first to demonstrate MS/MS on the chromatographic time-scale using a wide-bore capillary column¹⁸.

My research began with an evaluation of the performance of the BEDER-TOF mass spectrometer. An in-depth analysis of David Pinkston's dissertation led to a number of conclusions that provided the impetus for the development of the beam deflection TOF (BDTOF) mass spectrometer. Figure 27 of David Pinkston's dissertation shows a plot of theoretical and

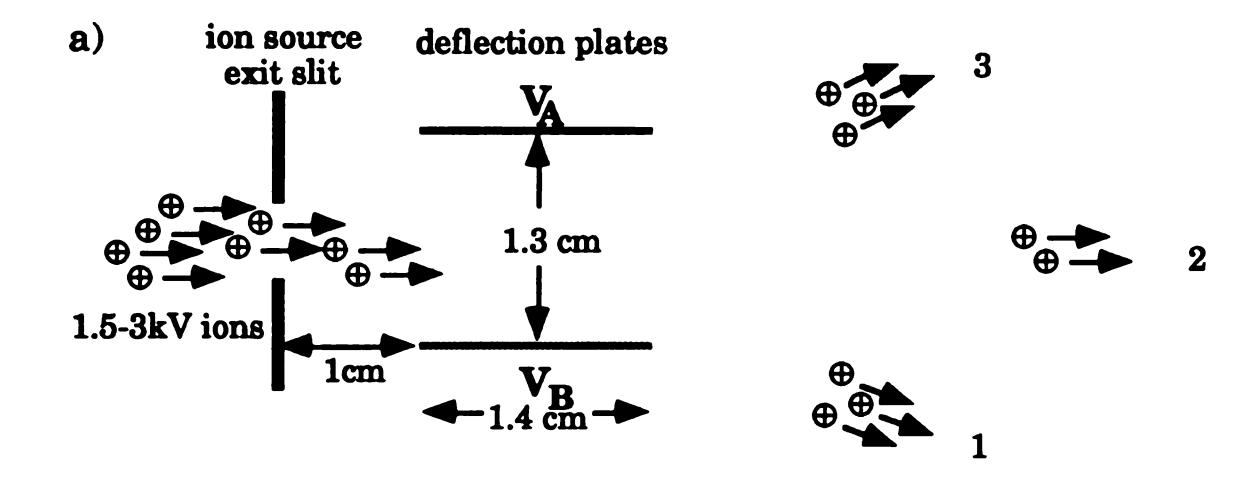
experimental resolution versus the exit slit width of the electric sector. Adjustment of the exit slit width controls the energy distribution of the continuous ion beam that is modulated to form a mass spectrum. In this figure, the experimental data points do not correlate with the theoretical data points. As the slit width was increased, i.e., allowing greater energy distribution in the continuous ion beam, the resolving power did not decrease accordingly. The experimental data suggest that the resolution of the BEDER-TOF mass spectrometer was not limited by the energy distribution of the continuous ion beam exiting the electric sector. The conclusion was drawn that the resolution was limited by some factor after the electric sector, namely, the mode of beam deflection implemented on the BEDER-TOF mass spectrometer.

Modifications to the BEDER-TOF mass spectrometer were severe enough to warrant the renaming of the mass spectrometer. The electric sector was removed from the mass spectrometer due to the apparent independence of the resolving power of the BEDER-TOF mass spectrometer with the energy distribution in the continuous ion beam. A benefit of the removal of the electric sector was an increase in total ion current of the continuous ion beam since it wasn't being dispersed by the electric sector. Of course, removal of the electric sector eliminated the capability of MS/MS by TRIKES, but the main objective of this research was to develop a GC/TOF mass spectrometer.

Much of the early work on the BDTOF mass spectrometer was directed towards optimizing the method of beam deflection because it appeared that this was limiting the mass resolving power of the mass spectrometer. Experiments were performed utilizing a number of beam deflection assemblies. A new set of deflection plates was designed with a factor of five decrease in capacitance, improving pulse rise/fall times. The pulsing/gating method used by Pinkston¹² was discarded for a single gate mode, operated at a 5 kHz rate. Figure 1.2 shows the final beam deflection system and the pulse timing utilized. Two pulses were used to form ion packets by applying a voltage pulse to each of two parallel deflection plates.

The pulses were held at two different potentials, and by reversal of the potentials applied to each plate, an ion packet would be produced at the time during which the electric field between the deflection plates was zero. This method of beam deflection proved quite successful, producing a resolving power of m/ Δ m of 1400 at m/z 132 corresponding to the nominal atomic mass of xenon as shown in Figure 1.3. The resolving power achieved by this procedure is better than unit resolution over the mass-to-charge ratio range of 20 to 500 u. 19

This is the first report of the use of two voltage pulses to form the ion packet in beam deflection.²⁰ Previous beam deflection methods utilized one voltage pulse applied to one-half of the gate and a d.c. voltage applied to the other half. Ion packet formation is accomplished by reversal of the electric field between the deflection plates of the gate. The new beam deflection circuitry provided control over the time when each pulse switched relative to the other. By simply changing the time at which each pulse changed magnitude (forming an ion packet), control of the effective d.c. voltage of the gate could also be optimized to focus the ion packet at the detector.



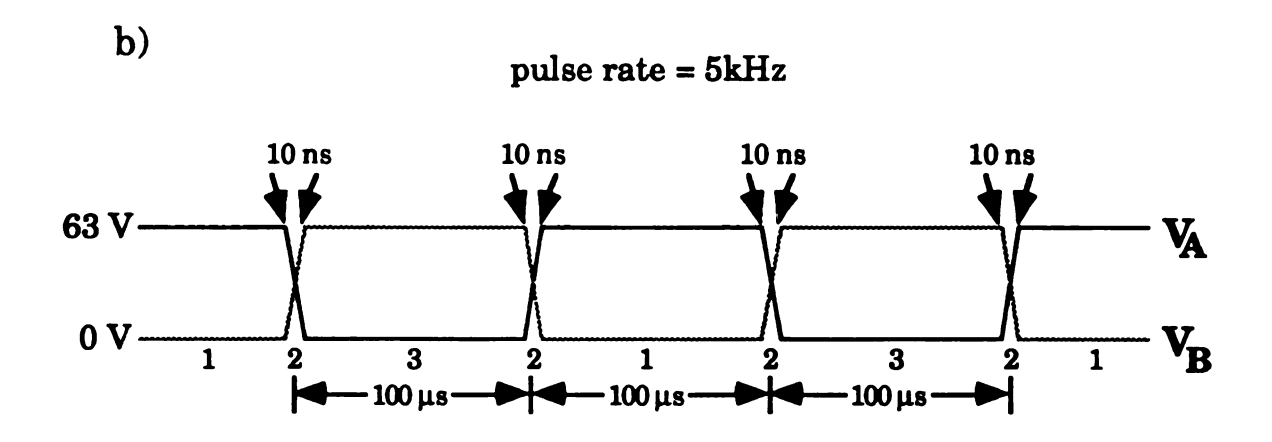


Figure 1.2 a) Schematic of beam deflection assembly located in the flight tube directly after the exit slit of the ion source. The beam deflection spacing and plate dimensions are also given. b) The repetition rate of mass spectral transient formation is 5kHz with pulse rise and fall times of 10ns. During time period 1, the ion beam is deflected downward. As the voltage applied to VA and VB changes during time period 2, the beam is swept across the detector surface, resulting in a mass spectral transient available for acquisition. The continuous ion beam is deflected upward during time period 3.

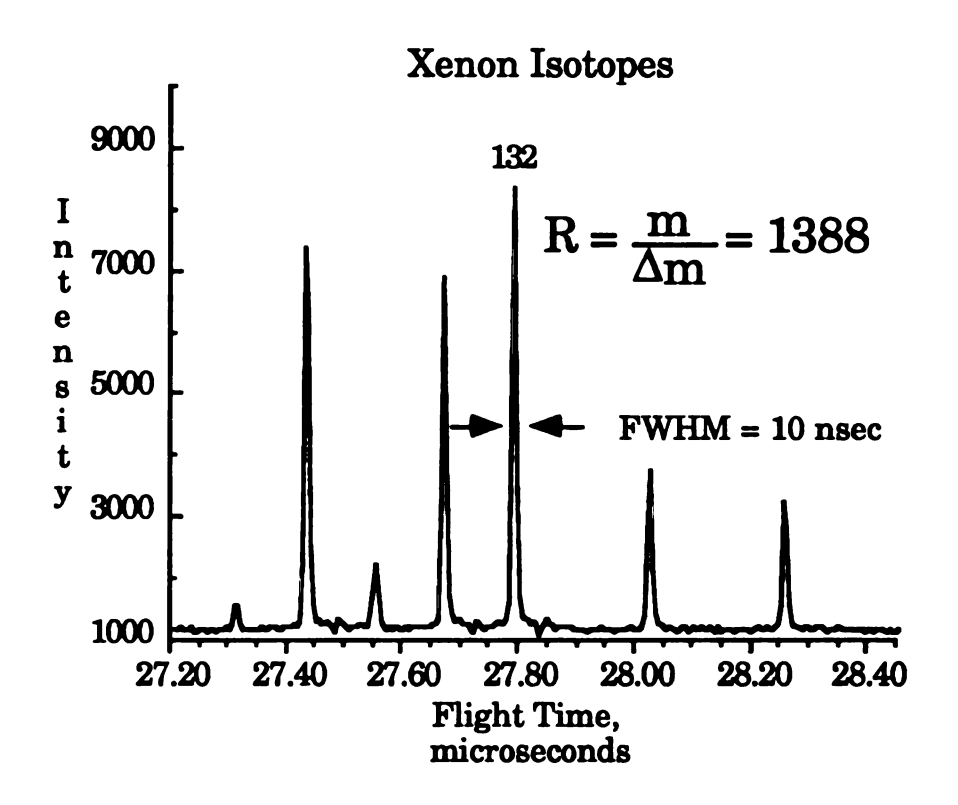


Figure 1.3 Mass spectrum of Xenon showing mass resolution with new beam deflection assembly of the BDTOF mass spectrometer.

The high mass spectral acquisition rate of TOF-MS coupled with TAD provided by the ITR is a powerful analytical combination that can be used to study ionization methods where rapid changes in the abundance of analyte ions occur in the ion source. Figures 1.4 and 1.5 demonstrate the capabilities of TOF-MS coupled with the ITR. A gas chromatograph was interfaced to the BDTOF mass spectrometer to show the capabilities of high mass spectral acquisition rates of TOF mass spectrometers combined with TAD in the context of complex mixture analyses. GC/MS data were acquired during the analysis of a trimethylsilyl derivatized mixture of urinary organic acids at 1 and 10 scans-per-second to show improvements in the chromatographic information available from the reconstructed total ion current (RTIC) chromatograms generated at higher mass spectral acquisition rates. Chromatographic peak shapes and areas are more accurately represented with the higher mass spectral acquisition rates due to the greater number of mass spectra available. Mass spectra of closely eluting components that are incompletely resolved chromatographically are easily made available by mass spectral subtraction with the 10 mass spectra/second data base. Regions of the chromatogram that contain coeluting components are identified by a 3-dimensional display of the data or by plotting mass chromatograms of selected ions.

There have been numerous accounts of time-dependent ion currents in the desorption/ionization (D/I) techniques of fast atom bombardment²¹ (FAB) and secondary ion mass spectrometry²² (SIMS). The BDTOF mass spectrometer/ITR may contribute to a greater understanding of the mechanism of ion formation in these D/I techniques²³ by utilization of the high mass spectral acquisition rates of TOF-MS and the high mass spectral

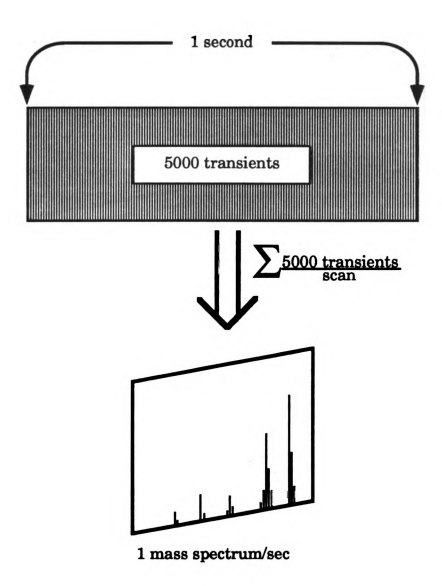


Figure 1.4 The BDTOF mass spectrometer operates with a mass spectral transient generation rate of $5000s^{-1}$. The summation of consecutive 5000 mass spectral transients by the ITR results in a mass spectral acquisition rate of 1 mass spectrum/second.

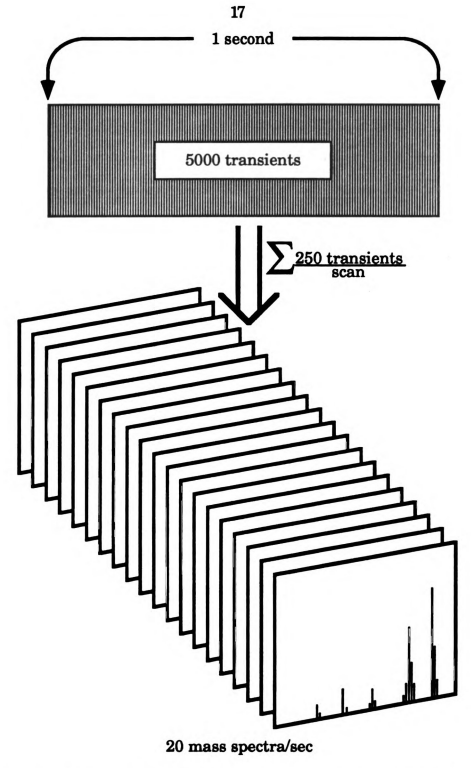


Figure 1.5 The BDTOF mass spectrometer operates with a mass spectral transient generation rate of 5000s⁻¹. The summation of consecutive 250 mass spectral transients by the ITR results in a mass spectral acquisition rate of 20 mass spectra/second.

acquisition rates available with the ITR. It has been shown that it can take many seconds to establish a "steady state" of matrix and analyte ion currents upon primary beam bombardment. 24,25

Another D/I technique, developed in this laboratory, potassium ion ionization of desorbed species (K+IDS)²⁶, also, produces time-dependent ion currents. This technique uses thermionic emitters²⁷ as sources of alkali ions for attachment to thermally-desorbed analyte molecules and fragments. This technique produces analyte ion currents for periods of time ranging from one second to many seconds. For the case of a one second desorption profile, the mass spectral information available rapidly changes due to the temperature gradient produced by the heating of the sample by the "potassium glass". The high mass spectral acquisition rates of TOF-MS may help elucidate the mechanisms of ion formation and a better understanding of the processes occurring in this D/I technique.

A preliminary investigation of K+IDS has been performed using the BDTOF mass spectrometer/ITR. Studies were performed to compare K+IDS spectra obtained with the BDTOF mass spectrometer under K+ chemical ionization (K+ CI) conditions of acetone to those obtained using a Hewlett Packard 5985 mass spectrometer under the same K+ CI conditions. A comparative study was performed to determine the effects of the accelerating voltage penetration into the ion volume of the ion source on the extent of conversion of gas phase K+ to gas phase (analyte + K+) by placing a wire grid across the ion volume exit slit. Some preliminary spectra have been collected on a number of samples.

Chapter 2 - Developments In Time-Of-Flight Mass Spectrometry

The first description of a "pulsed mass spectrometer with time dispersion" was given in 1946 by Stephens²⁸. Cameron and Eggers²⁹ developed a TOF mass spectrometer that formed ions by EI in an ion source and accelerated them into an evacuated tube. The ion beam was allowed to pass into the evacuated tube by deflecting plates for time periods close to 5 µs in duration, resulting in peak widths of 20-30 µs. The mass resolving power was limited by the design of the ion source and the large distribution of energies for each ion with these early instruments. Later, TOF mass spectrometers were designed using pulsed EI and pulsed acceleration from the ion source.^{30,31}

Time-of-flight mass spectrometers are simple in design, consisting of an ionization region (ion source) and dispersive region (flight tube), making them easy to construct and maintain at low cost. Mass spectra can be generated by a TOF mass spectrometer at high rates (up to 25 kHz) and is limited by the transit time of the heaviest ion to the detector, which is typically on the order of 100 µs. The availability of transient recorders (specifically the ITR) has allowed the acquisition of all of the transient mass spectra produced each second, expanding the use of TOF mass spectrometers.

Improvements in mass resolving power in TOF mass spectrometers were accomplished by minimizing or correcting for the initial spatial and energy distributions in the ions. Wiley and McLaren developed a mathematical model for an ion source with two accelerating fields.³² The Wiley and McLaren ion source was the first major advance in TOF-MS, with the first commercially available TOF mass spectrometer based on this This mass spectrometer demonstrated a mass resolving instrument. power $(m/\Delta m)$ of better than 600 for the ionic isotopes of xenon. A schematic of this mass spectrometer is shown in Figure 2.1. The first accelerating region of the ion source is labeled as s. The ions are formed in this region and then extracted by application of a positive voltage to the source backing plate. An important feature of this ion source is that the electric field, E_{s,} in region s is held near zero during the ion formation process to minimize the energy distribution in the ions. The region labeled d is kept at a constant electric field strength, Ed. The ions are accelerated into the field free region, D, separating into ion-packets of different m/z value. Ions of a given m/z that are formed at different positions in region s can be made to arrive simultaneously at the detector by varying the ratio of Ed and Es. This has been termed space-focussing and is independent of the m/z value of the ions.

Although this new TOF mass spectrometer had improved resolving power over a single-extraction-field ion source, the focussing of each m/z value was dependent upon ion source parameters. Wiley and McLaren introduced a method for improved resolving power for narrow mass windows called time-lag energy focussing of the ions. A delay time between

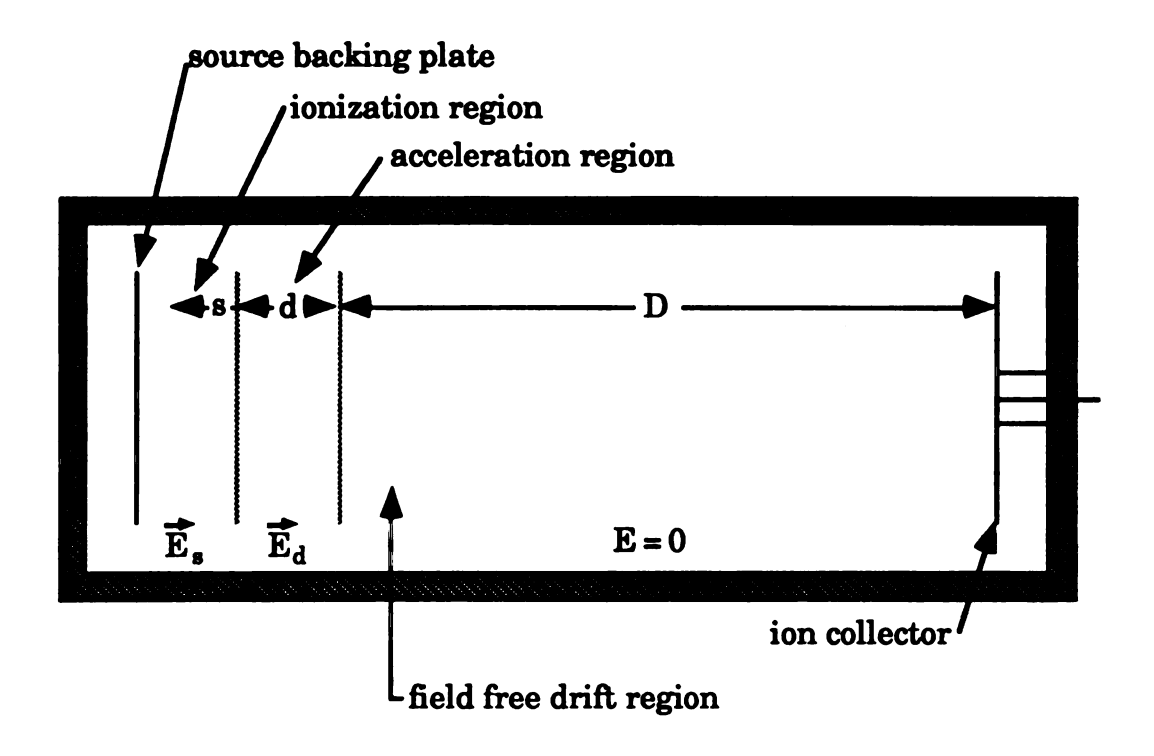


Figure 2.1. Wiley-McLaren ion source showing two extraction fields, $\vec{E_s} + \vec{E_d}$.

ion formation and application of an extraction pulse to the ion source backing plate results in ions of a given m/z value and distribution of energy to arrive simultaneously at the detector. This is more clearly understood by referring to Figure 2.2. This figure shows a theoretical plot of ion flight times versus initial ion position within region s of the ion source for three isomass ions. One ion has no initial energy, while the other two have the

same initial energy but with velocities in opposite directions (one with a velocity vector towards the detector, v_0 , and one away from the detector, $-v_0$). By allowing the ions to drift in region s from their initial positions for a time τ, the final velocity given to each of the three ions after extraction is dependent on their positions within region s. The ion with initial velocity away from the detector, -vo, will acquire more energy upon extraction than the ion with initial velocity towards the detector, v_0 , but will have a longer flight path. The ion with initial velocity, vo, will acquire less energy upon extraction and have a shorter flight path. The time-lag, τ , is optimized for each m/z value when the ions of initial velocity vo and -vo arrive simultaneously at the detector. Energy-focussing is achieved when isomass ions with different thermal velocities have flight times that are independent of their velocity distributions. Using a linear drift path and time-lag energy focussing, however, results in mass-dependent focussing of the ions. This limits the usefulness of this mass spectrometer because only a narrow range of m/z values is in optimum focus at the detector for each ion source extraction pulse and time-lag. Stein³³ showed that it was mathematically impossible to have both space and velocity-focussing using time independent, one-dimensional accelerating fields in TOF mass spectrometers.

Bakker published a discussion of time-focussing in TOF-MS.³⁴ Time focussing involves making the flight time for an ion independent of an its initial velocity or spatial distributions. Time-focussing is achieved when isomass ions with initial space or velocity distributions can be made to arrive at a point or line in space simultaneously. Mamyrin proposed the use of an electrostatic mirror to provide energy-focussing.³⁵

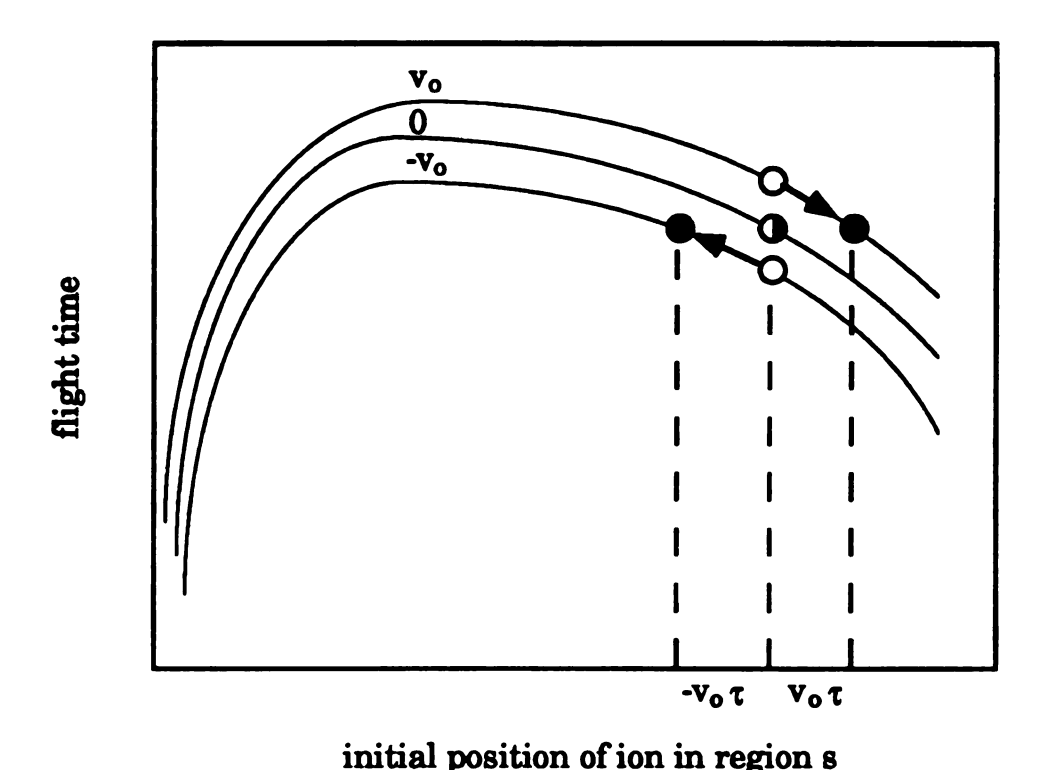


Figure 2.2. Plot showing ion flight times versus initial position of the ion in region s of a Wiley-McLaren ion source for three isomass ions with different initial velocities. By waiting for a time τ , after ion formation and before ion extraction, the flight time of the two isomass ions with the same initial velocities but opposite direction can be made to arrive at the detector simultaneously.

Poschenrieder derived a theoretical treatment of time-focussing using a combination of linear drift spaces with magnetic and electric sectors. 36,37 Using a combination of a magnetic sector with linear drift spaces and constant momentum acceleration, the flight time for ions of a given m/z value can be made to be independent of their initial thermal velocity distribution. Likewise, combining one or more electric sectors with linear drift spaces and constant energy acceleration provides ion flight times that

are independent of the initial energy distribution on the ions. Other TOF mass spectrometers have since been proposed that use multiple electric sectors and electrostatic mirrors to provide time-focussing. 38,39

The use of time-dependent, or dynamic electric fields to improve the mass resolving power has also received consideration. Time-dependent extraction voltages can be applied to a lens in the ion source or to a separate region in the ion flight path. Isomass ions with different initial velocities can be made to arrive simultaneously at the detector by applying the appropriate force to each isomass ion packet. In Impulse Field Focusing⁴⁰, the normal electric field, E_s , applied to region s of the Wiley and McLaren ion source is pulsed to a higher electric field strength, E_{τ} for a time, τ . The mass resolving power with impulse-field focusing has been theoretically determined to be better than unit mass resolution up to m/z 2600. Theoretical models for using post ion source time-dependent electric fields have also been considered. Theoretical and experimental data to support a post ion source time-dependent electric field has been demonstrated by Johnston, et. al.⁴³

Beam modulation techniques have been used in nuclear physics to provide isomass ion packets of well defined energy. 44,45 Anderson and Swann developed a theoretical description and experimental data of beam chopping and bunching of a continuous ion beam for nuclear physics. 46 Fowler and Good described two methods of beam modulation of a continuous ion beam. Impulse sweeping involves deflecting a continuous ion beam from its original path through an aperture using a set of deflection plates. Ions that pass through the aperture are defined by the time that the impulse is applied to the deflection plates. Differential

impulse sweeping forms ion packets using the rising and falling edges of a waveform. The width and duration of each ion packet is defined by an aperture placed in front of the detector.⁴⁷

Beam modulation was only successfully demonstrated in TOF-MS after the work of Bakker.^{6,7} Bakker developed a mathematical model of ion trajectories based on the dimensions of beam deflection plates and dimensions of the mass spectrometer such as length of the ion flight path and aperture defining the ion packet width. This model determined that the theoretical resolving power of a beam modulation TOF mass spectrometer is given by the following equation:

$$R = \frac{L^2V_0}{2DU(B+S)}$$

L is the ion flight path, V_0 is potential difference of the ion beam modulation applied between the deflection gates, D is the deflection plate spacing, U is the accelerating voltage, B is the ion beam width, and S is the aperture width. This model was confirmed by development of a TOF mass spectrometer that demonstrated that the mass resolving power varied by the square of the ion flight path. Also, according to this theory the mass resolving power is not dependent on m/z. A significant advantage to the use of beam modulation is that the ion source is operated in a continuous ion extraction mode. This removes the turn-around time as a limiting aspect of the mass resolving power. The continuous ion source also allows

high pressure ionization techniques to be implemented in TOF-MS. These were the main reasons for choosing beam modulation for this project. 13

More recently there have been other developments of continuous ion extraction TOF mass spectrometers. A TOF mass spectrometer has been developed based on Fourier transform techniques. This FT-TOF mass spectrometer modulates the continuous ion beam with a sinusoidal wave and modulates the electron current of the detector in phase. The ion signal is acquired as a function of the modulation frequency and a Fourier transform of the ion signal yields the time-of-flight mass spectrum. This mode of ion detection theoretically increases the duty cycle to 25 % which would greatly enhance the sensitivity available with TOF mass spectrometers. This work showed some preliminary data that reproduced the mass spectral quality available with an instrument operating in the normal pulsed ion extraction mode, however, the expected gain in sensitivity, due to the increase in the duty cycle, has yet to be realized.

Another development of a continuous ion source in TOF-MS is the orthogonal-acceleration TOF (oa-TOF) mass spectrometer.⁵⁰ This mass spectrometer accelerates ions from an ion source to 10 eV in one-axis and then accelerates them to 3000 eV in an orthogonal direction (TOF-axis) to a detector. The ion optics of the orthogonal accelerator are designed for space-focussing. A key feature of this instrument is the use of a collimating lens to make ion trajectories parallel. Variations from these parallel trajectories mainly result from the translational energy distributions in the ions. Ions entering the orthogonal accelerator are in positions similar to those necessary for the optimum time-lag for each m/z value in a conventional TOF mass spectrometer. For optimum resolving

power, the ion flight time between ion formation in the ion source and extraction from the orthogonal accelerator must be equal to the optimum time-lag necessary to focus the ions at the detector. A theoretical mass resolving power at m/z 2000 of m/ Δ m > 2000 (FWHM) is predicted.

Chapter 3 - Design of BDTOF Mass Spectrometer

A simplified schematic diagram of the BDTOF mass spectrometer is shown in Figure 3.1. This figure shows the major components of the mass spectrometer used for ion beam manipulation, focussing and detection. The first part of this chapter provides a detailed description of these different components either designed or modified for the mass spectrometer along with the circuit diagrams of the circuits that supply the necessary voltages. A discussion of the performance characteristics of the BDTOF mass spectrometer will follow including mass resolving power and mass range in suitable focus for each transient mass spectrum. A comparison of mass spectrometer performance to the BEDER-TOF mass spectrometer will round out this chapter.

A. Ion Source

Ion source design requirements are different for a TOF mass spectrometer incorporating beam deflection methods compared to those of the more common "pulsed extraction" ion source. Time encoding of the ions formed in a commercially available TOF mass spectrometer is usually accomplished by applying a voltage pulse to a repeller in the ion source. Each of the source lenses in this type of ion source has a wide aperture (up to 5 mm in diameter) to increase ion transmission efficiencies to the detector. The utilization of beam deflection methods in a TOF mass

spectrometer requires a narrowly-focussed, continuous ion beam exiting the ion source to achieve adequate mass resolution. Also, successful implementation of high pressure ionization techniques is possible only if the ion source and flight tube regions of a TOF mass spectrometer are differentially pumped. This is a necessary requirement to minimize ion losses due to ion-neutral collisions in the flight tube.

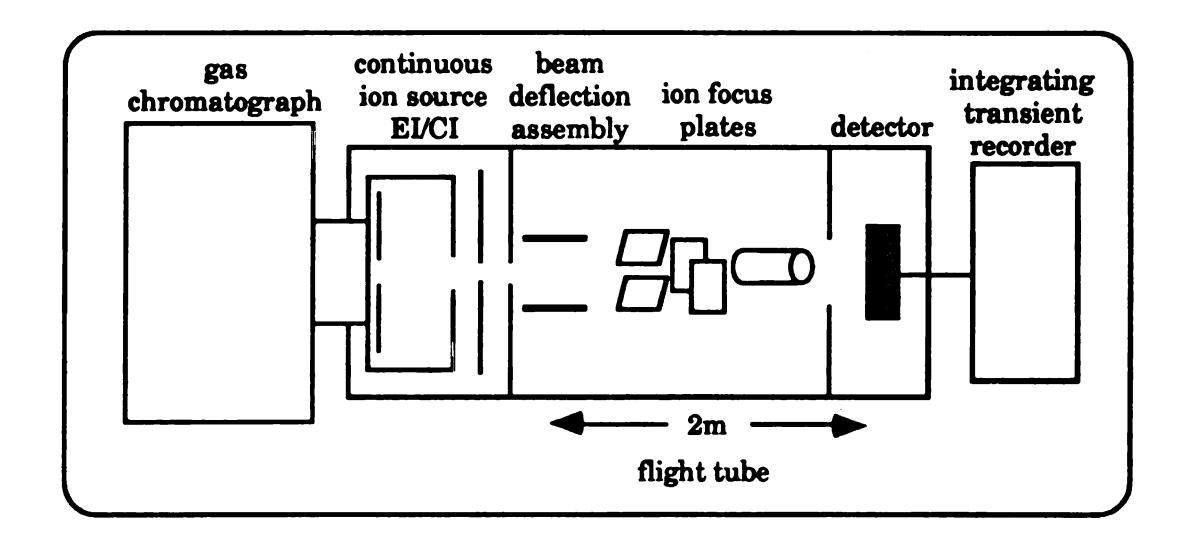


Figure 3.1 Schematic diagram of GC/BDTOF mass spectrometer (not to scale). Shown are the ion source, flight tube, beam deflection assembly, ion focus plates, detector and integrating transient recorder.

The ion sources used in the BDTOF mass spectrometer were adapted from mass spectrometers that used electrostatic and magnetic analyzers because these mass spectrometers also require a narrowly-focussed ion beam. During the course of these studies there were two different ion sources used in this mass spectrometer. The Dupont 21-491B double-

focussing mass spectrometer ion source was the one originally used in the BEDER-TOF mass spectrometer and also for the BDTOF mass spectrometer. The JEOL DM303 double-focussing mass spectrometer ion source was a gift from JEOL, U.S.A., Peabody, MA. This ion source was adapted for the GC/MS research.

1. Dupont 21-491B ion source

This ion source has been adapted from a Dupont 21-491B double-focussing mass spectrometer. The ion source is simple in design, consisting of two repellers in the ion volume and one set of focussing lenses to collimate the ion beam exiting the ion source. Figure 3.2 is a drawing showing the ion source. For a more descriptive drawing, see the Dupont 21-491B operating manuals. The ion source did not have an electron trap and therefore, the electron current of the electron filament could not be regulated as ionization current, but only as total emission current from the filament. Focussing the ion beam involved tuning of the two repeller voltages and the focus right voltage. The ion source exit slit is held at ground potential. A voltage divider provides the ion volume and focus left voltages.

Dupont 21-491B ion source

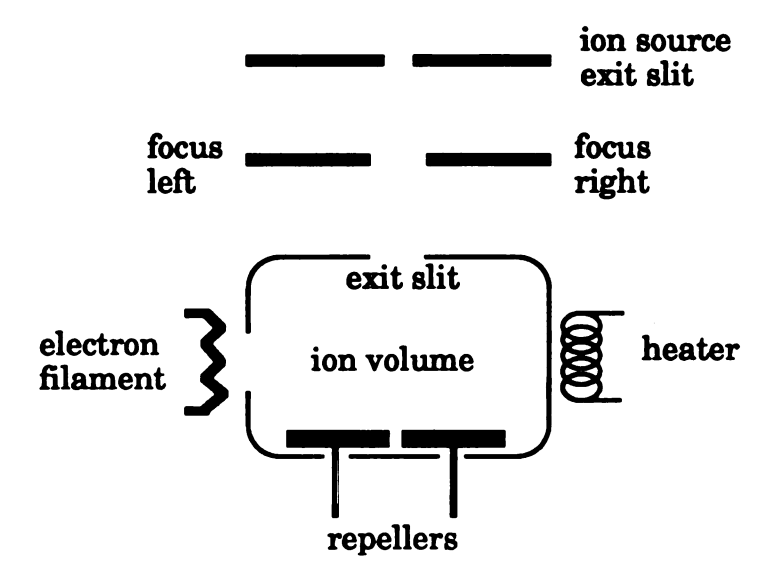


Figure 3.2 Dupont 21-491B ion source.

2. JEOL DM303 ion source

This ion source was adapted to the Dupont 21-491B ion source housing. A simple drawing of the components of this ion source is shown in Figure 3.3. This ion source consists of a repeller, two set of focussing lens, and X-Y deflector plates for ion beam focussing. The electron current is regulated on the ionization current measured on the electron trap. High voltage is supplied by a Bertan model 205A-05R high voltage power supply, Bertan Assoc., Inc., 3 Aerial Way, Syosset, N.Y. 11791. The original JEOL electronics were not available, so a duplicate of these electronics was designed by M. Rabb of the electronics shop of the Chemistry Department.

A schematic of the duplicate electronics is shown in Figure 3.4. Table 3.1 contains information concerning connections to the upper and lower octal sockets on the Dupont ion source housing for the ion source. Table 3.2 contains pin lettering for an amphenol connector that connects circuit

JEOL DM 303 ion source

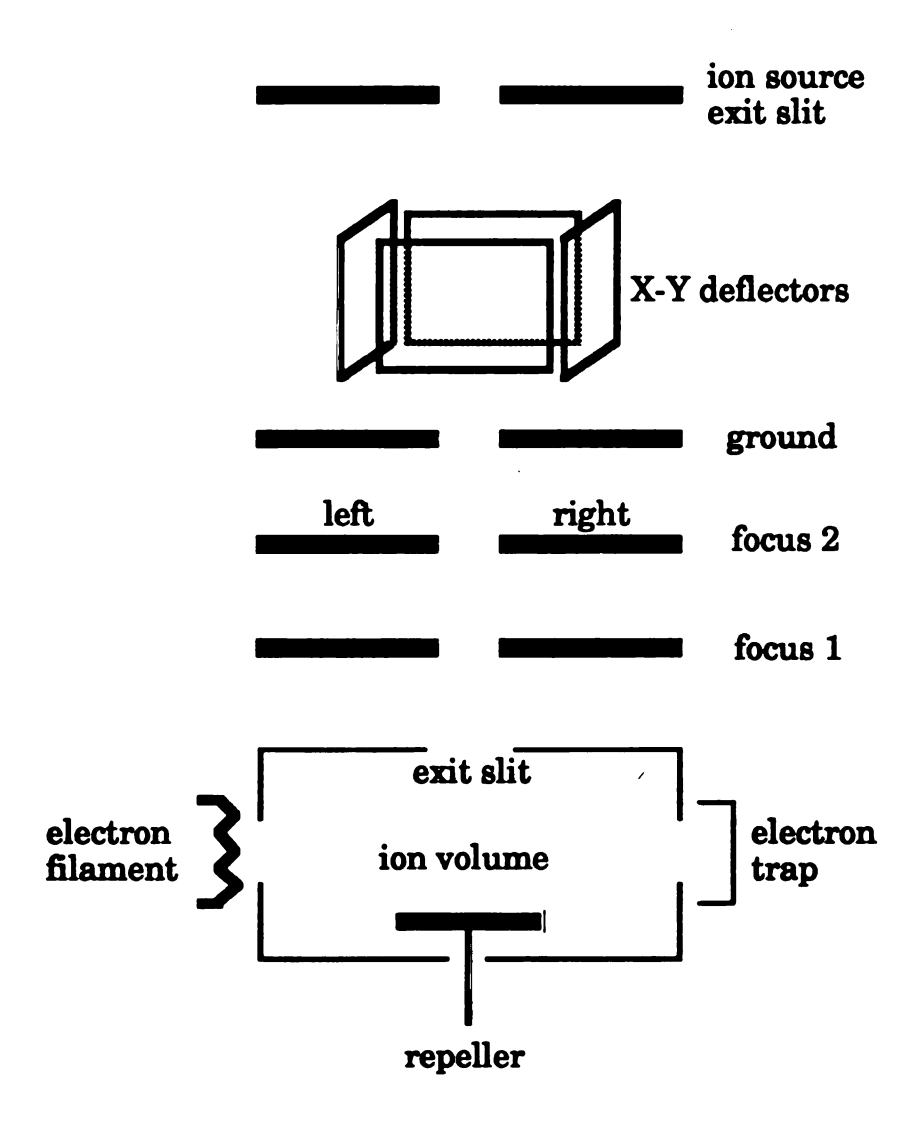


Figure 3.3 JEOL DM303 ion source.

connections to the ion source elements. The filament voltage is variable from 0 to -300V (relative to the ion volume). The electron trap voltage is maintained at an ion source bias voltage of +11V. The voltages for the ion volume and focus 1 (left and right) lens are derived from the voltage divider in Figure 3.5. Focus 2 has the left and right electrodes connected and derives its voltage from a separate voltage divider network. The voltage applied to the focus 2 lens is variable from 0 to V_A. A typical operating voltage for focus 2 is a few hundred volts. The X-Y deflector plates have a voltage range variable from ±200 V derived from the power supply in Figure 3.6.

Table 3.1 Upper and lower electrical connections on Dupont ion source housing for JEOL DM303 ion source.

Table 3.1				
pin number	upper octal socket	lower octal socket		
1	chamber	filament		
2	upper X-Y deflector	heater		
3	lower X-Y deflector	spare		
4	focus left 1000V	electron trap		
5	focus right 800-1200V	thermocouple		
6	focus 2 (left and right)	thermocouple		
7	repeller	heater		
8	spare	filament		

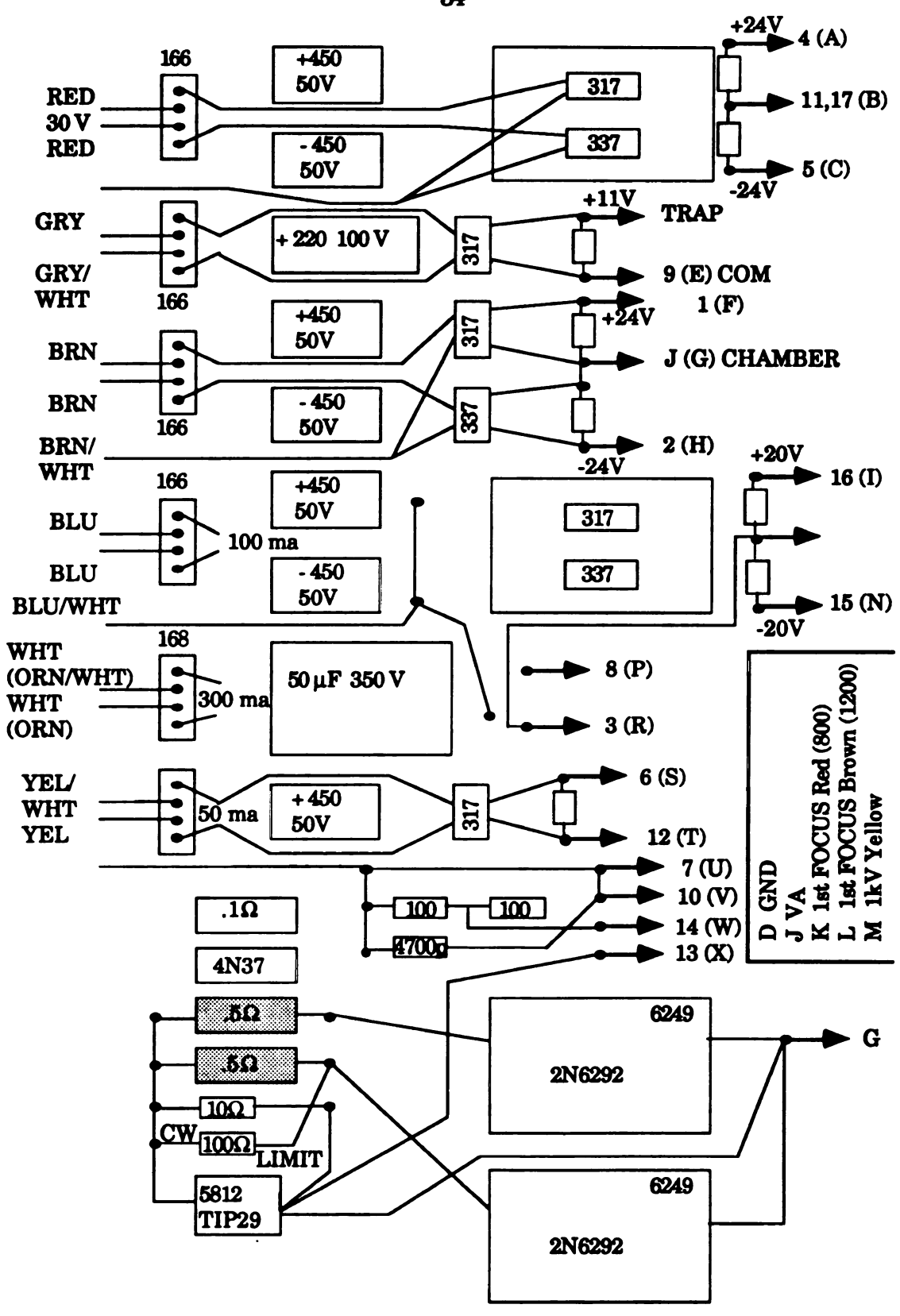


Figure 3.4 Electronic diagram of duplicate circuit for JEOL DM303 ion source.

Table 3.2 Connector (amphenol) pin numbering for JEOL DM303 ion source voltages and ion source elements along with those of the original Old Hirose connector used by JEOL.

Table 3.2						
amphenol connector	voltage and/or connection	Old Hirose connector	amphenol connector	voltage and/or connection	Old Hirose connector	
A	+24V	4	L	1 st focus 1200V (yellow)		
В	common	11,17	M	1 st focus 1000V		
C	-24V	5	N	-20V	15	
D	ground		P	+300V (filament)	8	
E	11V (electron trap)	9	R	common (filament)	3	
F	+24V (repeller)	1	S	11V	6	
G	common	(J) chamber	Т	common (11V)	12	
H	-24V (repeller)	2	Ū	filament	7	
I	+20	16	V	filament	10 (H)	
J	VA		W	100Ω C.T.	14	
K	1 st focus 800V (red)		X	filament control	13	

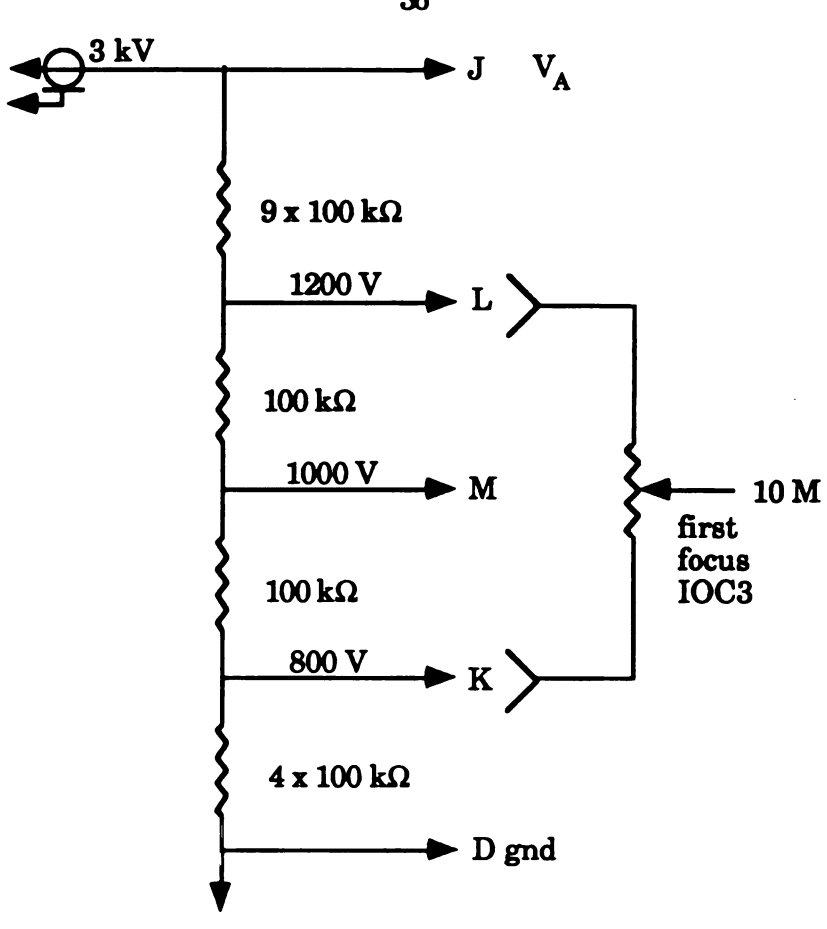


Figure 3.5 Voltage divider for JEOL DM303 ion source. Provides VA and First Focus 1 (left and right) voltages.

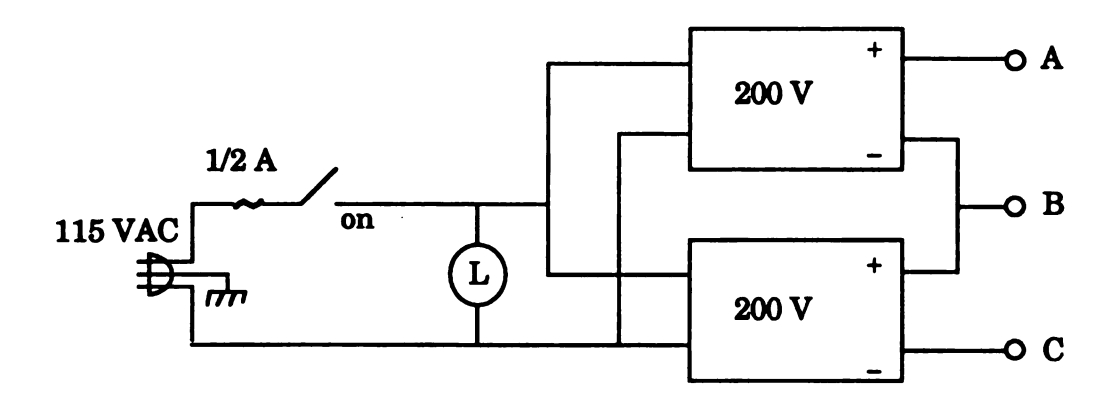


Figure 3.6 Electronic diagram of $\pm 200V$ power supplies for DM303 ion source X-Y deflector plates.

B. Gas chromatography interface

The GC/MS interface is a modification of the aluminum block heater used on the JEOL HX110 mass spectrometer. The aluminum block heated the region from the gas chromatograph to the flange on the ion source housing. The end of the aluminum block going into the HP 5790A gas chromatograph was modified to fit through the oven wall insulation, flush to the inner wall of the oven to maintain high interface temperatures throughout the transfer line. Inside the ion source housing there is a separate aluminum fitting machined to heat the capillary column from the housing flange to the ion source. This aluminum piece was heated with a Watlow C1E13 cartridge heater (HiWatt, 2130 Enterprise, Suite 104, Kentwood, MI). These two heating blocks overlapped by approximately one inch on the housing flange. The interface was wrapped in insulation to maintain a constant temperature the length of the interface. The gas chromatographic interface was tested for cold spots by injecting a standard hydrocarbon mixture containing C9, C10-C26 (even-numbered carbons) hydrocarbons with a temperature program of 50 to 325°C at 20°C per minute. A separate Variac controlled the heating of the aluminum block and the aluminum fitting. The temperature of each component of the interface was gradually increased until the peak shape for C26 showed no evidence of chromatographic peak tailing.

C. Beam Deflection Assembly

Much time was spent developing a successful beam deflection geometry and method. Successful beam deflection (with the BEDER-TOF assembly) was only accomplished after tedious tuning of the pulse width and delay time, along with the d.c. offset voltage of the ion packet production gate. These parameters for the ion packet production gate had to be synchronized to the select gate, which deflects one of the two ion packets formed with the ion packet production gate from reaching the detector. The select gate pulse was never successful in completely deflecting the second ion packet from reaching the detector. Instead a d.c. signal consisting of random ion events at the detector was observed on the oscilloscope that changed in width and delay with changes made to the select gate pulse. The grass signal was proportional to the intensity of the continuous ion current at approximately 5-10% of the peak intensity. Pinkston had to apply an unusually high voltage (close to 100 V!) to the horizontal steering plate located half way down the flight tube to only observe one transient mass spectrum on the oscilloscope. This "tuning" of the mass spectrometer diminished the intensity of the transient mass spectrum as well. All of these variables proved difficult to optimize.

1. Deflection Plate Geometries

The deflection plate geometry of the BEDER-TOF mass spectrometer used $1 \times 4 \times 1.4$ cm blocks of aluminum for the deflection plates (refer to David Pinkston's Dissertation, Figure 20 for details). These blocks were isolated from each other with teflon spacers. The size and design of this assembly resulted in a capacitance between each set of plates of 39 pF at a plate spacing of 2 mm. The capacitance between gates can affect pulse rise/fall times and also induce a voltage on an adjacent gate when pulse amplitudes are changing rapidly. The Avtec pulse generator used for beam

deflection with the BEDER-TOF mass spectrometer was discarded (due to failure of pulse integrity) along with the deflection plate geometry for better designs.

The plate geometry used on the BEDER-TOF mass spectrometer was replaced with a set of horizontal gates etched on a teflon circuit board. This was done mainly to minimize capacitive effects between adjacent gates affecting the voltage pulse applied each individual deflection plate. The active area of the original BEDER-TOF mass spectrometer deflection plate geometry was reduced to 1.4 cm in length by 2 cm in height with the same deflection plate separation of 2 mm. The capacitance between gates decreased to 7 pF.

Geometry studies of the deflection plates led to the conclusion that a greater plate separation provided higher resolution than the 2 mm spacing geometry for the same experimental conditions. Further improvements in the plate geometry were made by eliminating one set of the deflection plates (due to the problems mentioned previously). Eliminating one set of deflection plates (the select gate) and lengthening the pulse time to 100µs improved the success of beam deflection (discussed in more detail in the next section). Increasing the plate separation by a factor of 6.5 reduced the effect of fringing electric fields on the ion beam and created a more uniform electric field between the deflection plates. Also, the deflection plate assembly alignment to the exit slit of the ion source was less critical with the wider deflection plate spacing. The final deflection plate geometry and position relative to the ion source exit slit is shown in Figure 1.2.

2. Beam Deflection Methods

The following is a chronological description of the beam deflection methods implemented beginning on the BEDER-TOF mass spectrometer, including deflection plate geometries and pulse characteristics, and ending with the BD-TOF mass spectrometer.

Initial work on the BEDER-TOF mass spectrometer involved the Avtec pulse generator and David Pinkston's deflection plate geometry. The failure of the Avtec pulse integrity led to the design and construction of a new pulsing circuit by M. Rabb. The specifications for this circuit were as follows:

- 1. Output should consist of two independently controlled pulses with variable delay of 0 20 μ s and variable width of 0 20 μ s.
- 2. The pulse amplitudes were fixed at 63 V (because this was a typical operating voltage used by David Pinkston).
- 3. Pulse rate was variable from 1 to 10 kHz.
- 4. Pulse rise and fall times were less than 10 ns.

A d.c. voltage offset, variable from 0 to 63 V, was applied to one of the pulsing plates. The gate was "opened" by holding the gate pulse at 0 V and grounding the other gate plate. The gate was "closed" after one of the ion packets had passed through the gate by raising the gate pulse amplitude to 63 V. The mass resolution of the mass spectrometer with this new circuit was approximately 100 (m/ Δ m, with Δ m being the width of the peak at half

its maximum height, FWHM), with the baseline peak width for m/z 28 at 150ns.

At this point in time, the select gate of the beam deflection assembly was eliminated and the beam deflection electronics were modified in the following way:

- 1. The pulse width was changed to be variable from 5 μs up to 100 μs .
- 2. The pulsing circuitry would provide two voltage pulses. One pulse would switch from 63 V to 0 V on "edge 1" and the other pulse from 0 V to 63 V.
- 3. Variable delay of the rising and falling edges of each pulse from 0 to $5\,\mu s$.

The electronic diagram of this pulsing circuit is shown in Figure 3.7. This modification eliminated many of the drawbacks associated with the two-gate pulsing assembly. First, the pulse rate was reduced from 10 kHz to 5 kHz and the deflection pulse held for 100 µs after "edge 1", in exchange for the elimination of the select gate of the deflection assembly. Secondly, the application of a dynamic voltage pulse to each plate in the beam deflection assembly provided for both control over the effective d.c. offset voltage that formed the ion packet, thus providing a focussing effect for the ion packet, and also produced an electric field that changed magnitude twice as quickly compared to that from the old method of using one dynamic pulse and a d.c. offset voltage.

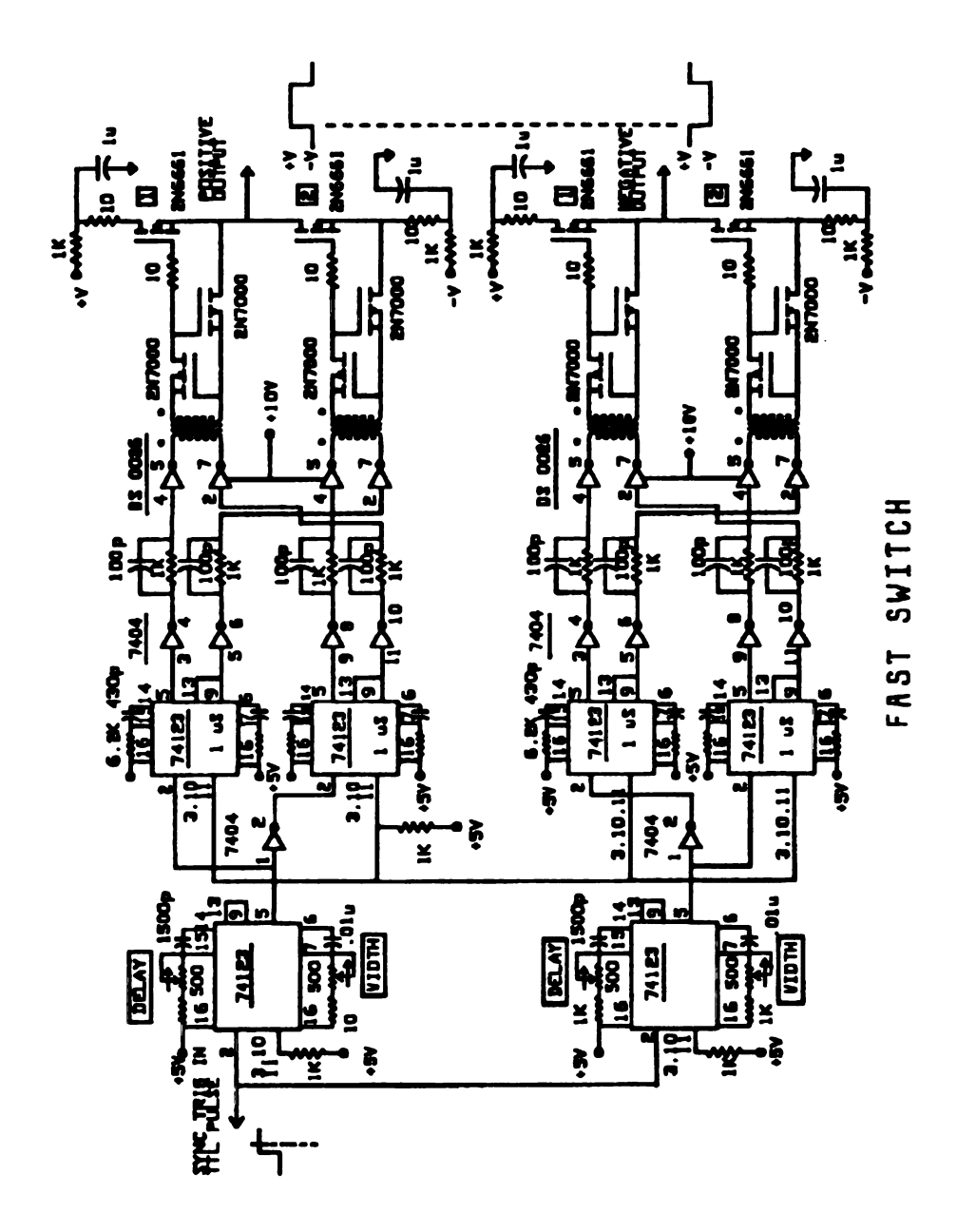


Figure 3.7 Electronic diagram of beam deflection circuit. This circuit provides two output pulses that alternate between 0 and 63 V at 5 kHz. The rise and fall times for each pulse are adjustable as is the relative time at which each pulse changes potential with respect to the other.

D. Detectors

Descriptions of each of the detectors used in this mass spectrometer are given along with the general performance characteristics of each. A flange was designed and machined from stainless steel to fit on the Bendix flight tube. The vacuum seal to the flight tube can be made with a silver wire or 1/16" diameter Viton o-ring. The flange is shown in Figure 3.8. There is a BNC feedthrough centered on the flange for mounting the detectors. Four high voltage feedthroughs are available for any necessary high voltage connections. The Galileo FTD-2003 channel plate detector requires two high voltage feedthroughs and the Becton Dickinson MM-1-1SG electron multiplier requires three.

1. Galileo FTD-2003

A microchannel plate (MCP) is a lead glass substrate containing many channels that are coated with a secondary emissive material. An MCP consists of up to 10⁷ channels that operate independently as electron multipliers. Primary ions or electrons that strike the wall of a channel will form 1 or more secondary electrons. A bias voltage up to 1000 volts across the channel will form a cascade of secondary electrons, multiplying the primary ion or electron current up to 10⁴. The schematic diagram of the voltage divider used for this detector is shown in Figure 3.9.

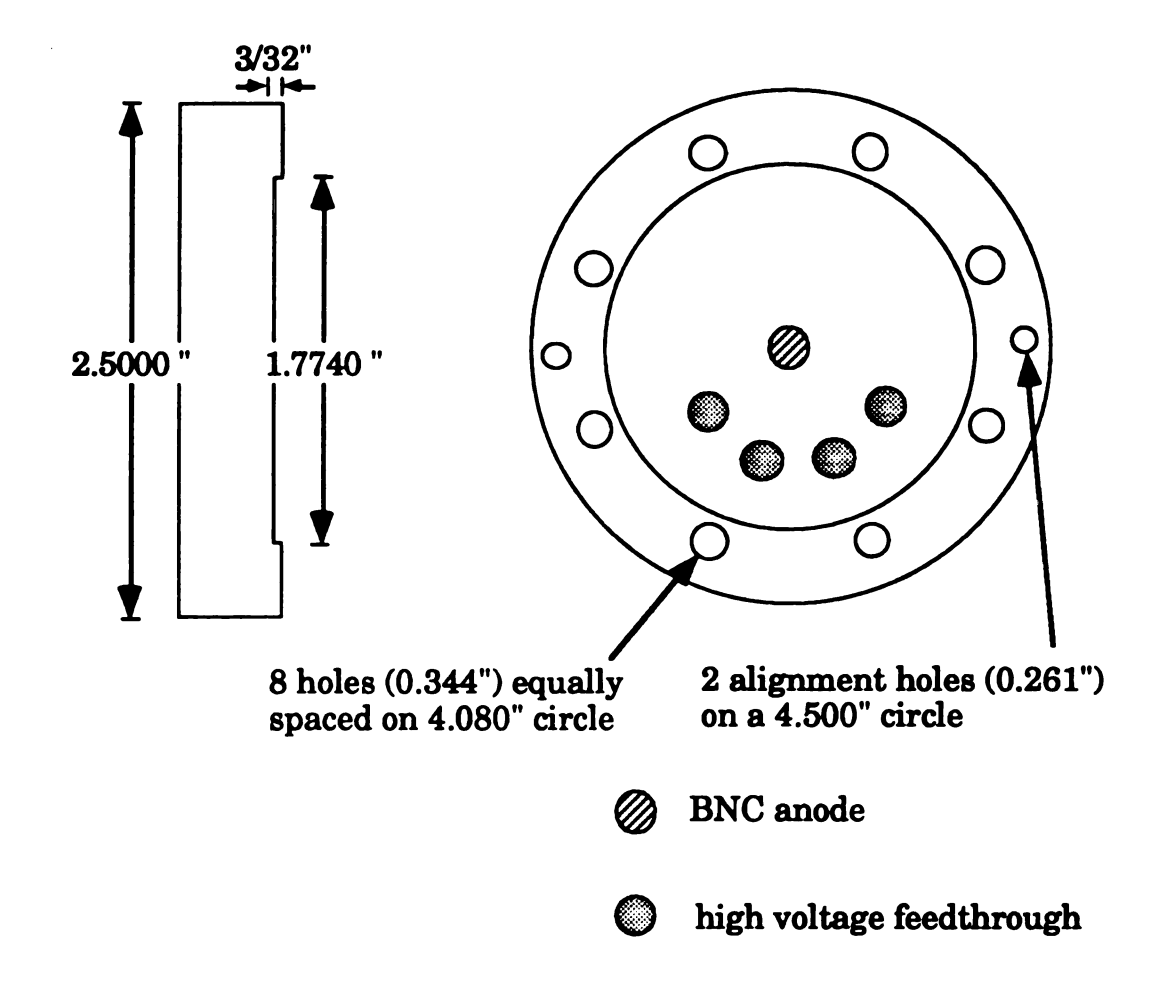


Figure 3.8 Galileo FTD-2003 and Johnston MM-1 detector mounting flange for Bendix flight tube.

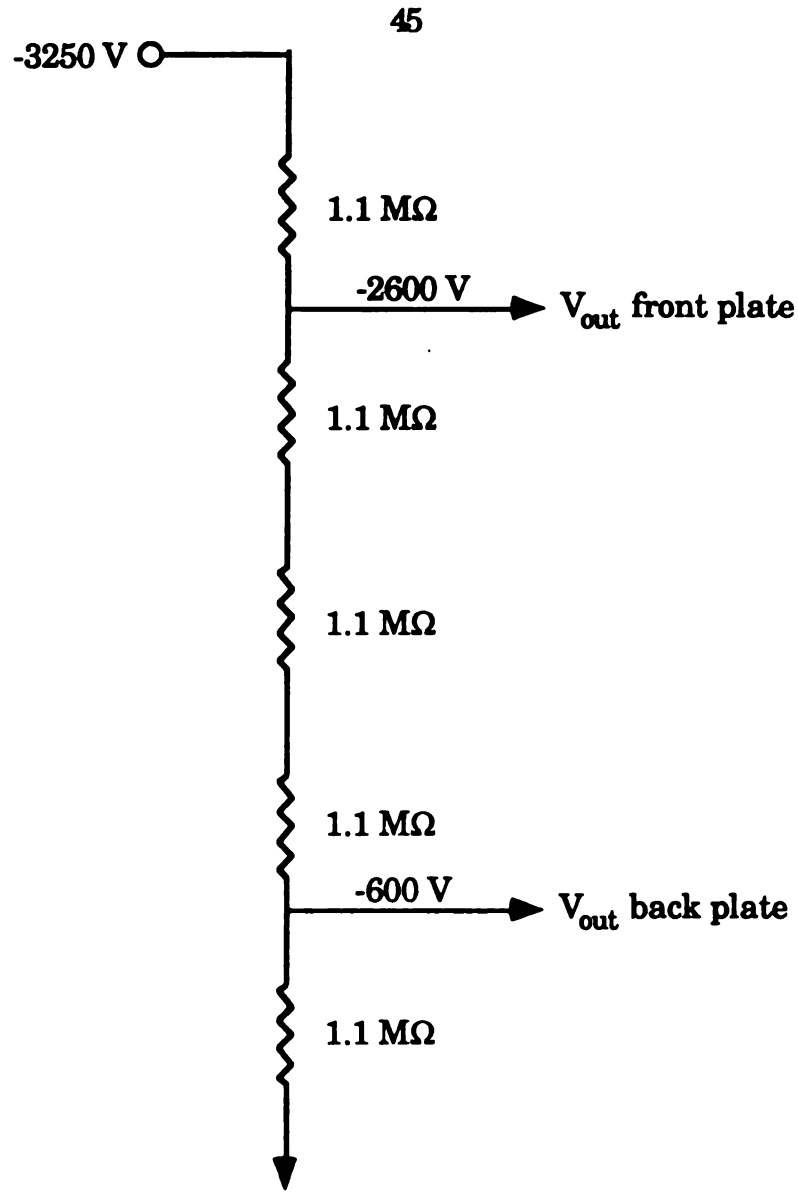


Figure 3.9 Voltage divider network for Galileo FTD-2003 channelplate detector.

The bias voltage is controlled by adjusting the input voltage at the top of the voltage divider. The channels are biased at an angle of 120 to minimize ion feedback through the channels of the MCP. The Galileo FTD-2003 detector consists of two MCPs in series providing a linear output current up to 10-7A. The output current of an MCP has a linear response to input

current provided that the output current does not exceed 10% of the bias current of the MCP. After a primary ion or electron strikes the wall of a channel and the cascade of secondary electrons leaves the channel, there is a "dead time" during which the channel will not respond to any incoming ions or electrons. This dead time can be related to the resistance and capacitance of each channel and is on the order of 20 ms. Since each channel operates independently, this does not limit the gain response of the MCP provided that a primary ion or electron does not strike a dead channel 20 ms after the previous one. The detection efficiencies for primary electrons and ions have been reported to be approximately the same⁵¹. For primary electrons and ions with energy ranging from 0.2-2 kV, the detection efficiencies ranges from 5-85%.

a. Standard multichannel plates

The standard MCP has a linear response of output current/input current of $10^{-7}A/10^{-11}A$. Typical bias currents are $10^{-6}A$ per MCP, which limits the linear response to output currents less than $10^{-7}A$. The dynamic range of a standard MCP is limited to 10^4 and drops off at output currents greater than $10^{-7}A$. The gain of the chevron assembly used in the Galileo FTD-2003 detector is 10^6 at the maximum operating voltage of 2000 V.

b. High output technology multichannel plates

The high output technology (HOT) MCP is of the same construction as a standard MCP, but constructed from a different lead formulation that can maintain output currents up to 60 times that of a standard MCP while providing a linear gain response. The HOT MCP has a linear response of output current/input current of 10-4A/10-8A. The dynamic range is the same as the standard MCP, but has a linear response up to 10-4A of output current.

2. Becton Dickinson MM-1-1SG electron multiplier

This electron multiplier is a 20-stage Be-Cu dynode assembly available from Becton Dickinson Diagnostic Instrument Systems, 7 Loveton Circle, Sparks, MD 21152. A wire mesh is located in front of the first dynode to deflect the primary ions towards the secondary emissive surface to increase detection efficiency. Each stage has a resistance of $1M\Omega$ making a combined resistance of $20M\Omega$ for the stack. The maximum voltage for the stack is 5000V (250V/stage) with a typical operating voltage of 3000V. The electron detection efficiency is reported at greater than 90% at 200eV, while the ion detection efficiency is greater than 90% at 3000eV. The ion detection efficiency decreases as the mass-to-charge ratio of the primary ion increases while it is higher at greater ion energies. A typical gain response has a linear output from 10^3 (at 1.5kV) to 10^9 (at 3.5kV).

The gain of the discrete dynode electron multipliers decreases over time due to operation at high output currents or contamination. The lifetime of the detector can be extended by increasing the voltage applied to the stack up to 5000V. The detector can be reactivated to recover the original gain characteristics of the detector when new as guaranteed by the manufacturer.

E. Detector Slit Assembly

The detector slit assembly (Figure 3.10) is positioned 4 1/2" from the end of the flight tube. This positions the slit assembly 1/2" in front of the detector. It is machined from aluminum and designed to fill the entire cross section of the flight tube to prevent stray ions and neutrals from striking the detector surface. The assembly is held in position by 4 thumb screws. A set of adjustable slits centered on the assembly allows a range of slit widths from 0 to 1/2 inch. The assembly also was designed to hold the Allison-group beam visualizer⁵² for ion beam visualization.

F. Preamplifiers

Both the Comlinear and the "in-house" preamplifiers were powered with a ±15 V power supply @ 200 mA (SOLA Electric, Elk Grove, IL 66007 cat. no. 84-15-02120-E).

1. Comlinear

The preamp used for most of this work is the Comlinear E220 I BNC 50 50 30 preamplifier, Comlinear Corporation, 4800 Wheaton Dr., Fort Collins, CO 80525, (303)-226-0500. This preamplifier converts the input ion current to a voltage, inverts the signal to produce a positive voltage, and provides a gain of 30. This device provides control of the d.c. offset voltage of the output signal with an adjustable resistor. The offset voltage of the A/D converter of the ITR requires the input d.c. voltage to be set near -250 mV. The exact

value varies from day-to-day and is dependent on preamp and ITR warmup time. The preamp and ITR require approximately 1 hour to warm-up.

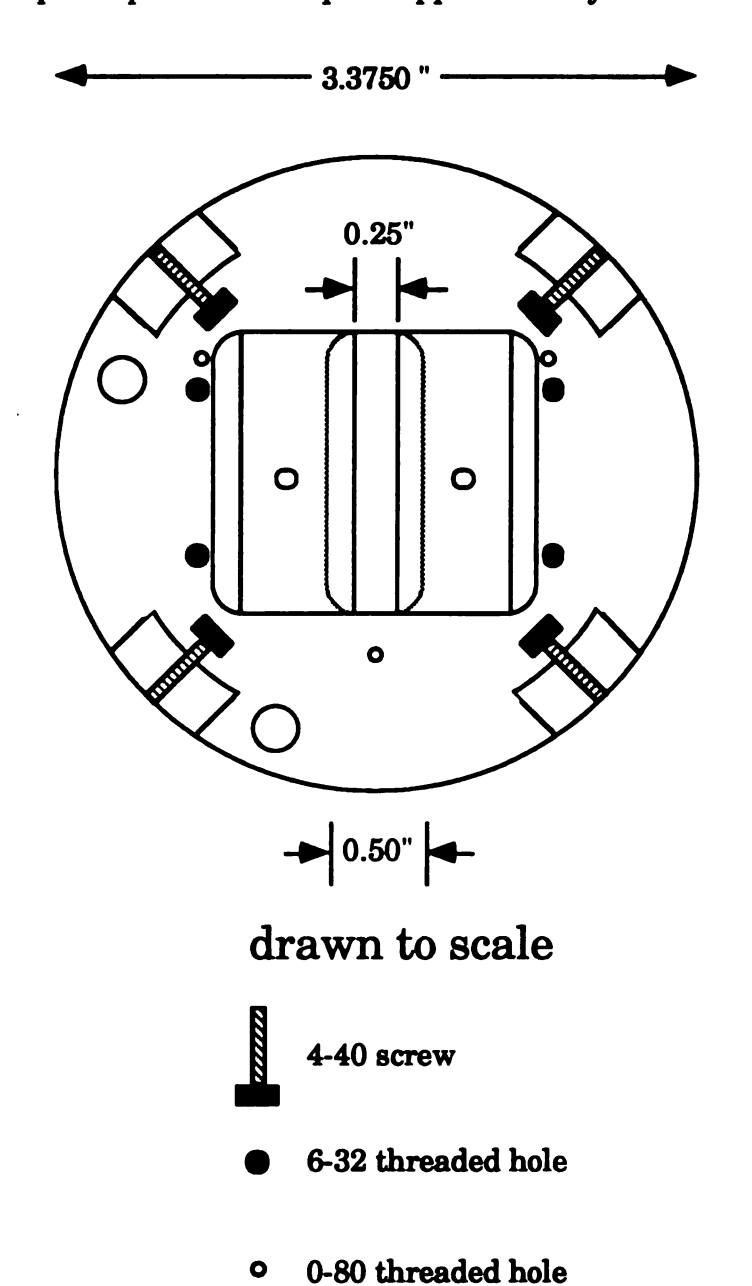


Figure 3.10 Detector slit assembly for Bendix flight tube. Provides for adjustable ion beam widths up to 0.50". This assembly also contains necessary holes and mounting threads for the Allison-group beam visualizer.

2. "in-house"

An "in-house" preamplifier was designed and constructed based on the Comlinear CLC404 wideband, high-slew rate, monolithic operational amplifier. A schematic diagram of the circuit layout is shown in Figure 3.11. This preamp was designed to invert the input signal and provide a gain of 81. Control of the output d.c. offset voltage also was provided with this circuit to interface to the ITR.

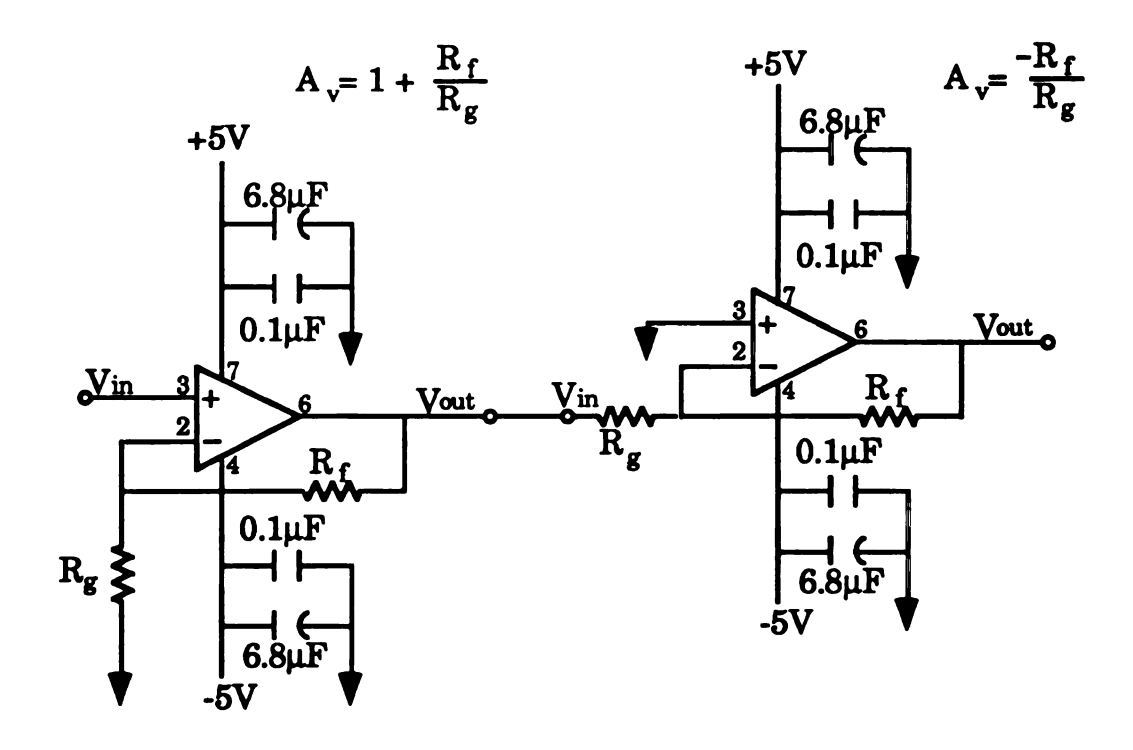


Figure 3.11 Electronic circuit diagram for "in-house" preamplifier built around two CLC404 high-slew rate operational amplifiers. $R_f = 501 \Omega$ and $R_g = 47 \Omega$.

G. Ion Focus Assembly

The ion focus assembly is a set of horizontal and vertical steering plates and an einzel lens located at the midpoint of the flight tube. These "steering plates" are used to deflect the ion packets toward the detector. The voltage divider designed for the ion focus assembly is shown in Figure 3.12. The 2000 V is supplied by a Ferranti Venus LR-2 200-2000VDC © 10mA d.c. to d.c. converter, Ferranti International 399 Smith Street, Farmingdale, N.Y. 11735. The voltages go through the beam deflection assembly circuit box that mounts on a flange located on the T-tube of the flight tube. The pin numbering of the T-tube flange is given in Figure 3.13 and listed in Table 3.3. There is a 5-pin Molex pin connector located inside the flight tube for the ion focus assembly that allows a quick disconnect to the ion focus assembly when removal of the T-tube is necessary. The pin numbering for the 5-pin Molex connector is given in Figure 3.14.

Table 3.3 Pin numbering on T-tube flange of flight tube for beam defection assembly and ion focusing assembly.

Table 3.3			
pin number	electrical connection		
8	vertical steering plate (top)		
9	vertical steering plate (bottom)		
10	horizontal steering plate (left)		
11	horizontal steering plate (right)		
12	ion lens		
16	beam deflection pulse (63 to 0V)		
18	beam deflection pulse (0 to 63V)		

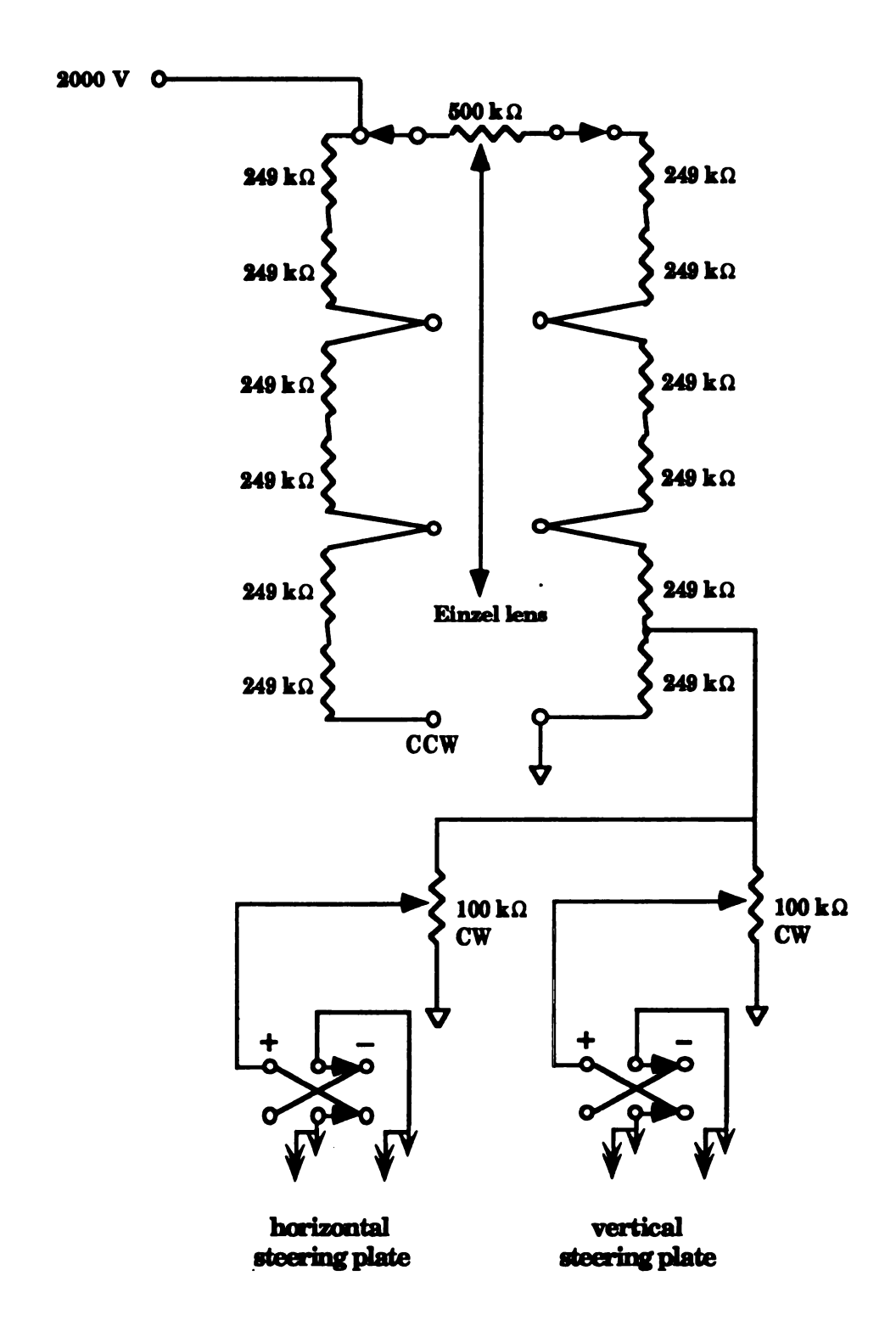


Figure 3.12 Electronic circuit diagram for ion focus assembly.

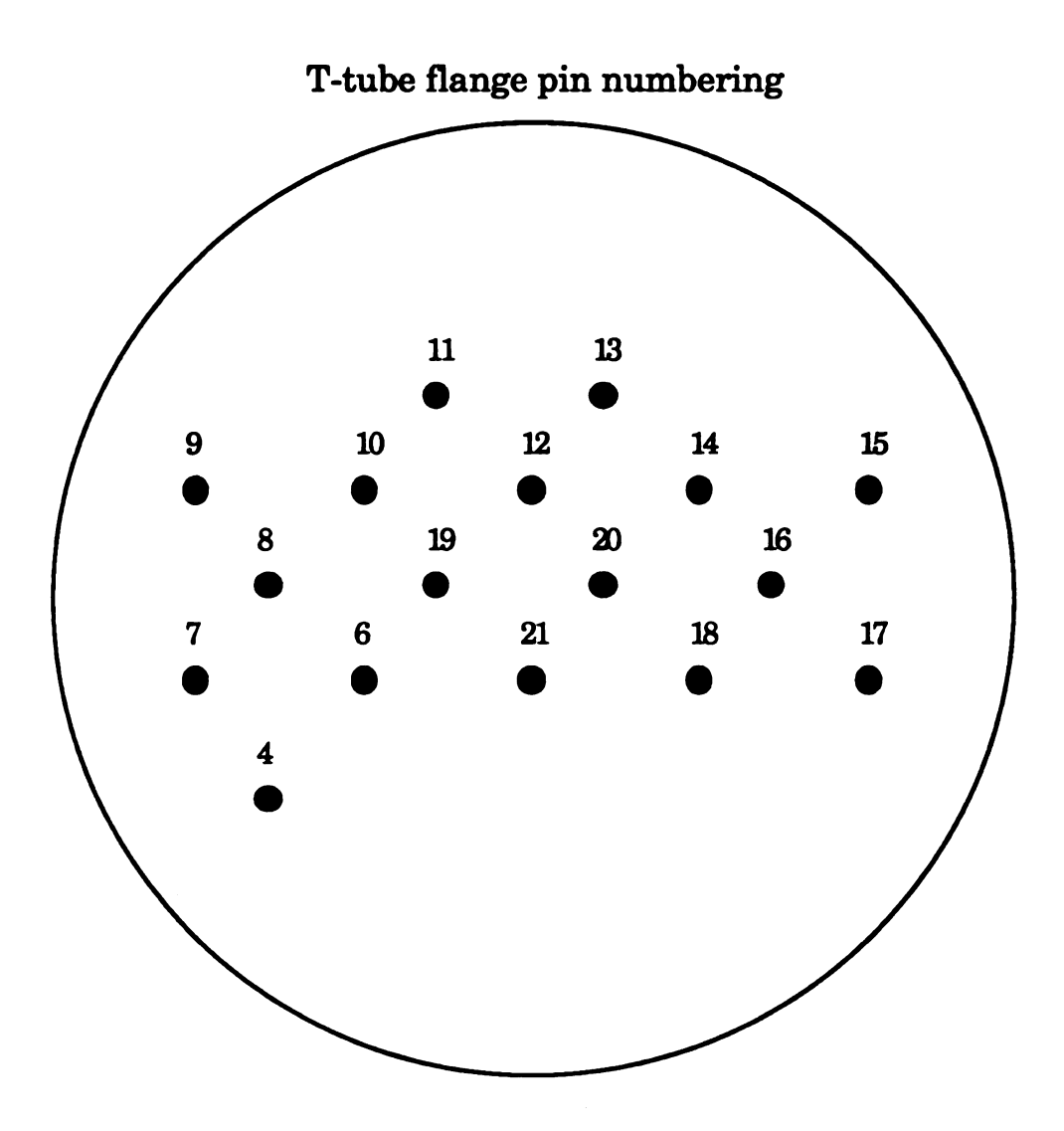


Figure 3.13 T-tube flange showing pin numbers. Table 3.1 contains a list of the electrical connections to this flange.

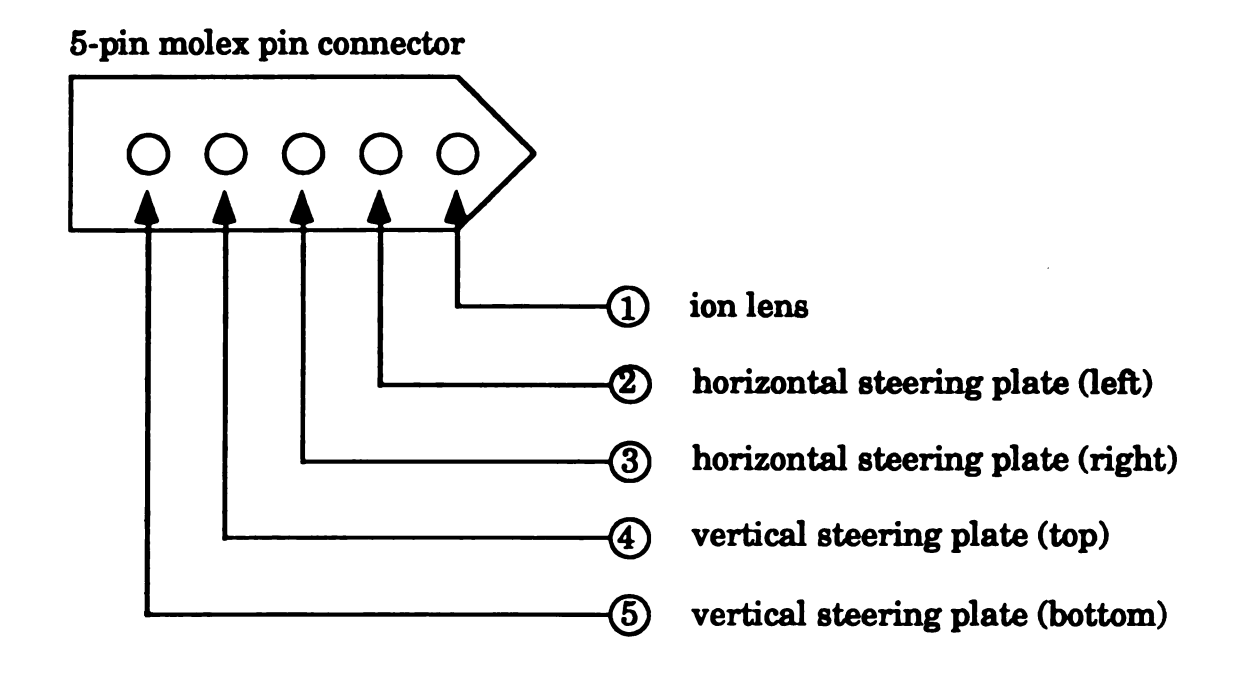


Figure 3.14 Five-pin Molex pin connector for quick disconnects to flight tube steering plates and ion lens.

H. Vacuum System

The exit slit of the ion source serves as a limiting aperture for this instrument that operates as a differentially-pumped mass spectrometer. This allows high pressure ionization techniques in the ion source while still maintaining flight tube pressures in the low 10-6 torr range. The ion source is pumped by a National Research Corporation model M0012 diffusion pump backed by an Alcatel roughing pump. The flight tube is pumped by a Varian model VHS-4 diffusion pump backed by an Alcatel roughing pump. A gate valve (K.J. Lesker model VR9-LP68) is located

between each diffusion pump and the mass spectrometer. The gate valves are air actuated, and are opened and closed by powering a Humphries solenoid (model 062-4E1-36). For mass spectrometer safety, the power to the solenoids is wired such that the gate valves will close due to power failure or pressure surges.

Improvements in the vacuum system of the BEDER-TOF were necessary before operation of the mass spectrometer could take place. The base pressure of the ion source and flight tube was in the 10-5 torr range when this project was begun. Many of the vacuum seals on the DuPont 21-491B ion source housing and electric sector were gold or silver wire gasket seals. These seals were leaking due to cross scratches on the flange surfaces on which the wire gasket seals were to be seated. These scratches provided channels through which air leaks were possible. The scratches were removed from each flange by hand sanding the flange surfaces with No. 220 sand paper to remove the major scratches; eventually, minor scratches were removed with polishing paper. Sanding motion was in a circular motion around the flange so that any fine scratches that remained would be concentric with the wire gasket seals thus minimizing the potential for further leaks.

The original adapter flange used to mate the Dupont electric sector to the Bendix flight tube was machined from aluminum and designed to use wire gasket seals. This particular area of the mass spectrometer was also a major source of vacuum leaks due to the high amount of stress placed on it by the design of the mass spectrometer frame supporting the source and flight tube. This piece was redesigned out of stainless steel and designed to use either wire gasket seals or rubber o-rings. The adapter flange was

designed to first mate to the source end of the mass spectrometer with either a wire gasket or an o-ring. The o-ring was used due to its greater tolerance during the process of connecting each half of the mass spectrometer. After the entire source assembly is connected to the support frame, the source and flight tube are connected by rolling the source frame up to the flight tube and adjusting the height of the source frame with the height adjustable table.

Further improvements in the vacuum system were made by redesigning the roughing lines between the rough pumps and the diffusion pumps. The roughing line on the flight tube was constructed from 1" o.d. copper tubing. A separate roughing pump was connected to the direct probe interface during the K+IDS experiments.

I. Integrating Transient Recorder

A brief description of the ITR is given here. For more descriptive information concerning the ITR, refer to reference 5. The ITR is a data collection system that digitizes data at 5 nsec resolution. This is accomplished with a 200-MHz flash analog-to-digital converter. The digitized data are passed to 16 high speed ECL (emitter coupled logic) summer cards where transients are summed to form a mass spectral scan. The integrated scans are passed across a VME bus to three Motorola 68020 parallel processors whereby time/mass calibration, and/or conversion to reconstructed mass chromatograms and/or real-time conversion to mass, intensity pairs occurs. The processed scans are written to a 300-Mbyte Priam disk drive. Each transient can be up to 80 µsec in duration (or

16,000 data points). The BDTOF mass spectrometer generates 5000 transient mass spectra each second.

J. Comparison of BEDER-TOF and BDTOF Mass Spectrometers

The design goals for the TOF project were to develop a TOF mass spectrometer that could provide sufficient mass resolving power over the entire m/z range of a typical GC/MS experiment. Commercially available GC/MS instruments have upper mass limits in the range of 650 to 800 u. Successful implementation of beam deflection in TOF-MS would require that the mass resolving power be better than unit mass resolution up to some m/z value in this mass range.

Perfluorotributylamine (PFTBA) is a compound commonly used to calibrate the m/z axis (or time axis in TOF-MS) since it has a number of peaks in its mass spectrum over the mass range up to m/z 614 (the molecular ion). Figure 3.15 shows the mass spectrum of PFTBA using the BD-TOF mass spectrometer and TAD. The mass spectrum is the result of integrating 5000 mass spectral transients over 1 second. Also shown in this figure are the raw data points for m/z 69 and m/z 502 to show that each ion is in focus at the detector for each mass spectral transient. This is a requirement to take full advantage of the capabilities of the ITR. Figure 3.15 demonstrates that the beam deflection method implemented on the BD-TOF mass spectrometer provides focussed mass spectral transients to the ITR over the mass range of most GC/MS applications.

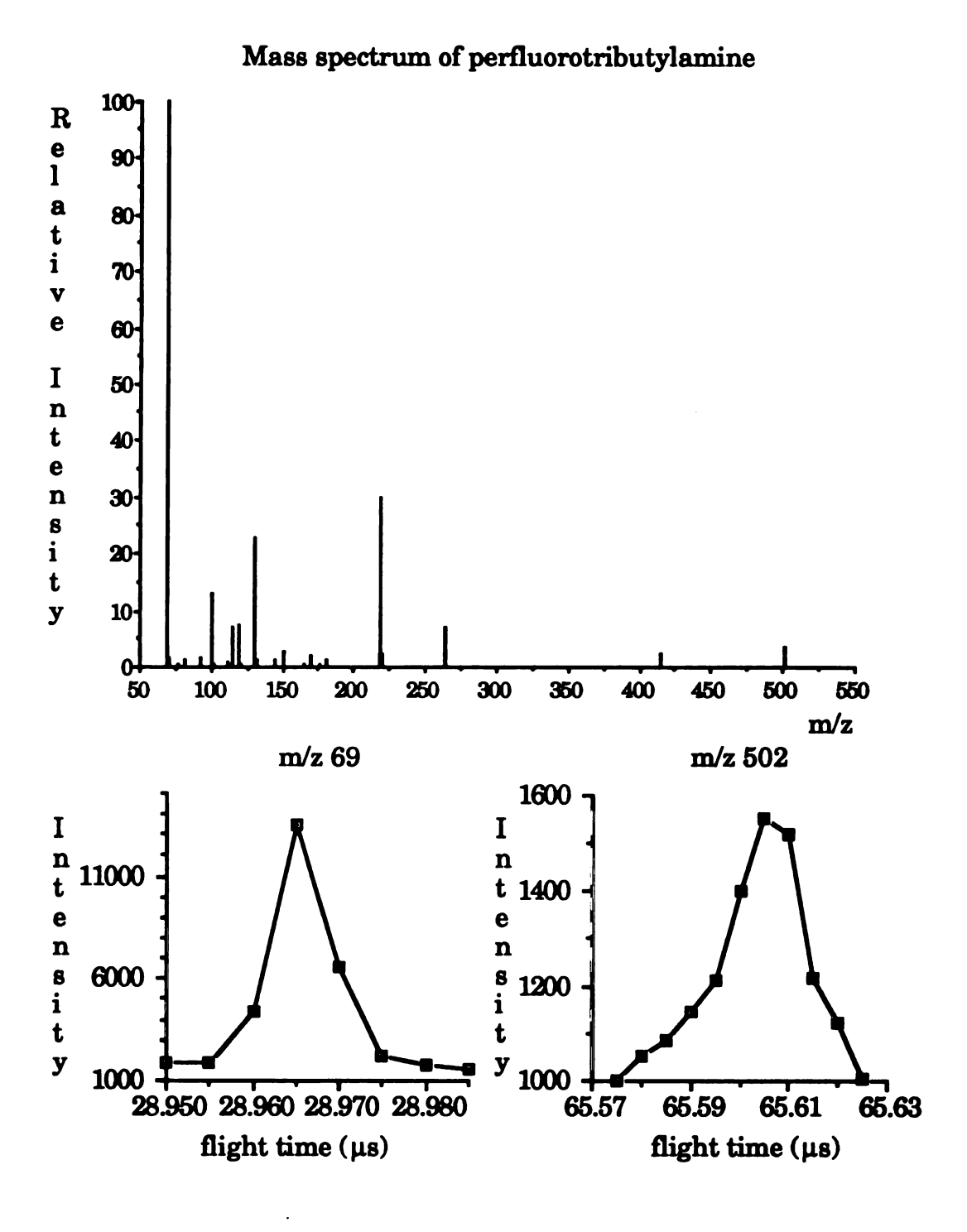


Figure 3.15 Mass spectrum of perfluorotributylamine obtained on the BDTOF mass spectrometer. Also shown are the raw data points for the peaks at m/z 69 and at m/z 502.

A comparison of the mass resolving power of the BD-TOF and BEDER-TOF mass spectrometers for each of the major ions in the mass spectrum of PFTBA is shown in Figure 3.16. The intensity of the peaks at m/z 502 and at m/z 614 are relatively weak and may result in an underestimate of the peak widths for these ions. The BD-TOF mass spectrometer provides better mass resolution without the use of an energy filter to minimize the energy distribution in the continuous ion beam than the BEDER-TOF mass spectrometer. An advantage to operating the mass spectrometer without the electric sector is the higher ion transmission efficiency, which improves the sensitivity of the mass spectrometer.

A plot of baseline peak widths vs $\sqrt{m/z}$ for the major ions in the mass spectrum of PFTBA in Figure 3.15 yields a slope of 3.7 x 10^{-9} s x $\sqrt{m/z}$. This slope can be used to calculate the upper m/z value that will have unit mass resolution (50% valley definition) using beam deflection. The peak width at half its maximum height can be approximated by one-half of the slope and setting it equal to Δt in the following equation:

$$\Delta t = \frac{L}{\sqrt{2eV}} (\sqrt{m/z + 1} - \sqrt{m/z})$$

Using L = 2.1m, V = 3000V, and $\Delta t = 1.85 \times 10^{-9} \text{s} \times \sqrt{\text{m/z}}$. An upper m/z value of 749 u is calculated to be resolved by this beam deflection method.

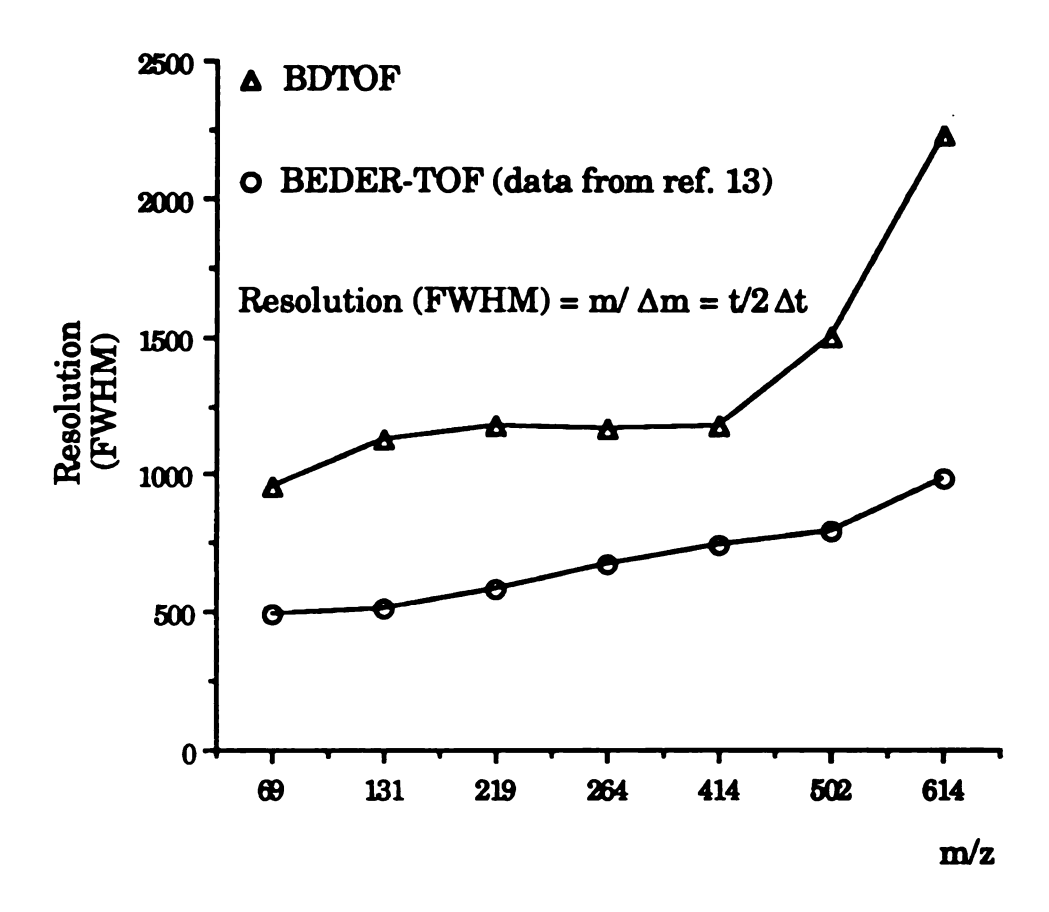


Figure 3.16 Comparison of mass resolving power of the BEDER-TOF and BDTOF mass spectrometers for the major ions in the mass spectrum of perfluorotributylamine. The resolution is based upon Δm (or its equivalent, $2\Delta t$) being the full width of the peak at half its maximum height (FWHM). The BEDER-TOF data are from reference 13.

Chapter 4 - Gas Chromatography/Beam Deflection Time-Of-Flight Mass Spectrometry

This chapter discusses developments in the area of GC/MS using the BDTOF mass spectrometer. Two examples are shown using highresolution capillary column gas chromatography. The first is an analysis of a simple 12-component mixture with a region of the RTIC chromatogram having unresolved chromatographic profiles for three of the components. The analysis of this sample mixture was performed at mass spectral acquisition rates of 1 and 20 mass spectra/second to show the advantages of higher mass spectral acquisition rates on representing the chromatography available and providing mass spectral data even for compounds that are represented by unresolved peaks in the chromatographic profile. The second example is the analysis of the TMSderivatized urinary organic acids in a normal urine sample. This example further demonstrates the advantages of acquiring the mass spectral data base at higher rates by comparison of the RTIC chromatograms and data available from mass spectral acquisition rates of 1 and 10 mass spectra/second to that available from a gas chromatograph using a flame ionization detector.

A. Grob programmed test mixture

1. Experimental

The gas chromatograph used is a Hitachi 663-30, fitted with an 18-m (DB-1, 0.18 mm i.d.) capillary column. The ion source and ion source housing from a double-focusing mass spectrometer, a DuPont 21-491B, is used to provide a continuous, narrow, focussed beam of ions produced by EI. Ions formed in the ion source are accelerated to a kinetic energy of approximately 3000 eV. Transient mass spectra are generated at a rate of 5.000 sec⁻¹.

A 12-component programmed test mixture was obtained from Supelco, Inc., Supelco Park, Bellefonte, PA 16823-0048, Cat. no. 4-7304. Table 4.1 lists the components and their concentrations in methylene chloride. A 1.0-µl injection of this mixture, split at 10:1 ratio, delivered approximately 50 ng/component to the column. A temperature program of 120°C - 200 °C at 20°C/min was used. The direct interface was maintained at a temperature of 250°C. The GC interface was direct, with all of the effluent from the gas chromatograph passing into the mass spectrometer ionization chamber.

Table 4.1 Components in methylene chloride for the Grob programmed test mixture in the order of elution.

Table 4.1					
Component	Conc.	Component	Conc.		
2,3-Butanediol	0.53 μg/μl	2,6-Dimethylaniline	0.32 μg/μl		
Decane	0.28 μg/μl	2-Ethylhexanoic acid	0.38 μg/μl		
1-Octanol	0.36 μg/μl	C10 acid methyl ester	0.42 μg/μl		
Nonanal	0.40 μg/μl	C11 acid methyl ester	0.42 μg/μl		
2,6-Dimethylphenol	0.32 μg/μl	Dicyclohexylamine	0.31 μg/μl		
Undecane	0.29 μg/μl	C12 acid methyl ester	0.41 μg/μl		

2. Reconstructed Total Ion Current Chromatograms

a. Comparison of 1 and 20 scans/second

Figure 4.1 shows the reconstructed total ion current (RTIC) chromatogram available with a mass spectrum acquisition rate of 1 mass spectrum/second of a standard test mixture⁵³ analyzed using the GC/BDTOF mass spectrometer/ITR. Several questions must be addressed concerning the results in Figure 4.1. Does the RTIC chromatogram generated from the data base acquired at 1 mass spectrum/second adequately represent the chromatography? Also, it was known that the mixture contained 12 components, but only 10 peaks are shown in the RTIC. The portion of the chromatogram containing the solvent peak and 2,3 butanediol is not shown here (Figure 4.1), so there should be 11 components represented by the RTIC chromatogram. To answer these questions, another aliquot of the test mixture was analyzed by the GC/BDTOF mass spectrometer/ITR, summing every 250 transient mass spectra, thereby generating 20 mass spectra/second. The RTIC chromatogram, resulting from the 20 mass spectra/second data base at approximately 2.5 minutes into the run, is shown in Figure 4.2a; the corresponding segment of the RTIC in Figure 4.1 between the vertical arrows, obtained from the 1 mass spectrum/second data base is shown for comparison. There are two obvious advantages to the faster mass spectral acquisition rate that can be seen upon comparing the RTIC chromatograms in Figure 4.2a. The 20 mass spectra/second data base offers 20 points/second to reconstruct the chromatographic profile more accurately in terms of peak shapes, relative heights, and relative areas. This feature of the data provides better quantitation of the components in

the mixture. The other advantage is that the RTIC chromatogram available from higher mass spectral acquisition rates more accurately represents the true chromatographic profile. It is obvious from the RTIC chromatogram generated from the data base acquired at 20 mass spectra/second, presented in Figure 4.2a, that this region of the chromatogram contains three components.

b. Deconvolution of closely eluting components

A common method of "resolving" chromatographically-unresolved components in a GC/MS analysis is to plot the intensity at an m/z value unique to each unresolved component versus scan number, generating mass chromatograms for each ion. Mass chromatograms suggest which scans would contain mass spectral information for particular components, allowing for qualitative and quantitative information to be obtained, even for overlapping components. The success of this approach depends on the mass spectral acquisition rate of the mass spectrometer and the identification of unique ions for each component. For example, a sufficient number of mass spectra must be acquired during elution of a chromatographic doublet for the mass spectral data base to be adequately time-resolved for identifying and deconvoluting overlapping components. The result of mass spectral interpretation is only as good as the quality of the mass spectra, which can be compromised due to skewing of relative peak intensities by scanning mass spectrometers, or due to spectral interferences from co-eluting components. Because the BDTOF mass spectrometer/ITR can generate many unskewed mass spectra each second,

mass spectral quality is superior and interferences are easier to identify and remove.

The high mass spectral acquisition rate allows the presence of three components to be recognized in this unresolved region of the RTIC chromatogram in Figure 4.2b. Can the three components be identified from the mass spectral data base even though the components coeluted? Because the components in the test mixture are known, as well as the type of column used for analysis, we were able to determine which components were expected to be in this region of the chromatogram. One of the expected components is 2,6-dimethylphenol. Instead of searching through the 200 mass spectra that contain mass spectral data for a match of the data to a library mass spectrum of this compound, we can display the mass chromatogram of one of the dominant ions in the mass spectrum of 2,6-The library mass spectrum of 2,6-dimethylphenol dimethylphenol. indicates that the molecular ion is represented by the base peak at m/z 122. Figure 4.2b shows the mass chromatogram of m/z 122 and identifies the middle component as 2,6-dimethylphenol. Another component expected to be in this region of the RTIC chromatogram is undecane; the alkyl cation C₄H₉+, m/z 57, was selected as a designate ion for this hydrocarbon. The mass chromatogram at m/z 57 displayed in Figure 4.2b shows that the mass spectra of both of the other two components contain this alkyl cation.

The mass chromatograms at m/z 57 and 122 available from the data base acquired at 20 mass spectra/second provide information on the chromatographic peak shapes of the three components and can be used to identify scans from which mass spectra for the three components can be obtained. By choosing a mass spectrum that does not contain peaks at both

m/z 122 and m/z 57, one can obtain a pure mass spectrum for each of the three components represented here. A visual inspection of the mass chromatograms represented in Figure 4.2b shows a region (scans 190-200) where the ion current at m/z 57 is minimal. Because the mass spectra of the other two components have an intense peak at m/z 57, this is a region of the data base that should provide a reasonably pure mass spectrum of the middle component. The mass spectrum contained in scan 192 is shown in Figure 4.3a and is identified as that of 2,6-dimethylphenol. A similar procedure was used to obtain pure mass spectra of the other two components by choosing mass spectra that do not contain ion current at m/z 122. Ion current at m/z 122 is observed in scans 160-232. Figure 4.3b shows the mass spectrum in scan 159, which is identical with the library spectrum of nonanal. Figure 4.3c shows the mass spectrum in scan 240, which is identical with that of undecane.

c. Limits of Detection

The detection limit of the GC/BDTOF mass spectrometer/ITR at a mass spectral acquisition rate of 20 mass spectra/second was compared to that of the JEOL JMS-AX505H MS system, which is a commercially available double-focussing sector mass spectrometer routinely used for GC-MS analyses. The fastest scan rate available with the JEOL mass spectrometer, 0.9 seconds/decade (e.g., m/z 50-500), which generates 1.1 scans/second, was used for the comparison.

Complete mass spectra were collected during the analysis of the standard test mixture at various concentrations at the mass spectral acquisition rate described above for each mass spectrometer. Mass

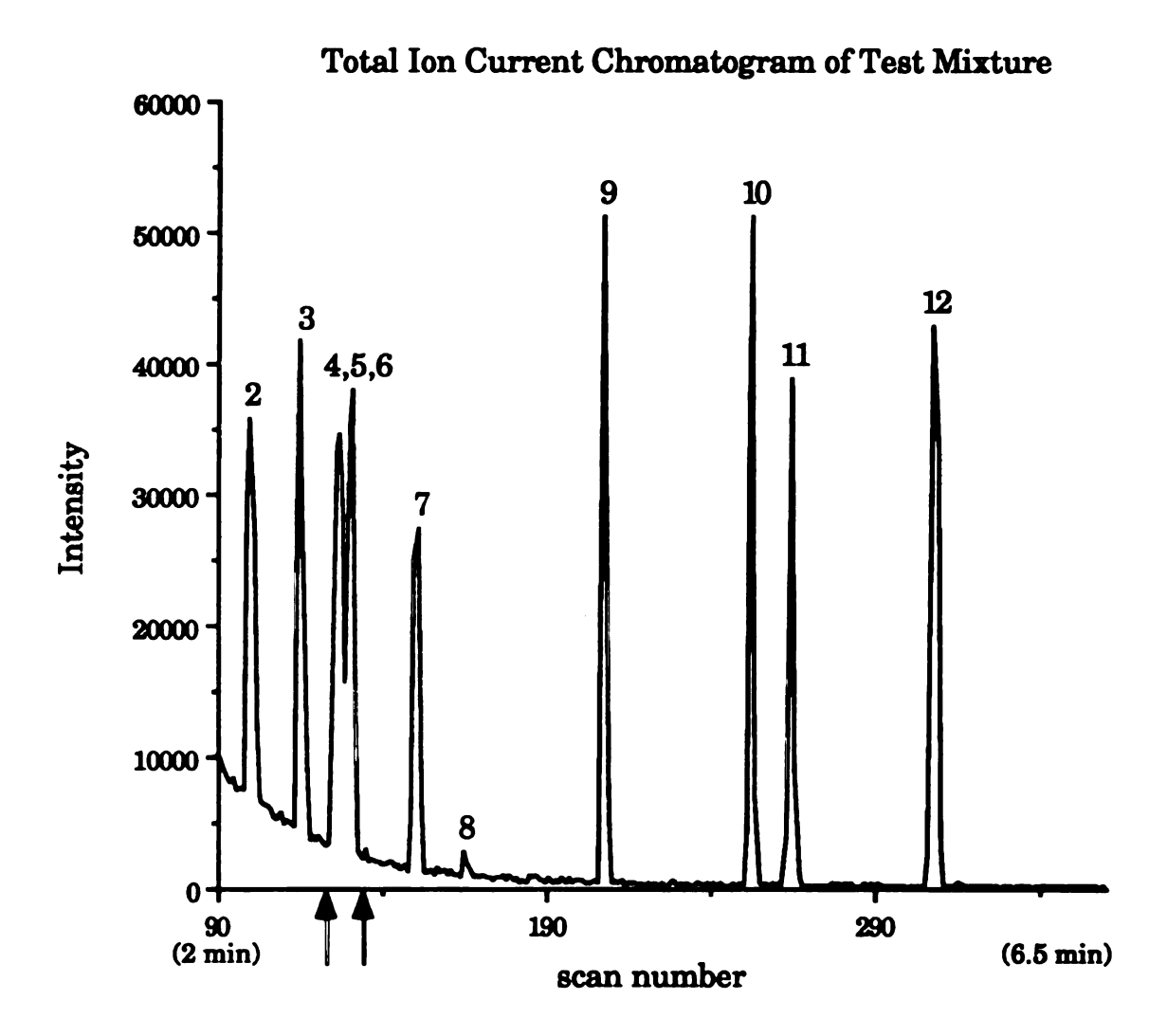


Figure 4.1 Reconstructed TIC chromatogram generated from the data base acquired at 1 scan/second of standard Grob test mixture.

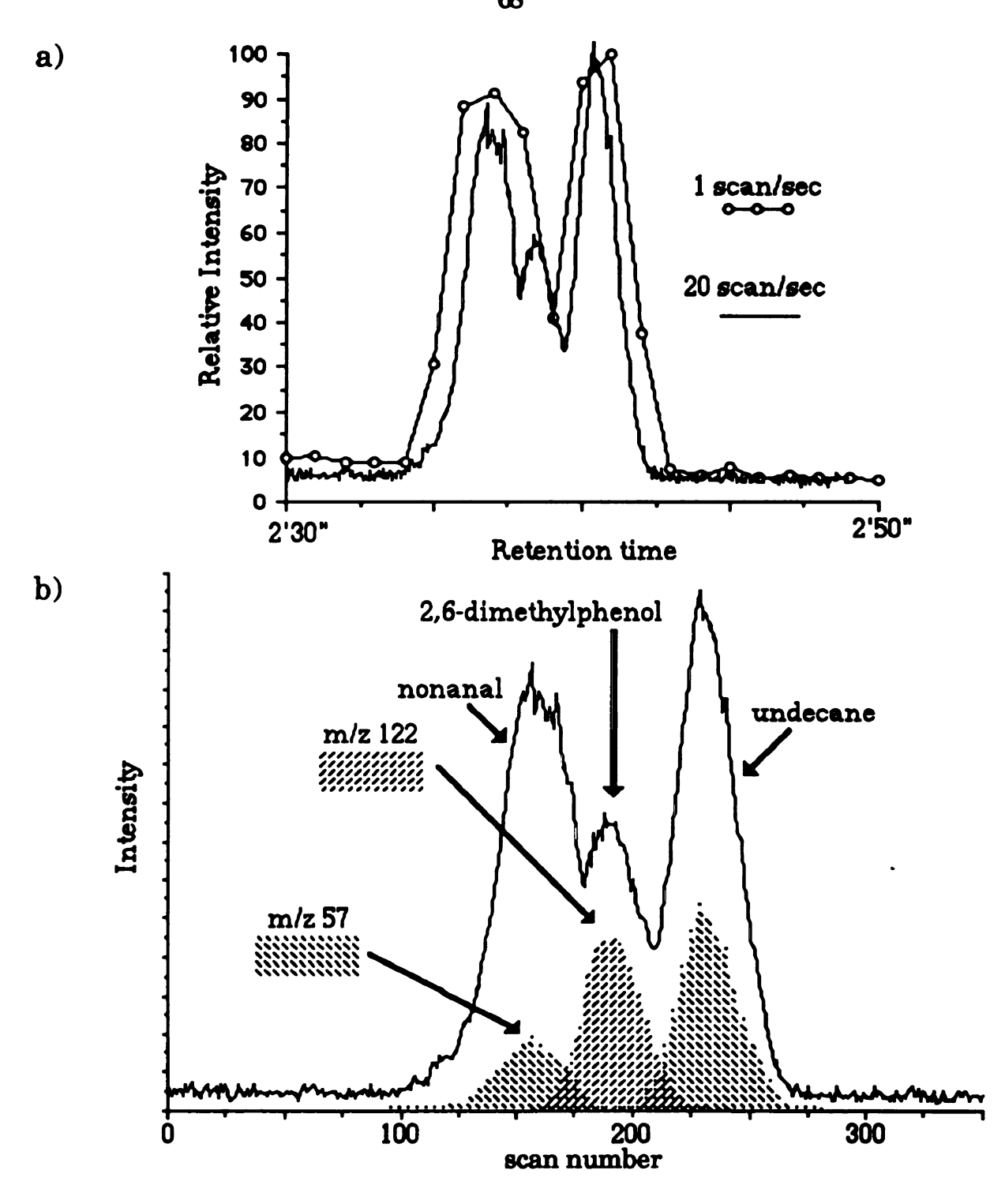


Figure 4.2 a) Comparison of RTIC chromatograms reconstructed from the data bases acquired at 1 and 20 mass spectra/second over the region of the chromatogram between the arrows in Figure 4.1. b) RTIC chromatogram is shown along with the mass chromatograms of m/z 57 and m/z 122 available from the 20 mass spectra/second data base.

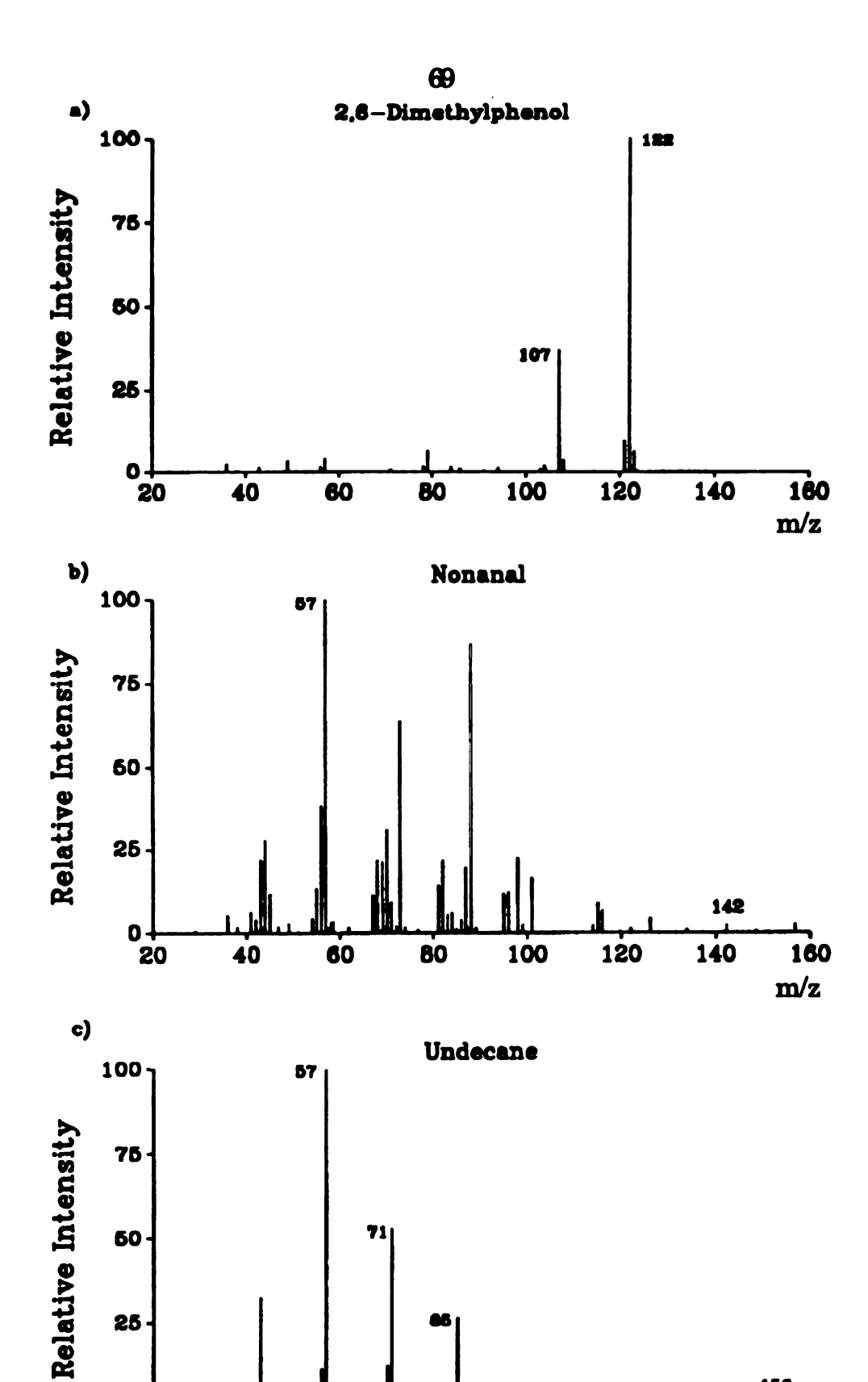


Figure 4.3 Mass spectrum in scan a) 192, b) 159, and c) 240.

m/z

chromatograms were reconstructed from the corresponding data bases. The area of the peak in the mass chromatogram at m/z 122 (corresponding to the mass spectrum of 2,6-dimethylphenol) was plotted versus the amount of analyte injected. The limit of detection was calculated using the method of regression analysis on each data set. The y-intercept of each regression line was used as an estimate of the blank signal, y_b . The signal, $y = y_b + 3s_b$, determines the limit of detection. The limit of detection calculated for both the scanning mass spectrometer and the GC/BDTOF mass spectrometer/TTR system was 0.6 ± 0.2 ng of 2,6-dimethylphenol.

B. Complex mixture analysis of TMS-derivatized organic acids of urine

1. Background

The results of analyses using the GC/BDTOF-MS/ITR system in the context of metabolic profiling of urinary organic acids is demonstrated. Metabolic profiling is an analytical method for quantitative and qualitative analysis of metabolites in complex mixtures extracted from physiological fluids such as urine or plasma⁵⁴. The metabolic profile, which is a chromatogram of the components of the mixture, portrays the relative amounts of these metabolites as derived from intermediary metabolism of proteins, carbohydrates, and lipids in the individual. The coupling of gas chromatography and mass spectrometry has played a crucial role in the development of methodologies for such analyses. The metabolic profile of urinary organic acids reflects metabolic status and allows for the identification of genetic disorders that perturb homeostasis. Improvements in metabolic profiling have been limited in the same way as have analyses

of other complex mixtures. Even with recent advances in capillary column technology, chromatographic resolution is not sufficient to separate every component in the mixture and, thus, some components in these complex mixtures may go undetected.

This example compares the results of the GC-only analysis of a urinary organic acid mixture using a flame ionization detector (FID) to those obtained by the GC/BDTOF mass spectrometer/ITR system at mass spectral acquisition rates of 1 and 10 mass spectra/second. The advantages of the higher mass spectral acquisition rates are demonstrated, both in terms of accurately representing the chromatographic profile and in providing a data base from which mass spectra can be obtained for closely-eluting components.

2. Experimental

The ion source was adapted from a JEOL DM303 mass spectrometer. The GC is a Hewlett Packard model 5790. The GC and BDTOF mass spectrometer are connected via a modified JEOL HX110 aluminum block interface, heated to 260°C. The detector is a Galileo FTD-2003 (Galileo Electro-Optics Corp., Sturbridge, MA) in which the standard multichannel plates (MCP) were replaced with high output technology (HOT) MCPs. The preamplifier was made "in-house". The urinary organic acid mixture was separated using a short capillary column, 6 m x 0.2 mm DB-5 (J&W Scientific), 0.4µm film thickness, using a column head pressure of 13 psig with helium as the carrier gas, splitless injection with an injector

temperature of 275°C, and a temperature program of 50°C to 325°C, at a rate of 20°C/min.

The urinary organic acid mixture also was analyzed on a Hewlett Packard model 5890 gas chromatograph with a flame ionization detector. The FID output was digitized by an HP 3392A printing integrator, with the peak width response set to 0.01 min, which digitizes the data at the highest sampling rate available (20-Hz).

The number of theoretical plates for the capillary column used for these analyses was determined on the GC/FID instrument. A two-component hydrocarbon mixture containing nonane and decane was analyzed isothermally at 120°C. The average value for the number of plates as determined by measurements on each of the two peaks was 51,000 plates.

The method of urinary organic acid extraction has been reported previously⁵⁵. The acidic metabolites isolated from 1 ml of a control urine sample were derivatized by mixing 25µl of pyridine and 100µl of bis(trimethylsilyl)-trifluoroacetamide/trimethylchlorosilane and heating at 80°C for 1 h. A 1.0-µl aliquot of the TMS-derivatized urinary organic acids was analyzed by GC/MS with mass spectral acquisition at 1 and 10 mass spectra/second, with the same column and GC conditions.

3. Chromatographic Profiles from the GC/FID and GC/BDTOF mass spectrometer/ITR

A comparison of the chromatograms obtained from analysis of a urinary organic acid mixture by GC-only with flame ionization detection

and by GC/MS with the reconstructed total ion current (RTIC) is shown in Figure 4.4. The RTIC chromatograms represent the analysis of the same quantity of this mixture and are generated from data acquired at 1 and 10 mass spectra/second on the GC/BDTOF mass spectrometer/ITR. A threeminute delay between injection of the mixture and data acquisition was used. The data base, obtained at 1 mass spectrum/second (providing only 1 RTIC point/second with which to reconstruct the chromatography), was generated by summing 5000 consecutive mass spectral transients, acquiring 600 mass spectra during the 10-minute analysis. Another data base, obtained at 10 mass spectra/second, was generated by summing 500 consecutive mass spectral transients, acquiring 6000 mass spectra during the 10-minute analysis. Table 4.2 lists several of the TMS-derivatized organic acids identified from data acquired at 10 mass spectra/second, with their retention times and relative amounts for each component. The components in the mixture were identified by comparison of retention times and mass spectra of each component to those in a reference library previously compiled in our laboratory using another GC/MS instrument.56 Components yet to be identified have been labeled as unknowns. Quantitation was achieved based on the area in the RTIC represented by 36 ng of the TMS-derivative of tropic acid (peak marked by an asterisk in Figure 4.4c) which was used as a coinjected internal standard.

The goal of any analysis by GC/MS is to obtain useful information for all of the components in a mixture represented by the RTIC chromatogram. Ideally, the RTIC chromatogram would provide an accurate representation of the chromatographic profile for retention times and quantitation of the components in the mixture. The data base from which the RTIC

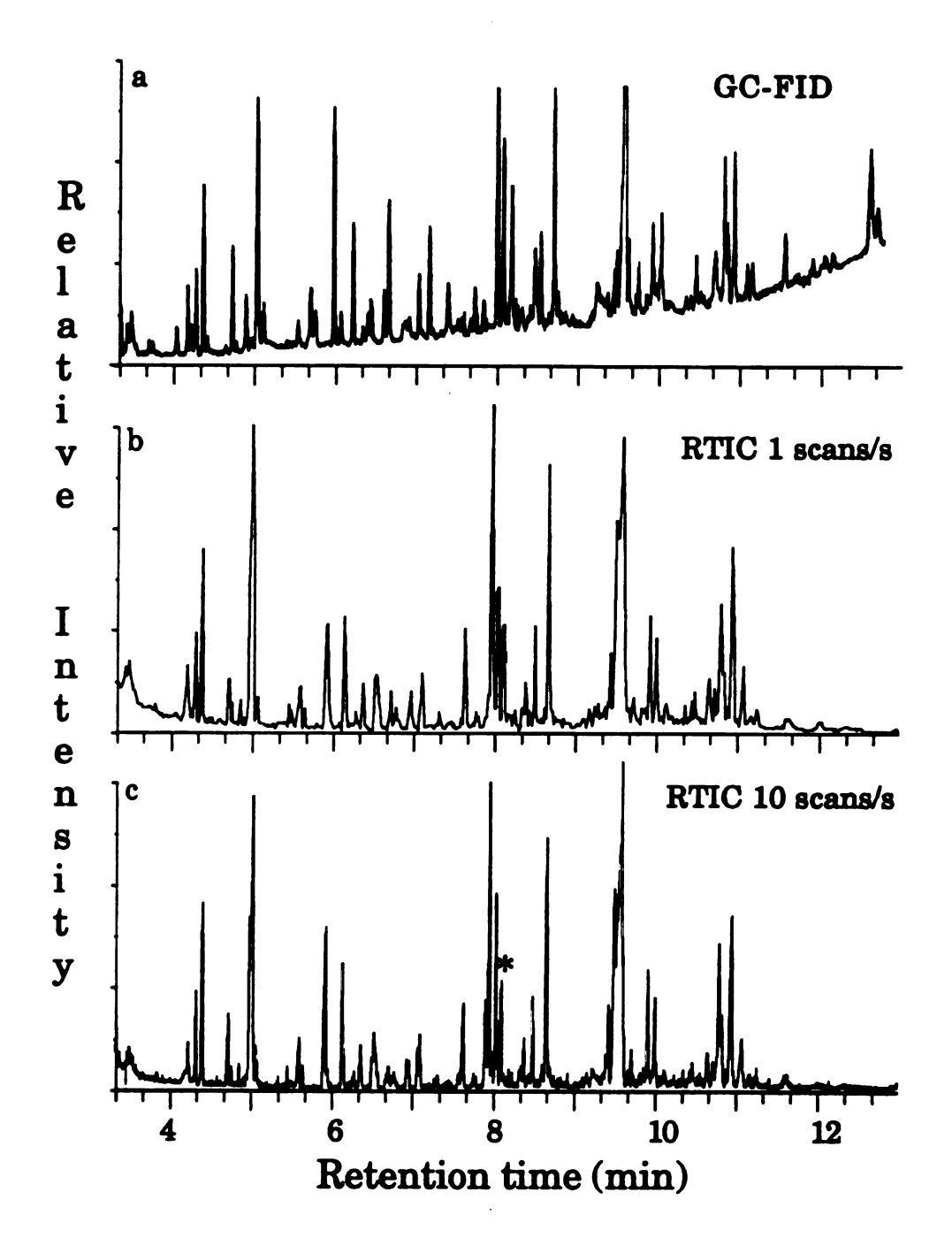


Figure 4.4 Complex mixture analysis of TMS-derivatized urinary organic acids. Comparison of a) GC-FID response to reconstructed total ion current chromatograms generated from mass spectral acquisition rates of b) 1 and c) 10 mass spectra/second.

chromatogram is generated should provide information to distinguish those components that are not fully resolved chromatographically. In capillary GC/MS, it is difficult to meet these criteria when mass spectra are generated at 1 mass spectrum/second or less. Mass spectral acquisition rates of 10 or more mass spectra/second are necessary to generate RTIC chromatograms that accurately represent the resolution achieved by the capillary GC column⁵⁷. The RTIC chromatogram in Figure 4.4c accurately represents the chromatographic peak shapes and areas as verified by comparison with the GC-FID chromatogram in Figure 4.4a.

Cram, et. al.,⁵⁸ have investigated the relationship between the number of data points required to represent the profile of a given chromatographic peak and the characteristic features of that peak shape as described by s, where s₂ is the variance that can be related to the mathematical function describing the profile. Mass spectral acquisition rates of 10 or more mass spectra/second are necessary to generate RTIC chromatograms that accurately represent the resolution achieved by the capillary GC column.⁵⁹ Based on the chromatographic peak widths for this analysis, the minimum number of data points that can accurately represent this profile is 10 mass spectra/second.

Selected segments of the complete RTIC chromatograms (shown in Figure 4.4) are shown in more detail in Figure 4.5. The RTIC chromatogram from the data base collected at 1 mass spectrum/second (Figure 4.5a) clearly does not accurately represent the chromatographic profile when compared to either the GC-FID chromatogram or the GC/BDTOF mass spectrometer/ITR RTIC chromatogram generated from

Table 4.2 TMS-derivatized urinary organic acids with a relative response greater than 2 μ g/mg creatinine.

Table 4.2. U	Table 4.2. Urinary Organic Acids in Mixture*,**					
Retention	scan	Acid	Relative			
time (min)	number	(or other compound)	Response			
$(\pm 0.002 min)$			μg/mg			
			creatinine			
4.328	798	lactic	27.0			
4.412	848	glycolic	59.7			
4.728	1038	oxalic	25.11			
4.767	1061	glyoxylic oxime	7.1			
4.863	1119	unknown	8.8			
4.928	1157	unknown	3.6			
4.988	1194	p-cresol	17.6			
5.035	1222	sulfuric	182			
5.080	1249	4-hydroxybutyric	14.4			
5.660	1477	3-OH-isovaleric	6.6			
5.775	1545	urea	9.4			
5.805	1564	unknown amino	18.8			
		acid				
5.853	1593	benzoic	7.2			
5.1137	1763	phosphoric	91.1			
5.1158	1776	unknown amino acid	7.4			
6.143	1887	succinic	31.7			
6.155	1894	tri-TMS-glycine	28.2			
6.285	1972	pyrocatechol	6.4			
6.365	2020	glyceric	13.4			
6.507	2105	4-deoxyerythronic	8.7			
6.542	2125	unknown amino acid	22.1			
6.560	2137	4-deoxythreonic	10.8			
6.708	2225	unknown	12.8			
6.958	2375	3-deoxytetronic	30.2			
7.092	2455	2-deoxytetronic	42.7			
7.432	2594	unknown	6.2			
7.642	2786	pyroglutamic	39.6			
7.768	2862	5-hydroxymethyl- 2-furoic	8.5			

Table 4.2 (continued)					
Retention	scan	Acid	Relative		
time (min)	number	(or other compound)	Response		
$(\pm 0.002 min)$		•	μg/mg		
			creatinine		
7.915	2950	erythronic (isomer)	46.6		
7.967	2981	erythronic	147		
7.998	3000	threonic (isomer)	11.8		
8.048	3030	threonic	89.2		
8.117	3071	internal std.	55.8		
0.111	60.1	tropic (36 ng)	50. 0		
8,208	3125	3-	3.5		
0.200	0	hydroxyphenylacetic	0.0		
8.358	3215	furan 2,5-	6.4		
		dicarboxylic			
8.393	3237	4-	15.1		
İ		hydroxyphenylacetic			
8.445	3267	2-aminoadipic	4.2		
8.502	3302	tartaric	37.6		
8.672	3404	2-deoxyribonic	116		
9.403	3843	arabinonic	32.6		
9.435	3862	ribonic	58.4		
9.565	3940	hippuric	297		
9.615	3970	citric	39.6		
9.720	4032	methylhydroxyphen	17.0		
		yl-hydracrylic			
9.922	4153	deoxyhexonic	49.9		
		lactone			
9.843	4106	glucono lactone	40.3		
10.357	4415	ascorbic	9.8		
10.657	4594	glucuronic	23.2		
10.803	4683	gluconic	81.0		
10.837	4703	gluconic	31.5		
10.953	4773	glucaric	111		
11.073	4845	galacturonic	39.3		

^{*} Quantitative results assuming identical ionization efficiencies for all compounds.

^{**} Table 4.2 contains information on compounds present at greater than 2.0 μ g/mg of creatinine.

the data base collected at 10 mass spectra/second (Figure 4.5b). Regions where there are two or more closely eluting components are represented by a single peak in the RTIC chromatogram in Figure 4.5a due to the small number of data points available with which to reconstruct the chromatographic peak profiles. For example, the segment marked "A" in Figure 4.5a suggests the presence of 3 components, while the data in Figure 4.5b clearly show that at least 5 components are eluting in this time period. Region "B" in Figure 4.5a may represent baseline noise; however, the data in Figure 4.5b show a chromatographic peak in that time window (see arrow). Similarly, region "C" becomes a chromatographic doublet (or possibly a triplet) when the mass spectral data base allows for adequate reconstruction of the chromatographic resolution (Figure 4.5b). If the RTIC chromatogram in Figure 4.5a were the only one available, an analyst would incorrectly interpret apparent "single peaks" as representing single components. However, the mass spectrum obtained by averaging the mass spectra across the peak, as is commonly done for data presumed to represent a single component, would be the sum of mass spectra from two or more components, thus making mass spectral interpretation difficult, if not impossible. Minor components in the mixture are also difficult to distinguish from the baseline in Figure 4.5a, again due to the insufficient number of data points (mass spectra) with which to reconstruct the chromatographic peak profiles.

4. Mass Spectral Deconvolution

An important difference between the RTIC chromatogram (Figure 4.4c) and the GC-FID chromatogram (Figure 4.4a) is that with the RTIC chromatogram additional dimensions of information are available in the mass spectral data base. The mass spectral data base can be used in two ways. Resolution of chromatographically-unresolved components is possible by plotting the ion current at specified m/z values versus scan number, generating a mass chromatogram.

One of the advantages of generating a mass spectral data base at 10 mass spectra/second rather than at 1 mass spectrum/second, is demonstrated in Figure 4.6. A portion of the RTIC chromatogram generated from the data base collected at 1 mass spectrum/second shown in Figure 4.6a has one "peak" in the vicinity of scan 125 that appears to result from a single component in the mixture. The 5-second peak width might be interpreted as resulting from overloading the column, and the scans 123 to 128 of the RTIC chromatogram, would be averaged and the resulting mass spectrum (mis)interpreted. In comparing Figure 4.6a to Figure 4.6b (reconstructed from the data base collected at 10 mass spectra/second), it is apparent that more than one component is eluting during this time period.

Differential comparison of adjacent mass spectra collected during a GC peak may help to discern the number of components present. For example, Figures 4.7a and 4.7b are the mass spectra in scans 1197 and 1220, respectively, from the region of the RTIC chromatogram in Figure 4.6b. The mass spectrum in Figure 4.7a has a number of peaks not observed in Figure 4.7b; the most obvious are at m/z 165 and m/z 180.

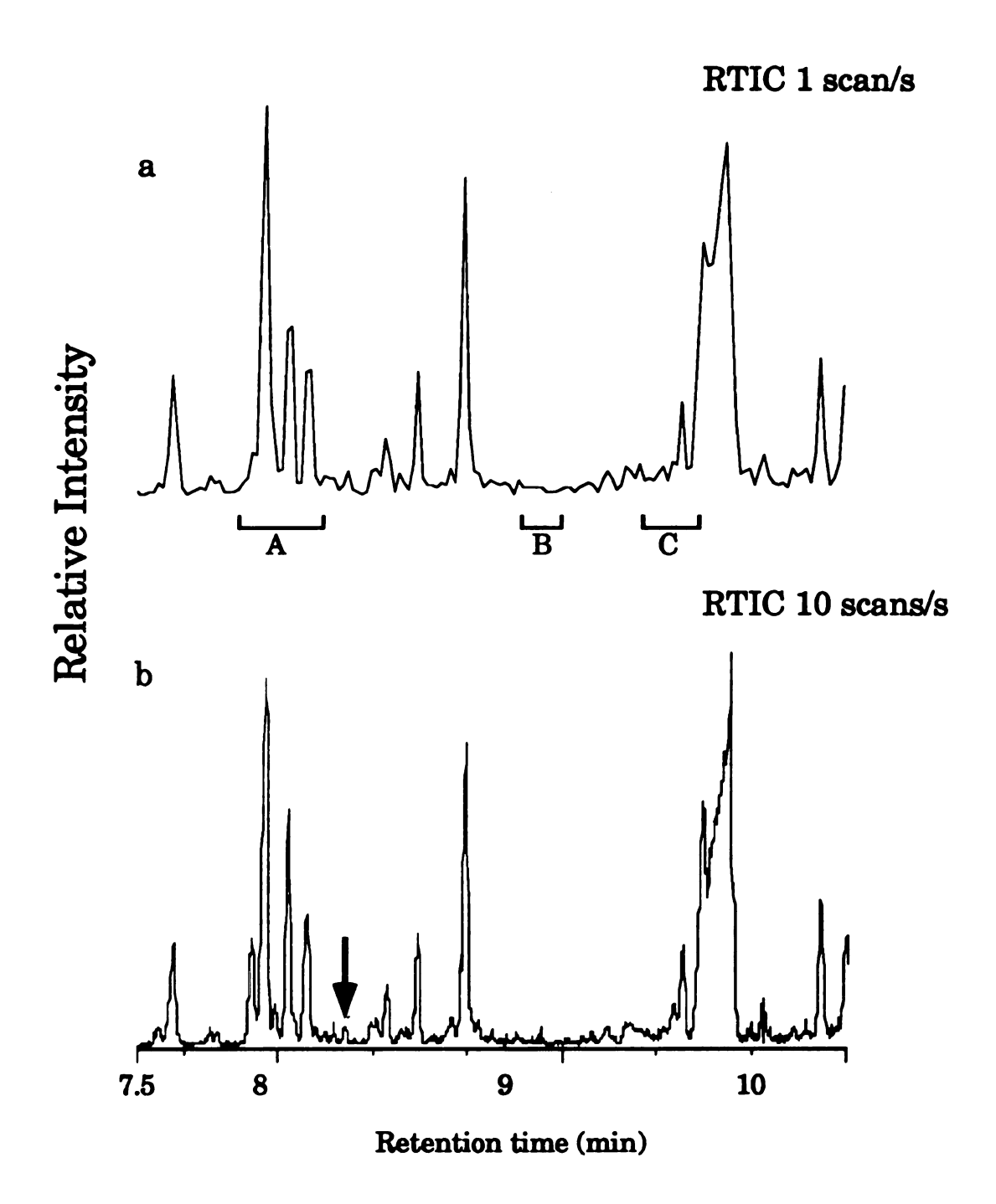


Figure 4.5 Selected region of RTIC chromatogram generated from mass spectral acquisition rates of a) 1 and b) 10 mass spectra/second showing improved representation of chromatographic profile at a higher mass spectral acquisition rate.

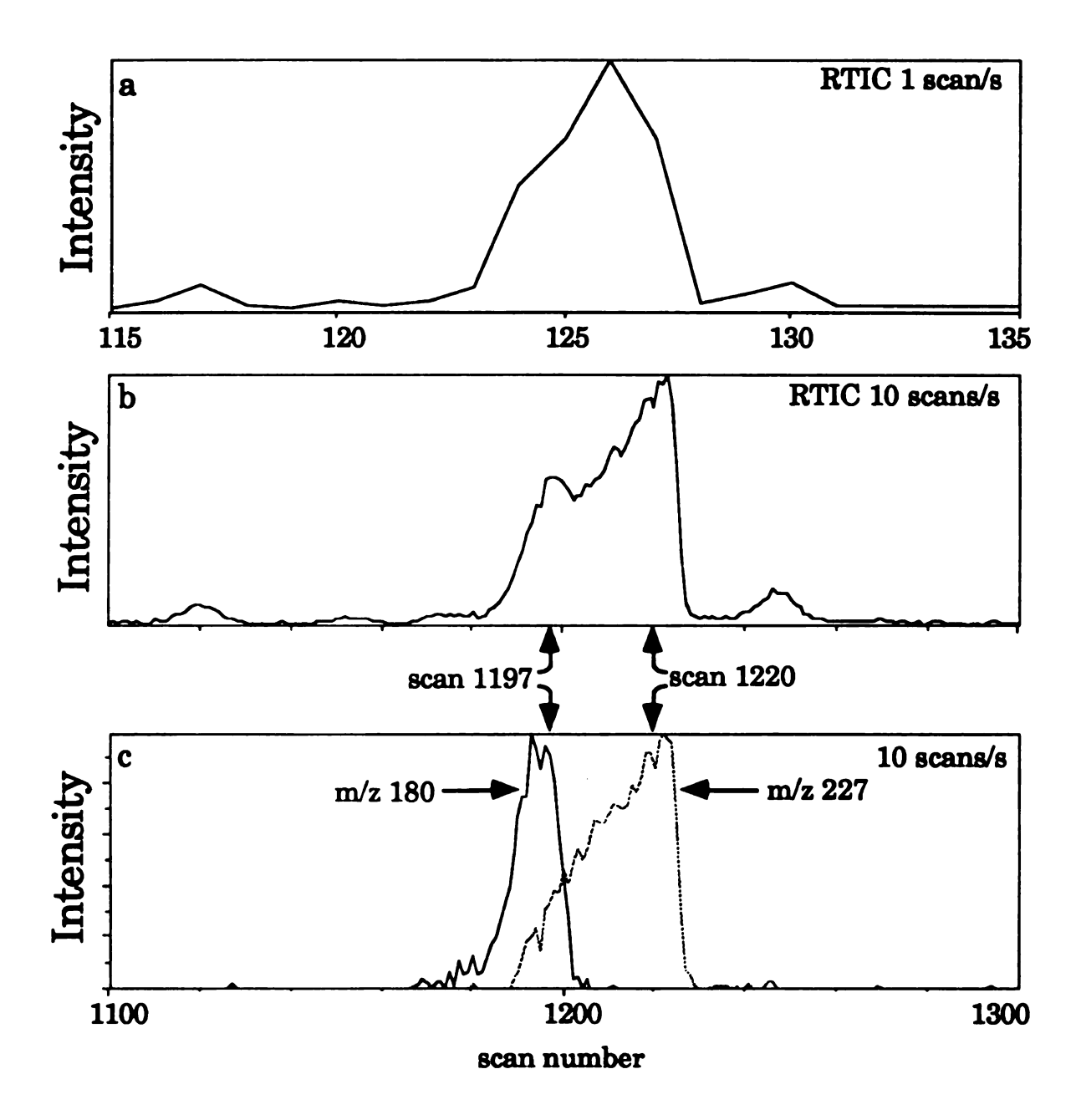


Figure 4.6 Comparison of RTIC chromatograms at mass spectral acquisition rates of a) 1 and b) 10 mass spectra/second for a chromatographic doublet. c) mass chromatograms at m/z 180 and at m/z 227 identifying two components.

Other peaks, such as those at m/z 73, m/z 147, and m/z 227 are found in both mass spectra. Because there are peaks that are not found in both scans, one can assume that there is more than one component represented by the peak in the RTIC chromatogram in Figure 4.6b. The relative intensity at m/z 147 and m/z 227 in Figures 4.7a and 4.7b remains constant, which indicates that both mass spectral peaks represent the same component. Also, the mass chromatograms at each of these m/z values correlate with each other. By plotting the signal intensities at m/z 180 and m/z 227 versus scan number, the elution profiles of the two components can be resolved, and these individual profiles realized (Figure 4.6c).

Mass spectra can be obtained after identification of a unique ion for each component. Ion current at m/z 180 is observed in scans 1180 to 1203. Thus, the data in Figure 4.6c show that the mass spectrum in scan 1220 is representative of the second component with no mass spectral interferences from the first, and can be interpreted as such. The mass spectrum in scan 1197 contains mass spectral data from both of the components. A mass spectrum representative of the first component can be obtained by mass spectral subtraction. By subtracting the peak intensities at m/z values representative of the second component found in scan 1220 from those in scan 1197, a mass spectrum for the first component will result. The base peak in scans 1197 and 1220 is at m/z 147, which represents only the second component. The ion current at m/z 147 in scan 1220 is 34,384 arbitrary units (AU) and 14,704 AU in scan 1197. Subtracting 43% ((14,704 AU/34,384 AU) x 100%) of the ion currents at all of the peaks in scan 1220 from those peaks in scan 1197 will remove all of the ion current indicative of the second component, leaving only peaks indicative of the first component.

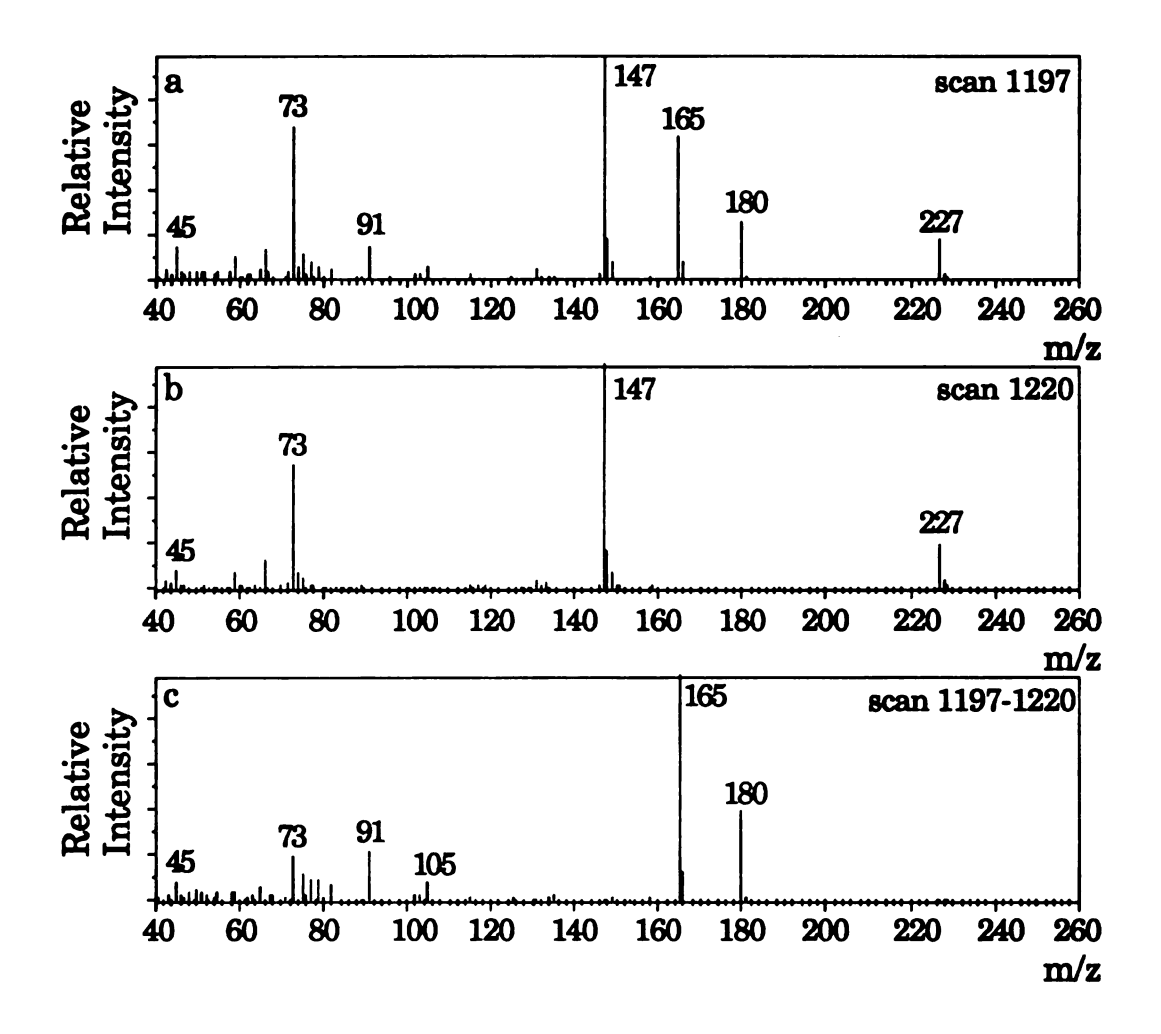


Figure 4.7 Figure 4.7a shows the mass spectrum in scan 1197 that has mass spectral information for both of the components eluting over the peak profile shown in Figure 4.6c. Figure 4.7b shows the mass spectrum in scan 1220. The mass spectrum shown in Figure 4.7c is the result of subtracting 43 % of the ion currents in scan 1220 from the corresponding ones in scan 1197.

The mass spectrum resulting from this mass spectral subtraction is shown in Figure 4.7c. This powerful operation is only possible with unskewed mass spectra, such as those obtained by TOF-MS.

The first component represented in the RTIC segment in Figure 4.6c has been identified as the TMS-derivative of p-cresol. The molecular ion, M+·, is represented by the peak at m/z 180; the characteristic ion, (M-15)+, due to the loss of a methyl group from the trimethylsilyl group, is represented by the peak at m/z 165. The second component has been identified as the bis-TMS-derivative of sulfuric acid. The molecular weight of this compound is 242 u, and the mass spectrum shows a peak at m/z 227 for the characteristic ion corresponding to (M-15)+.

Another example is illustrated in Figure 4.8a, which exemplifies the situation commonly encountered where two components elute so closely that neither a conventional chromatogram nor the RTIC chromatogram generated from a data base acquired at 10 scans/second shows clear evidence for the presence of two components. The data in Figure 4.8 represents the 10-second portion of the chromatogram from 6.05 min to 6.22 min. The peak profile in Figure 4.8a gives no indication that there is more than a single component eluting from the capillary column. However, the mass spectra found in scans 1551, 1555, and 1557, as shown in Figures 4.9a-c, show that more than one component could be eluting in this time window, based on the fact that the relative intensities at m/z 189 and m/z 210 do not rise and fall together. Confirmation of this assumption is provided by plotting mass chromatograms for each of these m/z values as

shown in Figure 4.8b, and noting that the maxima of the peaks in the two profiles occur at different times.

Mass spectra for each of the two components represented in Figure 4.8b can be obtained from the mass spectral data base. Referring to Figure 4.8b, scans 1540 to 1550 only contain mass spectral data for the first component. These scans were averaged to provide the mass spectrum shown in Figure 4.9d. A mass spectrum for the second component in the RTIC peak can be obtained by averaging the mass spectra in scans 1560 to 1570, shown in Figure 4.9e.

The first component represented by this peak profile has been identified as bis-TMS-urea. The ion current at m/z 189 represents the characteristic loss of a methyl group from the TMS ester of urea. The second component represented by this peak profile has yet to be identified. Based on its mass spectrum shown in Figure 4.9e, the molecular ion appears to be at m/z 225 with an intense ion at m/z 210 representing the loss of a methyl group. There is a peak at m/z 73 and at m/z 147 which represent one and two TMS groups, respectively. Since the molecular weight of this unknown is an odd mass, this compound has an odd number of nitrogens. The weight of two TMS groups (73 u per TMS group) is subtracted from the molecular weight determined by interpretation of the mass spectrum, the molecular weight of the unknown is 81 u (Note that each TMS group replaces a hydrogen so that the effective weight gain or loss for each TMS group is 72 u.). The odd molecular weight for this compound indicates one or three nitrogens. The most probable empirical formula for this molecular weight is C₅H₇N.

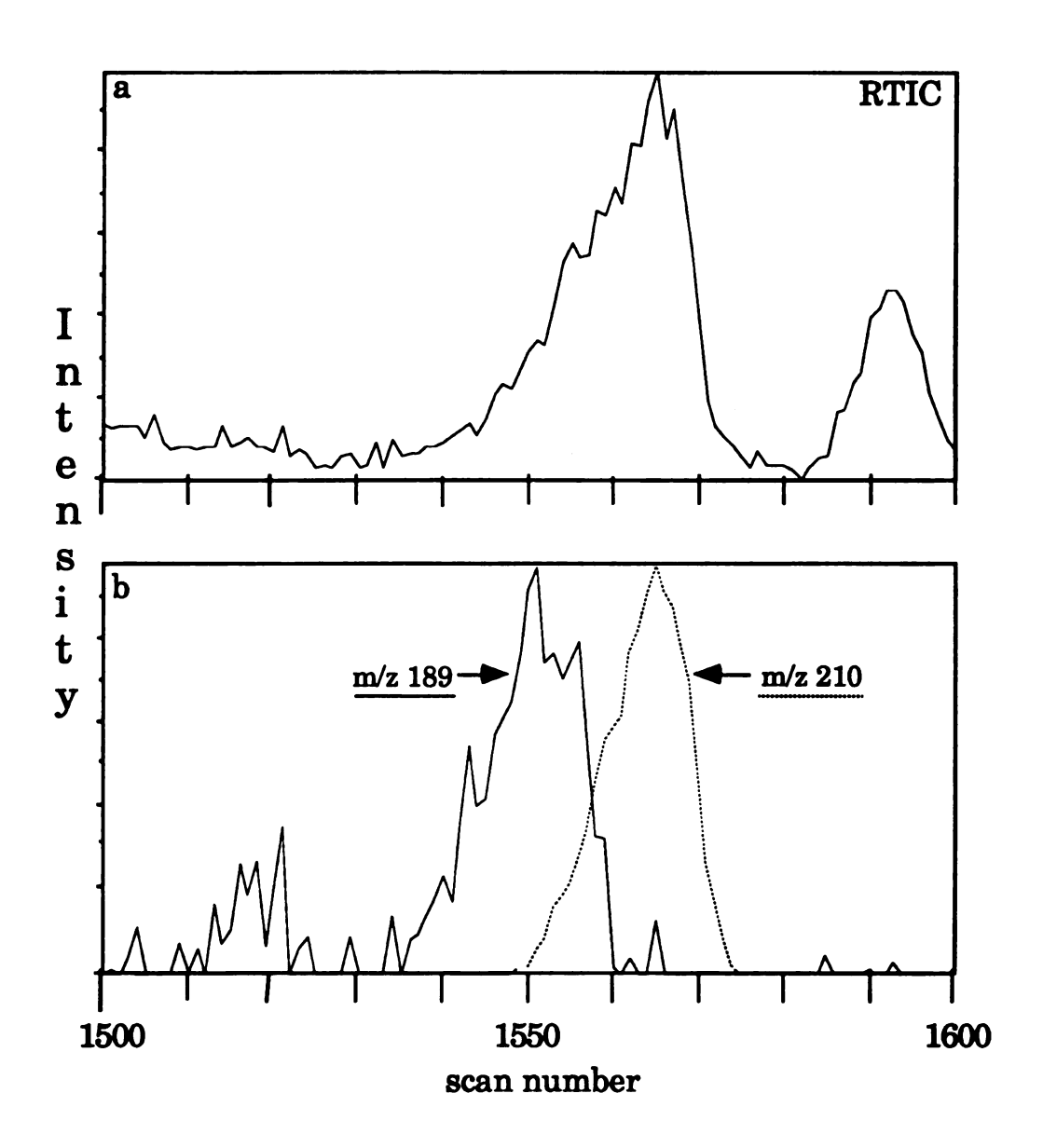


Figure 4.8 Figure 4.8a is a region of the RTIC chromatogram generated from the 10 scans/second data base. Figure 4.8b shows the mass chromatograms at m/z 189 (solid line) and at m/z 210 (broken line). The difference in the maxima of the two peaks indicates the presence of two components.

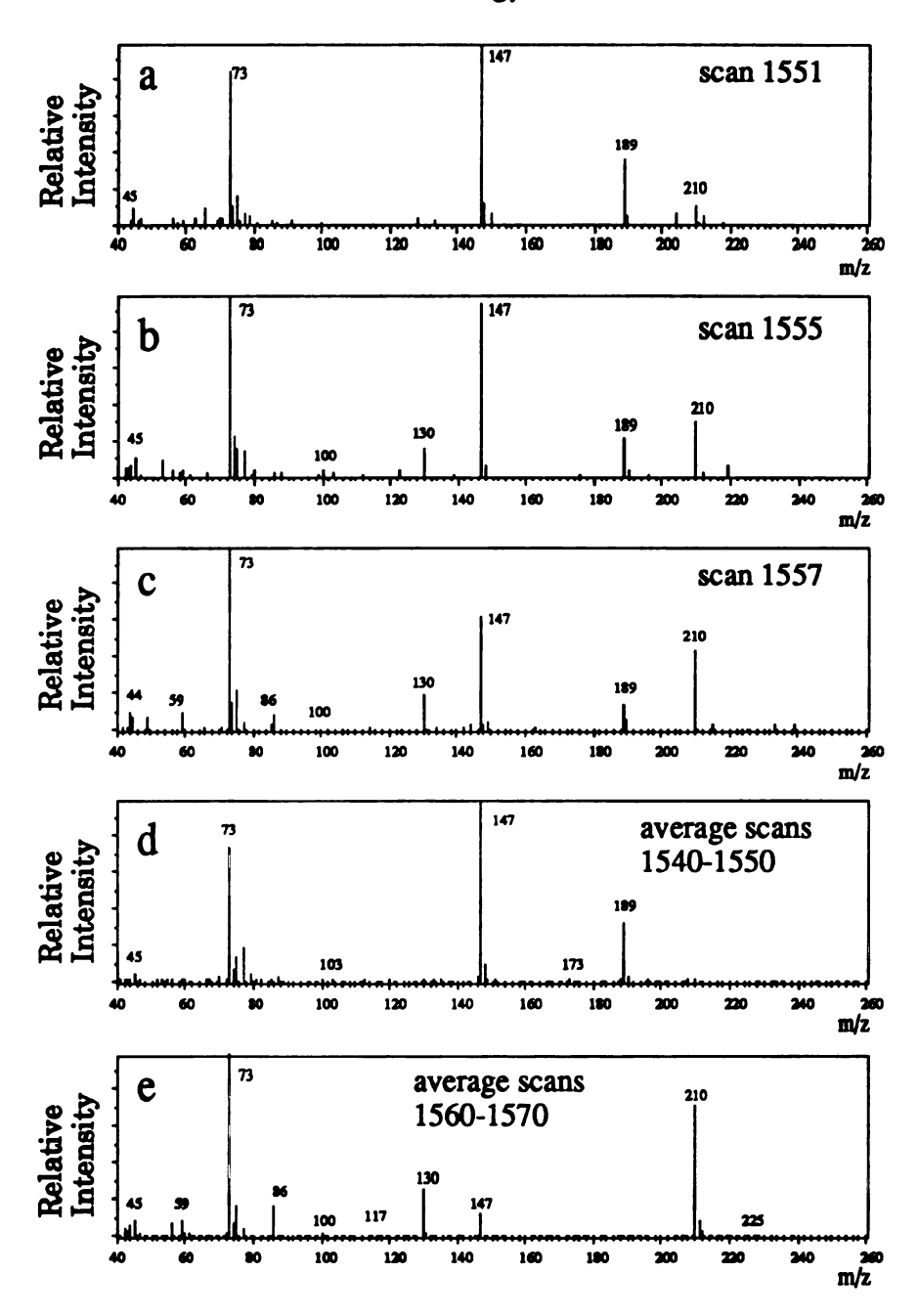


Figure 4.9 Comparison of mass spectral data (Figures 4.9a-c) in scans 1551, 1555, and 1557 over the peak profile in Figure 4.8. The changes in the relative intensities at m/z 189 and m/z 210 indicates the presence of more than one component. Figure 4.9d is the mass spectrum resulting from averaging scans 1560 to 1570. Figure 4.9e is the mass spectrum resulting from averaging scans 1540 to 1550.

A more dramatic example of a reconstructed chromatographic peak profile, suggesting, incorrectly, the elution of a single component, is shown in Figure 4.10a. The peak shape and width are consistent with elution of a single component at this retention time. The mass spectral data in scans 1883, 1890, and 1899, are shown in Figures 4.11a-c, respectively. The most obvious differences are the changes in relative intensities at m/z 147, m/z 174, and m/z 247 in the three mass spectra, suggesting the elution of at least two different components. Mass chromatograms at m/z 174 and m/z 247 are shown in Figure 4.10b. Again, the mass chromatograms do not overlap completely, indicating the presence of two components. By identifying a mass spectral peak for each of the components in the chromatographic peak profile, a mass spectrum for each component is obtained. A comparison of the mass spectra shown in Figures 4.11a-c shows that scan 1883 only has ion currents indicative of one of the components.

Similarly, scan 1899 only has ion currents indicative of the other component. Selection of these scans is more clear upon examination of the overlapping mass chromatograms shown in Figure 4.10b. Note that at the maximum intensities at m/z 174 and m/z 247, the retention times, shown in Figure 4.10b, only differ by 0.8 seconds, but one can still obtain a mass spectrum for each of the components directly from the data base acquired at a rate of 10 mass spectra/second. The two components represented in Figure 4.10 have been identified as bis-TMS-succinic acid and tri-TMS-glycine, respectively. The TMS ester of succinic acid has a molecular weight of 262 u and its mass spectrum shows a peak for the characteristic (M-15)+ ion at m/z 247.

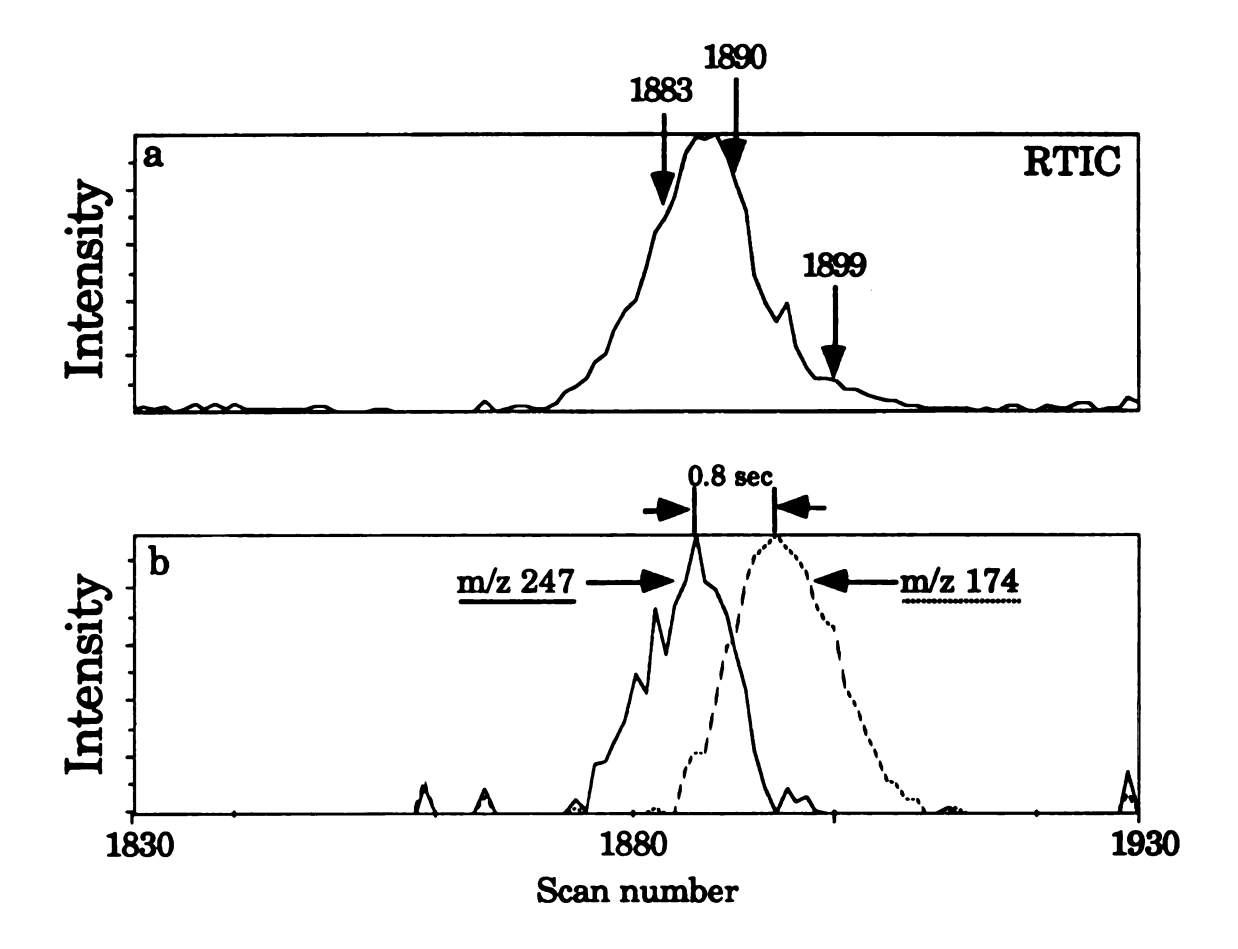


Figure 4.10 Figure 4.10a is a region of the RTIC chromatogram generated from the data base acquired at 10 scans/second. Figure 4.10b shows the mass chromatograms at m/z 174 (broken line) and at m/z 247 (solid line). The difference in the maxima of the two mass chromatograms indicates the presence of two components.

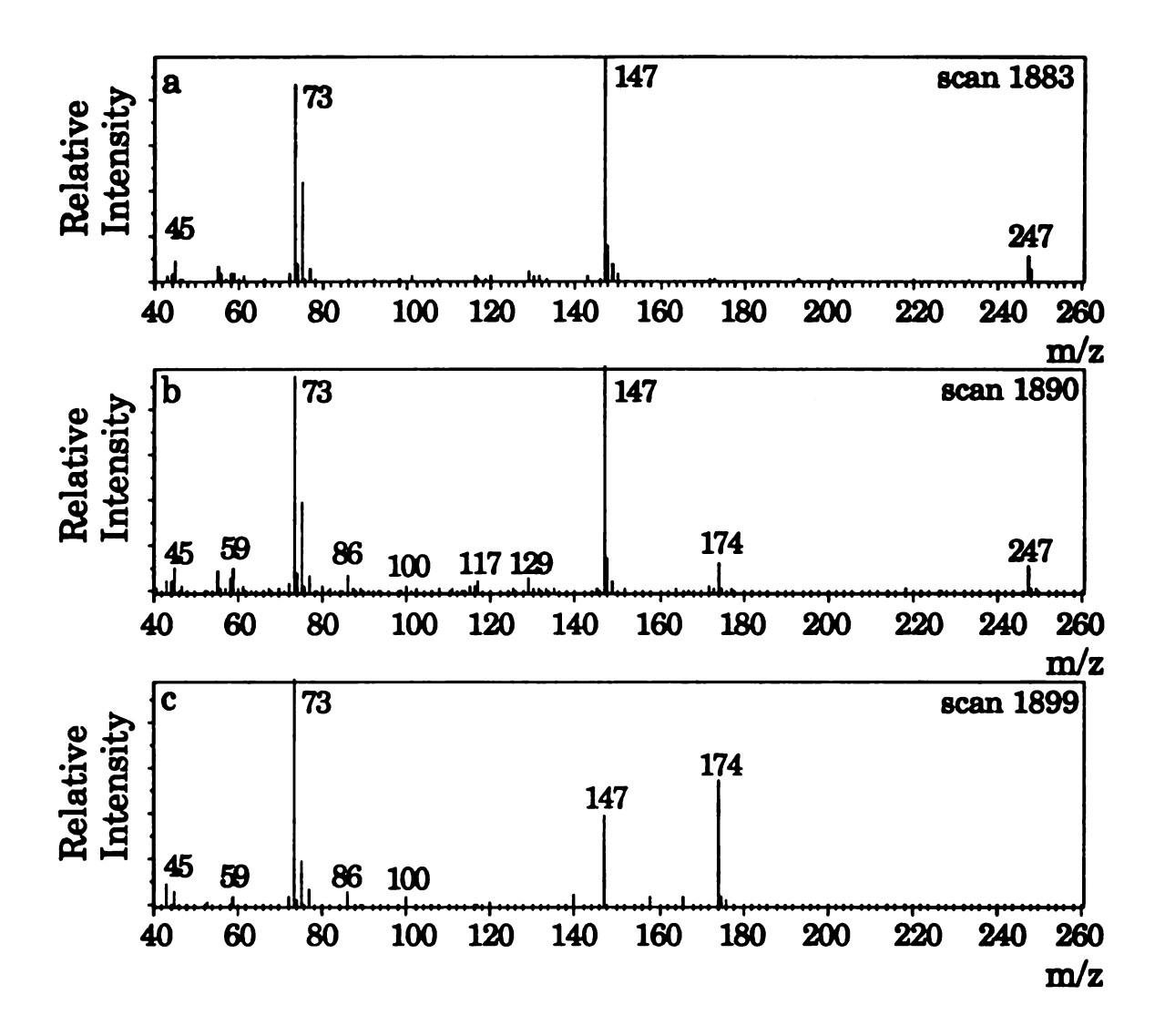


Figure 4.11 Comparison of mass spectral data (Figures a-c) in scans 1883, 1890, and 1899 over the peak profile in Figure 4.10. Comparison of the mass spectral data in each scan shown indicates that Figure 4.11a (scan 1883) represents the first component in the peak profile, Figure 4.11b (scan 1890) contains mass spectral data for both components, and Figure 4.11c (scan 1899) is the mass spectrum of the second component represented by the poorly resolved doublet in Figure 4.10b.

5. Three-dimensional data presentation

Three-dimensional (3-D) plots of mass spectra versus scan number are another useful means of displaying data consisting of a large number of scans per chromatographic peak⁶⁰. These 3-D plots are constructed by plotting mass chromatograms for all m/z values in a given region of the RTIC chromatogram. This allows the temporal profiles of each mass chromatogram to be compared to indicate which chromatographic peaks result from more than one component. An example of a 3-D plot is shown in Figure 4.12 over the chromatographic peak in the metabolic profile represented in Figure 4.10. The 3-D plot clearly shows evidence for the two components over this region of the RTIC chromatogram. components have peaks in common at m/z 73 and m/z 147, but there are a number of peaks that are unique to one or the other component. The two major peaks that are unique to each of the components occur at m/z 174 and m/z 247 (as in Figure 4.10b). Chromatographic profiles for the two components can be recognized by plotting mass chromatograms at m/z 174 and m/z 247. The mass spectrum of each component can be obtained by examining the mass chromatograms as shown previously.

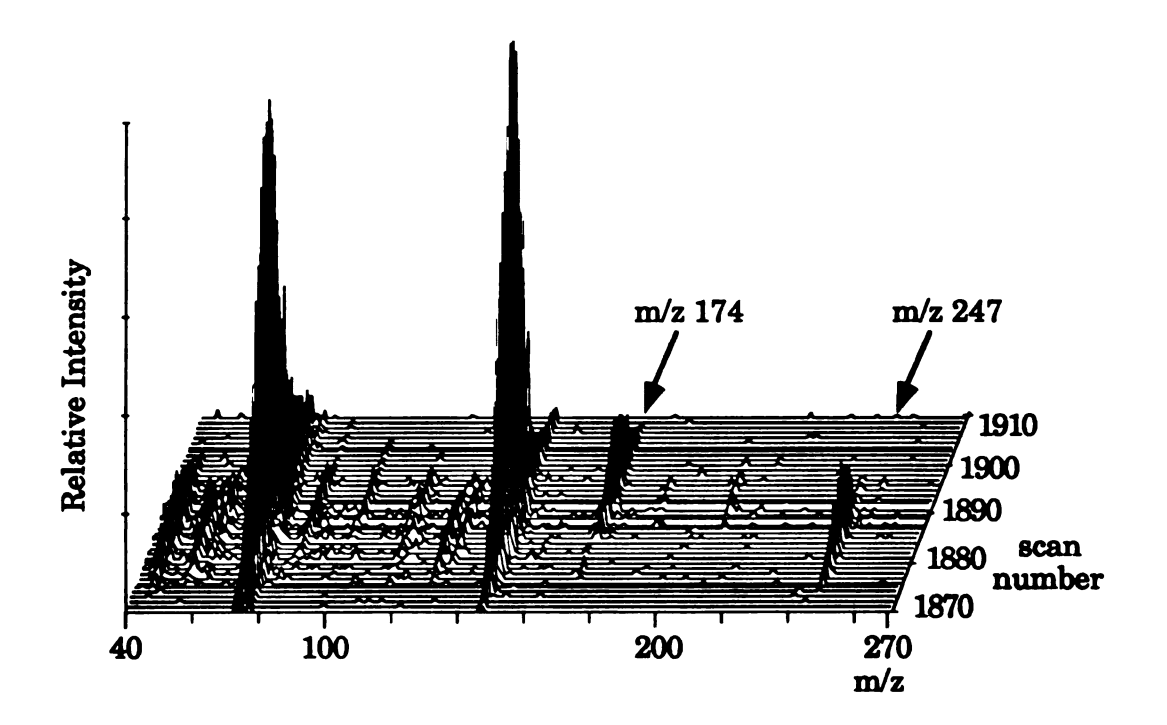


Figure 4.12 3-dimensional plot of scan range 1870 to 1910 of data base acquired at 10 mass spectra/second.

6. Conclusions

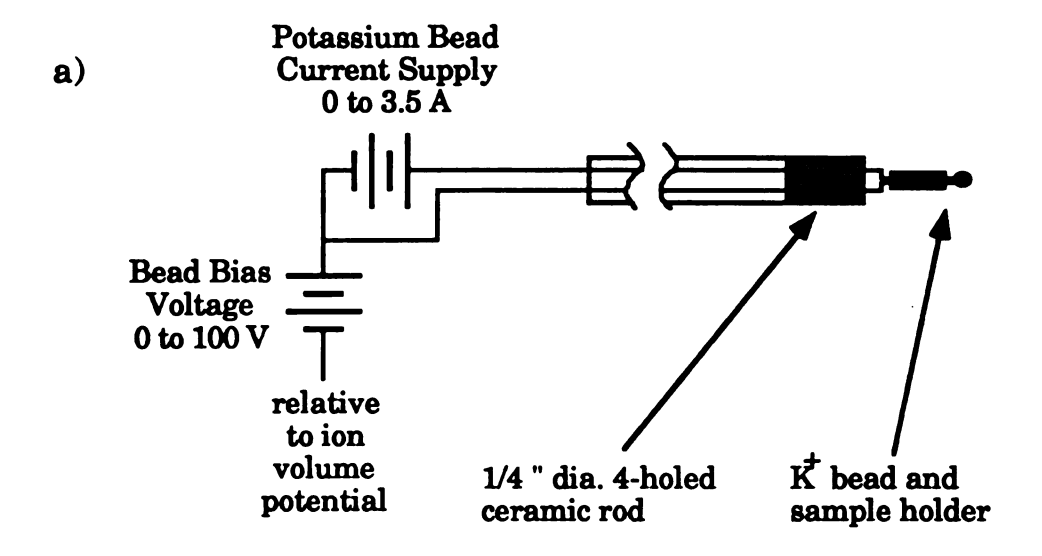
A GC/MS instrument based on beam deflection time-of-flight mass spectrometry can perform complex mixture analyses by generating complete mass spectra at a rate appropriate for specific chromatographic conditions. The mass spectral acquisition rate for an analysis is dictated by requirements to accurately represent the chromatography and provide data with good signal-to-noise. The utility of this unique system is demonstrated in the context of realistic problems encountered in the analysis of the complex mixture of organic acids extracted from human urine. problems in such analyses frequently manifest themselves as components that are chromatographically unresolved. It is further demonstrated that long capillary columns, with high numbers of theoretical plates and peak separation, are not necessary with this technology. Rather, an analysis can be performed on a short capillary column giving the same analytical information, but with reduced analysis time. The typical analysis time for this metabolic profile was reduced from 1 hour to 15 minutes (this particular analysis time was limited by the rate at which the GC temperature could be increased). The success of these analyses is due to the nature of the BDTOF-MS instrument combined with the ITR. In this application, each of the 10 mass spectra acquired each second is the sum of 500 transient mass spectra. The high mass spectral acquisition rate provides a data base that can be used to accurately represent the chromatographic information and that facilitates the identification of each of the components in a complex mixture. Quantitation of each of the components is facilitated due to the greater number of points available with which to determine peak shape, width and area. The "unskewed" nature of the mass spectrum in each of the scans facilitates preparation of "pure" mass spectra by deconvolution of nearly co-eluting components using mass spectral subtraction. For the data presented here, compounds with retention times differing by 0.1 sec, can be analyzed. The three-dimensional presentation of the data allows the user to identify peaks that are representative of poorly-resolved components, display the corresponding mass chromatograms, and then choose scan and background scans for subtraction to obtain mass spectra for closely eluting components.

Chapter 5 - Potassium Ion Ionization of Desorbed Species (K+IDS)

A. Background

Blewett and Jones⁶¹ developed the use of alumino-silicate glasses, doped with metal oxides, as a source of gas phase metal ions. By heating a mixture of 2SiO₂:1Al₂O₃:1K₂O, copious amounts of gas phase K+ are produced. The development of K+IDS as a complementary ionization technique to chemical ionization has been introduced in this laboratory.⁶² With K+IDS, samples are thermally desorbed into the gas phase by radiative heating by the potassium emitter. The thermally desorbed neutrals are "sampled" by gas phase K+ resulting in the formation of K+ adduct ions. The desorption products are dependent on the rate of heating and final temperature of the potassium glass used in an analysis. The two competing rates of decomposition and desorption of intact molecules determine the mass spectrum obtained for an analysis. Desorption of intact molecules is favored at high temperatures, while decomposition is favored at lower temperatures.

Previous work on K+IDS was performed on a Hewlett Packard 5985 quadrupole mass spectrometer. This mass spectrometer operates with the source at ground potential and a mass range up to 1000 u. The original K+IDS probe shown in Figure 5.1 was designed with only a potassium glass that also functioned as a sample holder. Sample analysis by thermal desorption from the potassium glass was accomplished as the current



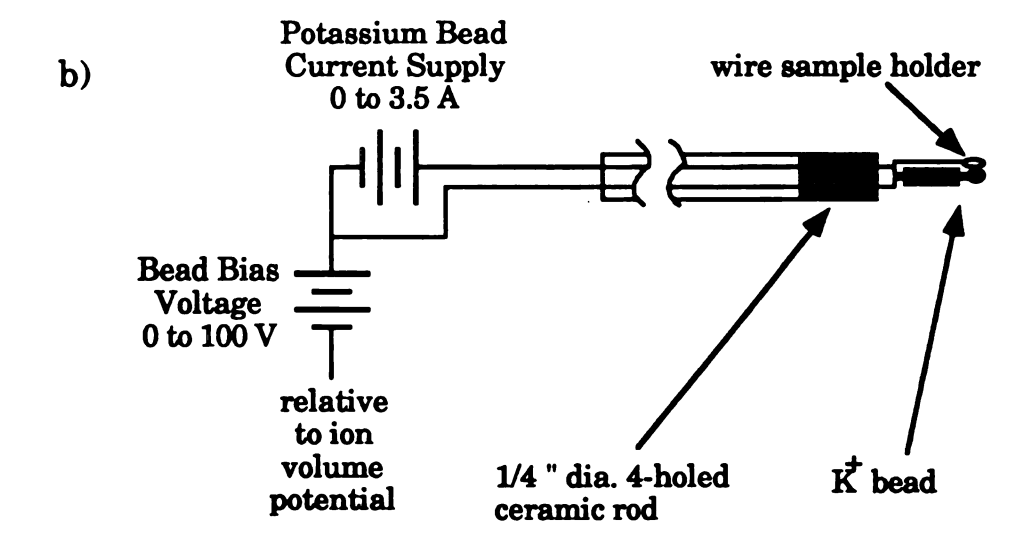


Figure 5.1 Previous K+IDS probe designs used on HP 5985 mass spectrometer. First design used by Bombick used the potassium emitter as a sample holder. Later design of Kassel used separate wire sample holder for better temporal overlap of potassium emission and sample desorption. A 30-fold improvement in detection limits result from the separation of the wire sample holder and potassium emitter.

through the potassium glass was increased. This probe design did not take full advantage of this desorption technique because most of the sample was desorbed from the potassium glass before a sufficient amount of potassium ions were available for attachment to the desorbed sample. The overlap of potassium ion desorption and sample desorption profiles was improved with the separation of the sample from the potassium glass. Here, the temporal overlap of the desorption profiles of both the potassium ions and desorbed sample can be optimized by the spatial separation of the wire sample holder and potassium bead in the ion source. The separation of the wire sample holder and potassium emitter improved the detection limits of K+IDS by 30-fold.⁶³

K+IDS is a useful method for obtaining molecular weight information for a number of compound classifications⁶³. Most often in the analysis of thermally-labile compounds, molecular weight information is desired and thus a high final potassium glass temperature is used. Structural information is available with K+IDS by controlling the rate of heating and final temperature of the potassium glass and/or sample. A slower rate of heating induces more decomposition products that provide structurally significant ions. K+IDS is useful in the analysis of polymers⁶⁴ and complex mixtures.⁶⁵ The analysis of polymers by K+IDS is used to provide both structural information on the oligomeric units and information on the distribution of oligomers in the polymer^{66,67}.

The K+IDS analysis of palmitic acid using the BDTOF mass spectrometer is shown as an example in Figure 5.2. The K+IDS probe design using a separate wire sample holder and potassium emitter was used for this analysis. A 1-µl solution of palmitic acid in methanol was

placed on the wire sample holder and the methanol was allowed to evaporate. The probe was inserted into the mass spectrometer until the probe tip was in the center of the ion volume of the ion source. The current through the potassium emitter was ramped from 0 to 2.7 A in less than 2 seconds and mass spectral data was acquired at 10 mass spectra/second from m/z 30 to m/z 350. Figure 5.2 shows the sum of the ion currents in each scan versus scan number along with the desorption profiles at m/z 41 (K+ isotope ion) and at m/z 295 (MK+ ion of palmitic acid). The desorption profile for the MK+ of palmitic acid is approximately 0.8 seconds for this analysis. A sum of the mass spectral data in the scans over the desorption profile at m/z 295 is shown in Figure 5.3. This is the typical K+IDS mass spectrum of palmitic acid with only an MK+ ion formed in the analysis.

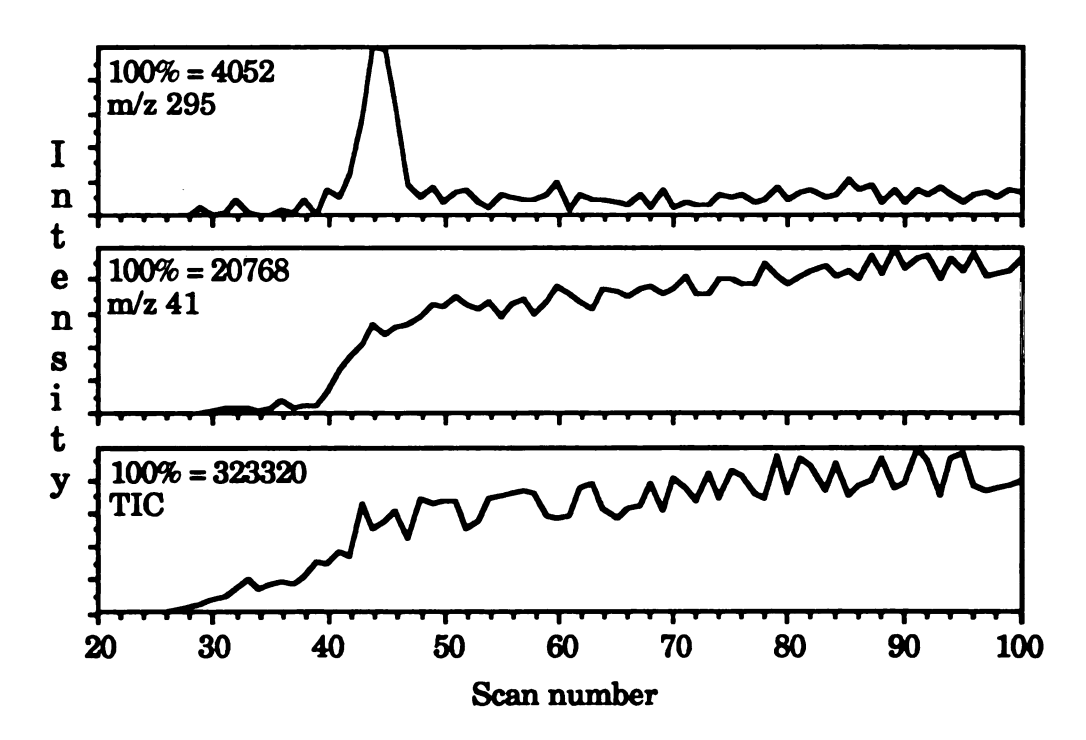


Figure 5.2 Total ion current and desorption profiles at m/z 41 and m/z 295 for the K+IDS analysis of palmitic acid. Bead current was 2.7 A at a mass spectral acquisition rate of 10 mass spectra/second.

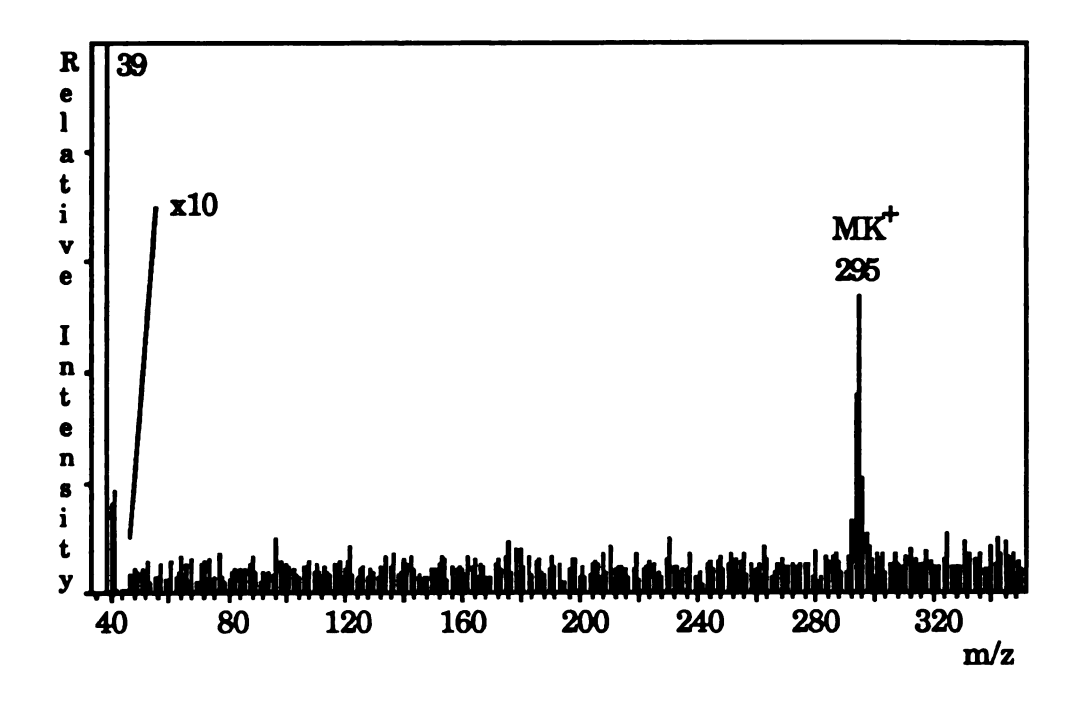


Figure 5.3 K+IDS mass spectrum of palmitic acid with MK+ at m/z 295. This mass spectrum is the sum of scans 42 to 46 from Figure 5.2. Bead current was 2.7 A with a mass spectral acquisition rate of 10 mass spectra/second.

The BDTOF mass spectrometer combined with TAD and the high mass spectral acquisition rates of the ITR may have a greater utility than a quadrupole mass spectrometer for K+IDS analyses. Figure 5.2 shows that a K+IDS analysis can be less than a second in duration. High acquisition rates of complete mass spectra are required when information on the rate of formation of all the analyte ions is desired. The high mass spectral acquisition rates will be useful in K+IDS applications that involve analyzing mixtures where there are desorption profiles being generated for each component in the mixture.

Rapid heating techniques have been used for the determination of the heats of vaporization of thermally-labile compounds.⁶⁸ Polyalcohols were rapidly heated from a rhenium filament and the desorbed neutrals reacted under CI conditions with methane and ammonia. The rate of appearance of the protonated molecules can be used to determine their heats of vaporization by plotting the rate of appearance versus the reciprocal of the absolute temperature. The slope of the resulting Arrhenius plot was used to obtain the heat of vaporization for each ion. Heats of vaporization for the polyalcohols studied were correlated to the degree of hydrogen bonding in each compound.

Light investigated the use of K+IDS as a rapid heating technique to determine the heats of vaporization of palmitic acid and sucrose.⁶⁹ The rate of appearance of K+ adducts of the desorbed neutrals was used as an approximation for the rate constant of the volatilization process. During a K+IDS analysis, the desorption of the sample was monitored versus temperature of the sample using a thermocouple as the sample holder. The temperature of the sample holder was calibrated for various final currents through the potassium bead. The slope of an Arrhenius plot of log of the rate of appearance of MK+ versus 1/T(K) yields the heat of vaporization for the desorbed neutral. The high mass spectral acquisition rates available with the ITR may provide more accurate determinations of the heats of vaporization and may be used to determine the heats of vaporization of several species in the same experiment.

B. Experimental

1. K+IDS probe design

When K+IDS was considered for study on the BDTOF mass spectrometer, a probe had to be designed that could operate at high ion source potentials (3-5 kV). Figure 5.4 shows the probe design and the materials used for its construction. The vacuum-lock inlet of the Dupont 21-491B ion source housing was designed for a 1/4 " diameter probe. High voltage isolation for the K+IDS probe was achieved by using 1/4 " diameter glass tubing. The two current supply leads for the potassium glass were passed through the center of this glass tubing. One of the leads was also passed through a second glass tube of 2 mm o.d. for electrical isolation from the other lead. High voltage feedthroughs were also necessary for this K+IDS probe. The base of the probe was machined from stainless steel to weld the stainless steel high voltage feedthroughs to the base plate. Electrical contact is made between the feedthroughs and the current supply leads by a screw-type pinch connector. The base plate containing the two high voltage feedthroughs was sealed to the base using a 1/16" o-ring seal. The 1/4" glass capillary was sealed to the probe base using a Cajon fitting. Probe disassembly was made possible by removing the probe base plate screws, loosening the Cajon fitting and then sliding the probe base up the length of the 1/4" glass tubing of the probe. The side of the base was also fitted with an SGE fitting to allow a capillary column to pass through the probe assembly up to the base of the sample holder. This setup allowed the continuous leak of volatile samples into the ion source for mass calibration of the time axis and performing K+ chemical ionization (K+ CI) experiments.

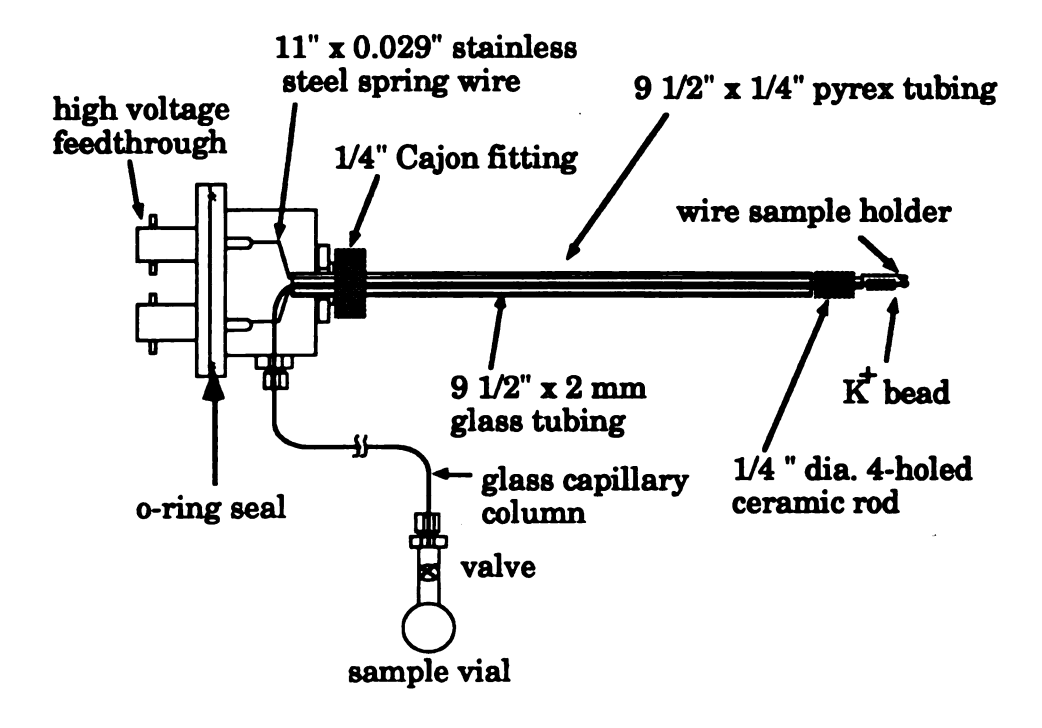


Figure 5.4 K+IDS probe designed for HV ion source of BDTOF mass spectrometer.

2. Electronic circuit modifications

The EI electron filament controls and electronics of the JEOL ion source power supply were modified to control the current and bias voltage of the potassium bead and sample holder. In Figure 3.4 there are two 0.5Ω resistors that are shaded. These resistors are used to control the current supplied to the EI electron filament. In the EI mode, the minimum unregulated current that the circuit can attain is 4 A. For a K+IDS experiment, the current supplied to the potassium bead typically ranges from 2 to 3 A. Two 0.3Ω resistors were added to each of the 0.5Ω resistors for a total of 1.1Ω . Adjusting the CURRENT LIMIT (100Ω resistor) provided

a range of potassium bead currents from 1 to 3.5 A. The bias voltage applied to the potassium bead is adjusted using the EI filament voltage (typically set to 70 V for EI). This voltage is typically set in the range from 0 to 5 V above the accelerating voltage. Potassium ion emission reaches a steady state condition within 3 s after the current supply is turned-on.

B. K+IDS by TOF-MS

Early work on K+IDS on the BDTOF mass spectrometer was directed at creating a benchmark by which to compare to the previous K+IDS work performed on the HP5985 quadrupole mass spectrometer. The best way to compare the performance of the BDTOF to that of the HP mass spectrometer is to compare the extent of conversion of K+ + M \rightarrow MK+ for known conditions. Also, the ion transmission efficiency for a TOF mass spectrometer utilizing a beam deflection system is not as high as that available with other mass spectrometers (assuming that a 10 ns "slice" is removed from a continuous ion beam for analysis using beam deflection, 99.995% of the continuous ion beam is not utilized).

In order to compare the extent of conversion of $K^+ + M \rightarrow MK^+$ of the HP5985 and BDTOF, it was necessary to find some data acquired on the HP5985 that showed both K^+ and MK^+ ions in the same mass spectrum. From the previous work on K^+ IDS on the HP5985, the only mass spectra reported that show the relative adduct ion intensities to the potassium ion intensities for the two major isotopes of potassium (m/z 39 and 41) were in Dan Bombick's dissertation (Figures 6-9). It is important to have both of the potassium isotope peak intensities to determine whether the major isotope

peak at m/z 39 is saturating the detector. Bombick performed a number of K+ CI experiments on different compound classes including aldehydes, ethers, ketones, and amines to show their typical K+ CI mass spectra. Experimental parameters included with the data in Figures 6-9 were the ion source pressure for the samples and the current through the potassium bead, but not the channeltron electron multiplier (CEM) voltage used for these K+ CI experiments. The voltage used determines the gain of the CEM detector and, therefore, it is an important parameter to determine the feasibility of K+IDS on the BDTOF mass spectrometer.

The K+IDS mass spectrum of acetone under K+ CI conditions was obtained on the HP5985 to determine the CEM voltage that would produce a mass spectrum with both of the potassium isotope ion currents "on-scale" with the acetone adduct of potassium at a partial pressure of 1 x 10^{-4} torr of acetone. The CEM voltage was adjusted to 1200V to obtain this mass spectrum. This provided a benchmark for a direct comparison of the extent of conversion of K+ + M \rightarrow MK+ for the K+IDS/BDTOF experiments.

Bombick had reported that the energy of the potassium ions used in a K+IDS experiment greatly affected the adduct ion intensities. An "addition bias window" ranging from 0 to 5 V for the energy of the potassium ions results in the best extent of conversion of $K^+ + M \rightarrow MK^+$. One of the major differences between the HP5985 and the BDTOF mass spectrometers (other than the mode of ion separation) is the accelerating potential used in each instrument. The HP5985 mass spectrometer uses an accelerating potential of approximately -(10 V + 100 mV/amu) compared to 1.5-3kV with the BDTOF.

The electric fields in the ion volume of the Dupont 21-491B ion source were modeled using SIMION⁷⁰ to determine the penetration of the accelerating potential into the ion volume. SIMION is a program that allows a user to define electrode surfaces and the potentials applied to them to determine the electric field lines for that geometry. A SIMION model of the Dupont ion volume of the ion source used for the K+IDS experiments is shown in Figure 5.5. Each potential field line in this figure represents a 1 volt change. The ion source voltage is 3000 V, the repeller is 3005 V and the focus lens is at 1000 V (not shown). Figure 5.5 shows considerable penetration (by as much as 20 V) of the accelerating field into the region of the ion volume. The tip of the K+IDS probe containing the potassium glass and sample holder is located midway between the repeller and ion source exit slit of the ion source. The penetration of the accelerating potential into the ion volume may contribute to a greater energy distribution of the potassium ions emitted from the potassium bead than those in an ion source in a quadrupole mass spectrometer operating with a lower accelerating potential.

1. Grided versus Gridless Ion Source

The results of the SIMION modeling of the Dupont ion source led to a series of experiments to compare the K^+ CI extent of conversion of K^+ + $M \rightarrow MK^+$ for an ion source with a wire mesh grid placed across the exit slit of the ion volume relative to no grid in the ion source. A wire mesh grid placed across the ion source exit slit will reduce the penetration of the accelerating potential into the ion volume.

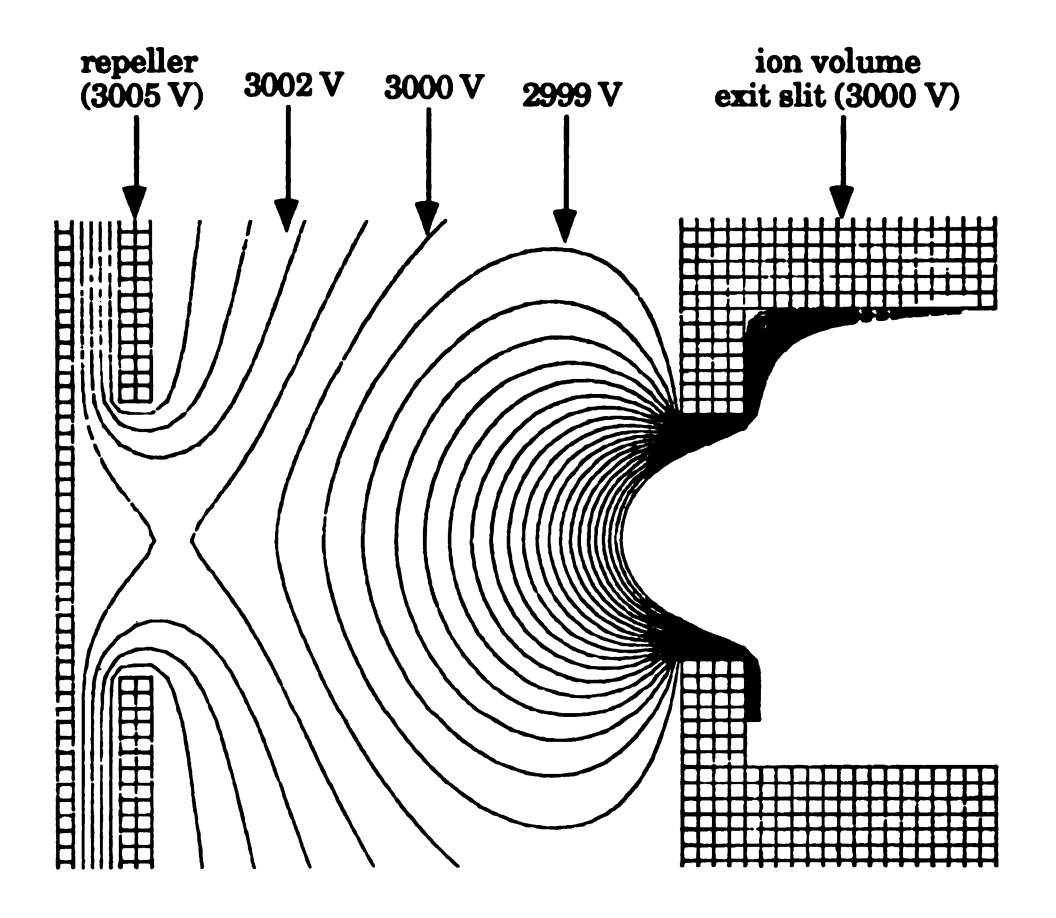


Figure 5.5 SIMION model of Dupont ion source with a repeller voltage of 3005 V, ion volume exit slit voltage of 3000 V, and focus lens voltage of 1000 V (not shown). Each electric field line represents a change of 1 V. A penetration of 20 V into the ion volume of the ion source is evident.

Experimental

The experiments for the gridless and grided ion sources were performed using the same probe assembly and potassium bead to minimize systematic errors. The current through the potassium glass was set to 2.6A with a bias voltage less than 5V. The K+ CI mass spectrum of acetone

was collected at a number of pressures ranging from 3.6 x 10⁻⁵ torr to 1.6 x 10⁻⁴ torr as measured by the ionization gauge attached to the ion source housing. Data collection was initiated and then the current supply to the potassium bead was applied. Scan 0 is not necessarily 'time zero' because everything is manually controlled and the time between starting data collection with the ITR and flipping the switch for the current supply is not constant. Data were recorded at 10 mass spectra/second for periods ranging from 10 to 20 seconds in duration.

Results

The intensity of the ion current at m/z 39, an isotope of potassium, saturates the preamplifier and A/D of the ITR at a potassium bead current of 2.6 A. The ion current for the potassium isotope peak at m/z 41 did not saturate the preamplifier and was used to compare the extent of conversion for the grided and gridless ion source. Figure 5.7 shows the desorption profiles at m/z 41 and at m/z 97 for the gridless ion source at 1.6×10^{-4} torr of acetone in the ion source. The information at the top of each figure contains the file name, ion source pressure, mass spectral acquisition rate, and whether there was a grid (w/ grid) or no grid (w/o grid) in the ion source. Figure 5.7 shows the desorption profiles at m/z 41 and at m/z 97 for the grided ion source at 1.2×10^{-4} torr of acetone in the ion source. A steady-state ion current was established after a few seconds for each of these experiments.

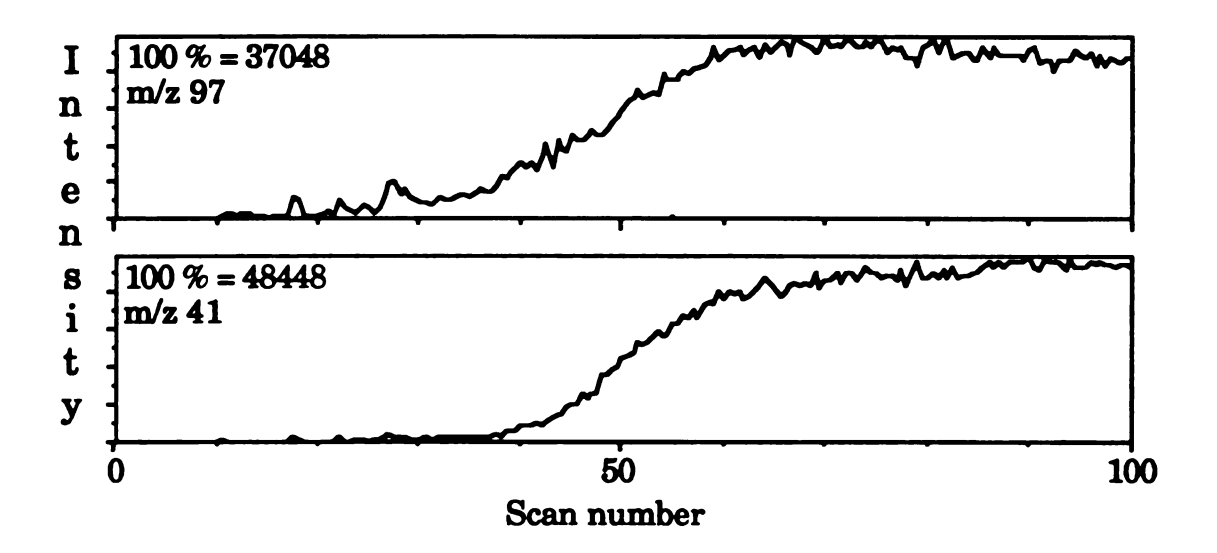


Figure 5.6 Desorption profiles of $(M + K)^+$ at m/z 97 and K⁺ isotope at m/z 41 for gridless ion source at 1.6 x 10⁻⁴ torr partial pressure of acetone and 10 mass spectra/second.

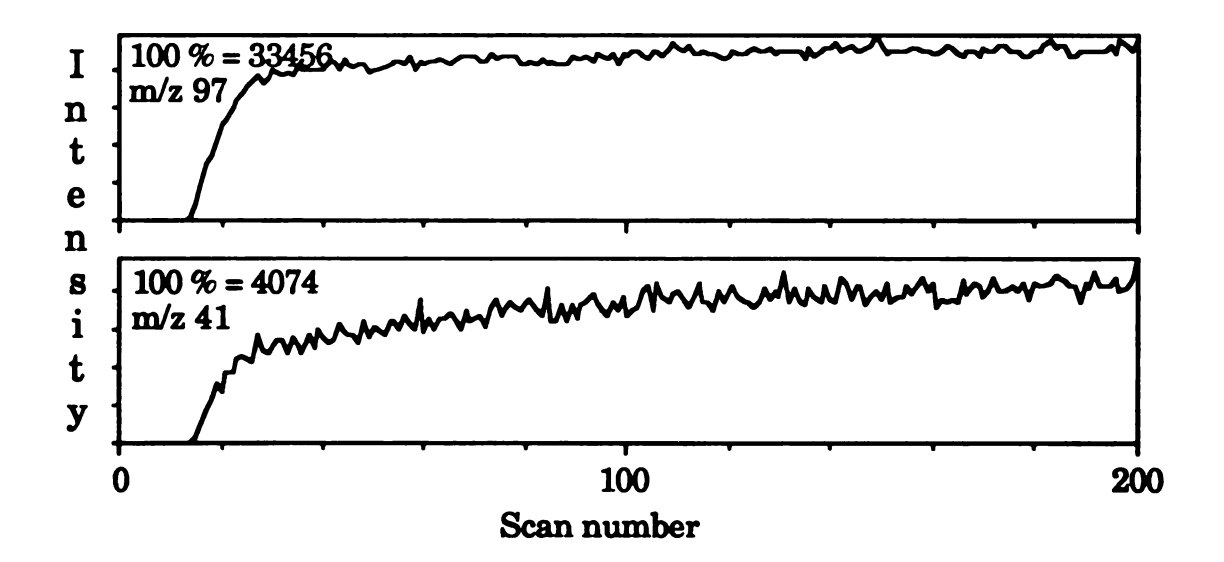


Figure 5.7 Desorption profiles of $(M + K)^+$ at m/z 97 and K⁺ isotope at m/z 41 for grided ion source at 1.2×10^{-4} torr partial pressure of acetone and 10 mass spectra/second.

Mass spectra for the gridless and grided ion source are shown in Figures 5.8 and 5.9, respectively. The mass spectrum obtained with the gridless ion source was at a higher pressure than the one with the grided ion source, but the relative abundance of the (acetone + K)+ ion at m/z 97 to that of K+ at m/z 41 is much less than that with the grided ion source. In fact, the K+ CI mass spectrum for the grided ion source shows ion currents at m/z 155 and at m/z 213 as well. These ions are the (2M + K)+ and (3M + K)+ ions, where M is one acetone molecule. The increase in the extent of conversion can be attributed to the increase in ion residence times in the ion volume of the ion source due to the grid minimizing the drawout potential of the accelerating voltage.

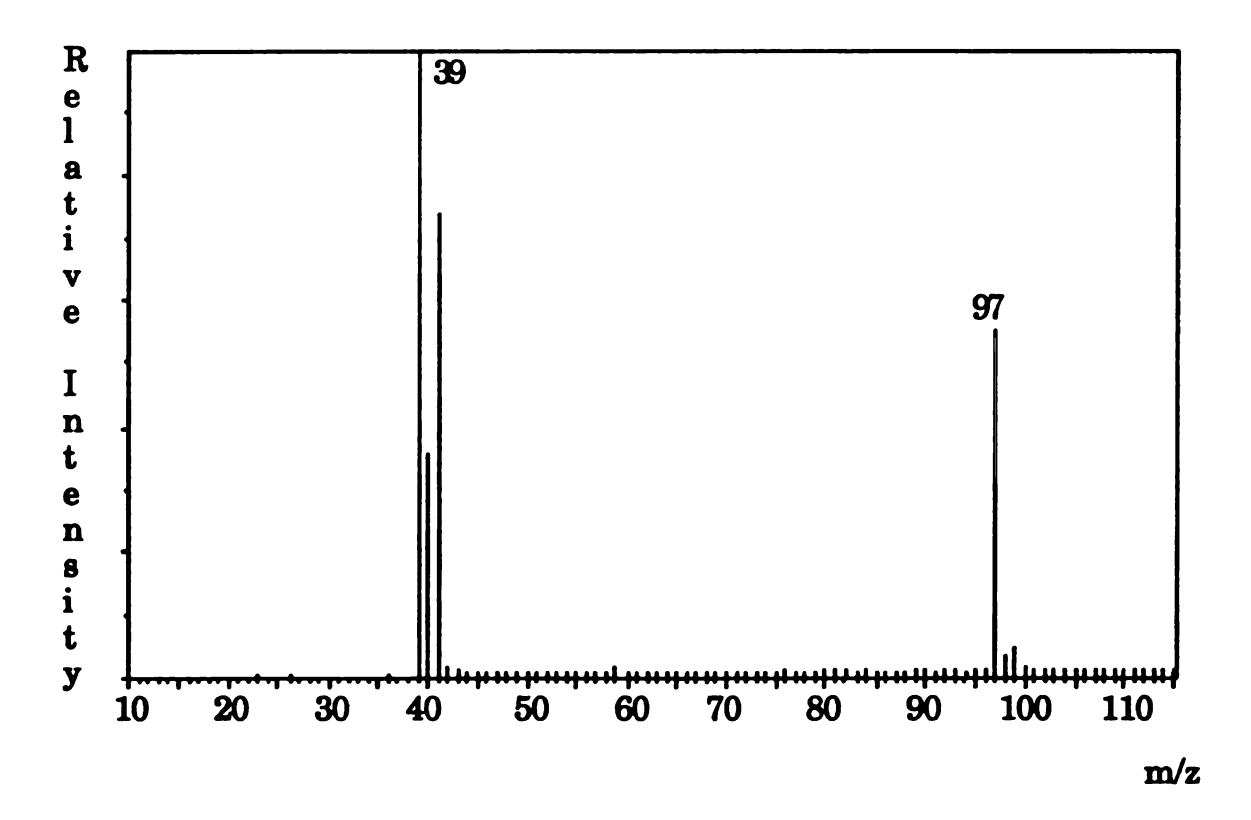


Figure 5.8 K+ CI mass spectrum of acetone in the gridless ion source at 1.6×10^{-4} torr at 10 mass spectra/second. Bead current is 2.6A.

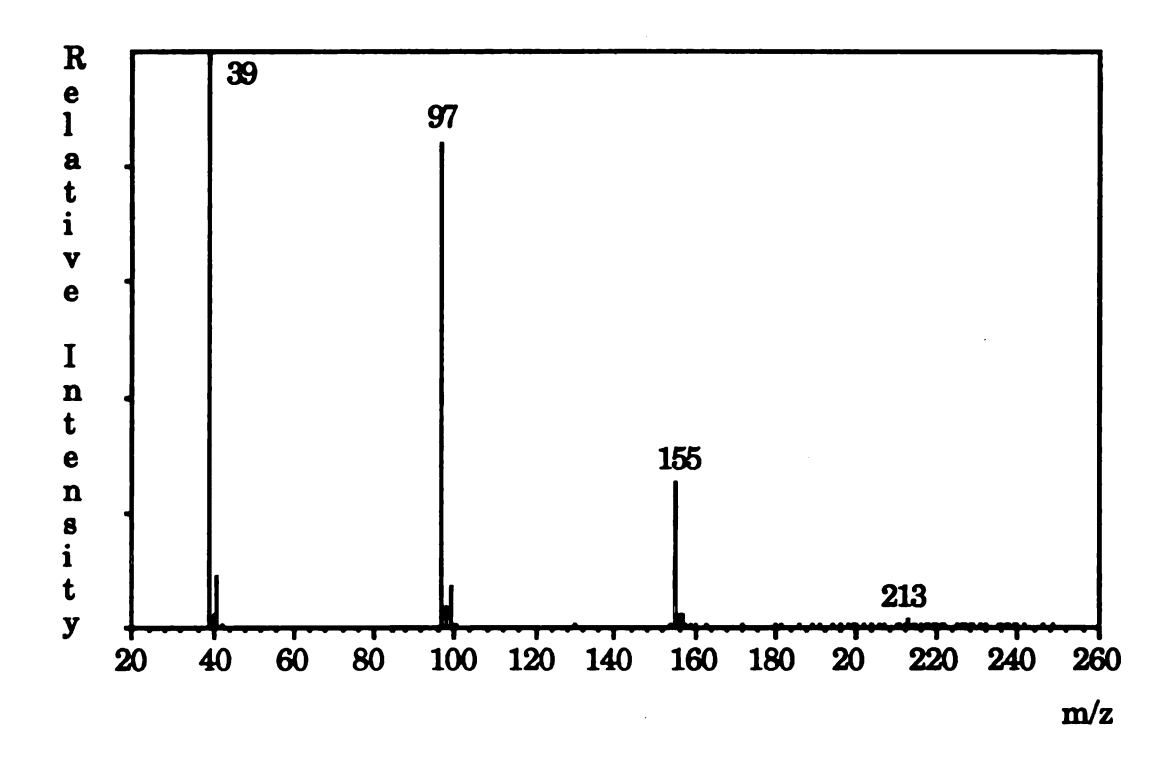


Figure 5.9 K+ CI mass spectrum of acetone in the grided ion source at 1.2×10^{-4} torr at 10 mass spectra/second. Bead current is 2.6A.

This result in an increase in conversion of gas phase K^+ to $(M + K)^+$ prompted data collection for the grided and gridless ion source at a number of partial pressures of acetone in the ion source. Table 5.1 contains the intensity at m/z 41 and at m/z 97 for the adduct ion of acetone for the gridless ion source. The values reported for the intensity at m/z 41 and at m/z 97 are the average of scans 60 to 100. Table 5.2 contains the intensity at m/z 41 and the $(M_n + K)^+$ ions at m/z 97, m/z 155 and m/z 213 for the grided ion source. The data are the average of scans 100 to 200. The abundance of

the potassium isotope peak at m/z 41 decreases at higher pressures due to "cooling" of the potassium bead by gas phase acetone molecules.

The grided ion source data are plotted in Figure 5.10 to show the general trends in the adduct ion intensities with partial pressure of acetone. The ITR data system can only sum up to 65,536 peak intensity counts for each time bin in each scan; if the ion current for a particular time bin "saturates" the ITR, the "excess" ion current is subtracted from 65,536 and that difference stored as the peak intensity. Based on the general trend of the ion current at m/z 97 in Figure 5.10 up to 9.5 x 10⁻⁵ torr of acetone, it is apparent that this ion current saturated the ITR data system. At 1×10^{-4} torr of acetone in the ion source, the increase in extent of conversion with the grid in the ion source is approximately a factor of 15. This is more clearly shown in Figure 5.11, which compares the ratio of the acetone adduct ion at m/z 97 to that at m/z 41 versus the partial pressure of acetone for the grided and gridless ion source. Figure 5.11 also shows the multiple acetone adduct ions to potassium for the grided ion source. The remaining K+IDS data were collected with a grid in the ion source due to the improved extent of conversion with the grided ion source.

2. MK+ abundance versus pressure

The mechanism of adduct ion formation in K+IDS has been considered a termolecular process, at least for small analyte molecules. Previous work by Bombick showed improved sensitivity (by a factor of 2) when a collision gas at 1 x 10⁻⁴ torr N₂ was used in a K+IDS analysis of polyphenyl ether. Collisional stabilization of an excited MK+* adduct ion can result from collision with another gas phase molecule or with the walls of the ion

Table 5.1 Average intensity of K⁺ isotope peak at m/z 41 and (acetone + K)⁺ at m/z 97 for various partial pressures of acetone in a gridless ion source.

Table 5.1 Gridless ion source					
6e-05	2328	71			
8e-05	3175	1226			
1.1e-04	6607	4394			
1. 4e-04	6030	6437			
1.6e-04	4303	6499			
1.9e-04	5412	6696			

Table 5.2 Average intensity of K⁺ isotope peak at m/z 41 and (acetone + K)⁺ at m/z 97 for various partial pressures of acetone in a grided ion source.

Table 5.2						
Grided ion source						
Source pressure of acetone (in torr)	Intensity at m/z 41	Intensity at m/z 97	Intensity at m/z 155	Intensity at m/z 213		
3.6e-05	5126	1010 ⁻	215	269		
4.3e-05	8541	7436	592	363		
5.6e-05	9922	19707	2117	446		
9.5e-05	7570	51923	15551	1496		
1.2e-04	5785	57520	25978	3069		
1.6e-04	4485	61330				

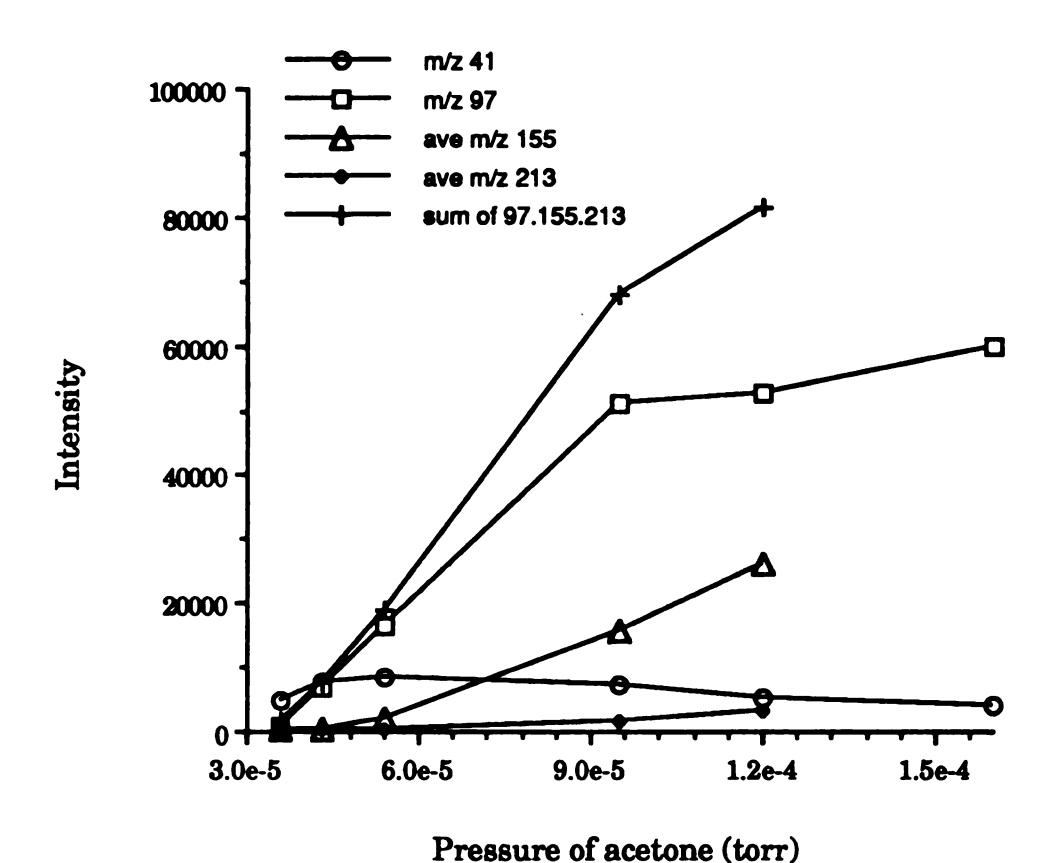
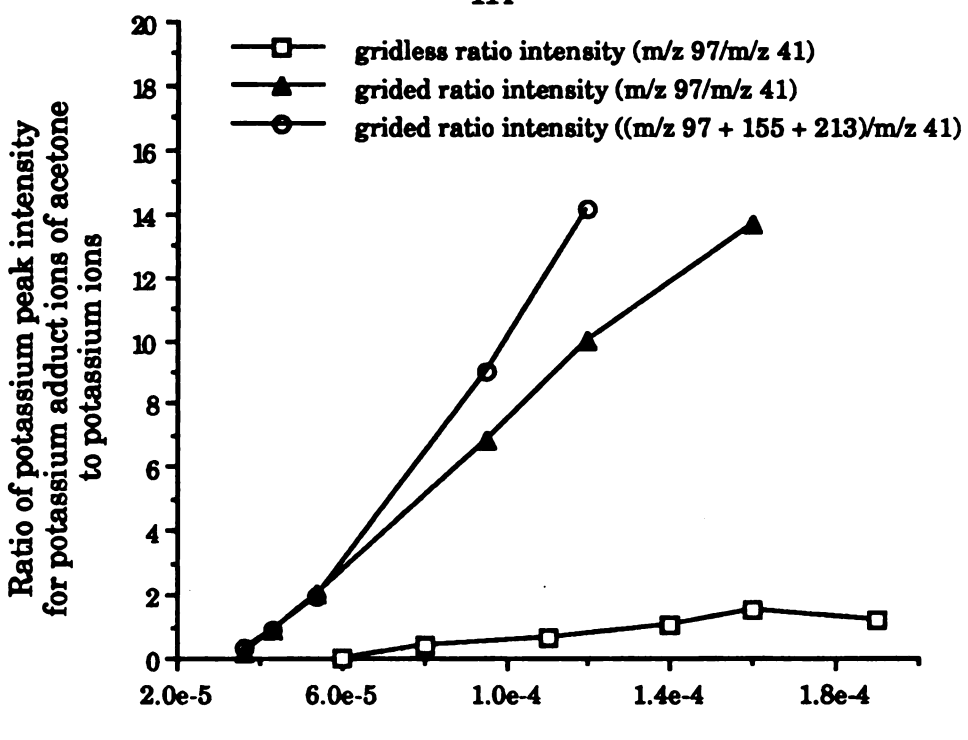


Figure 5.10 Plot of adduct ion peak intensity versus partial pressure of acetone in the grided ion source. Shown is the intensity of the potassium isotope at m/z 41 along with the intensity of the acetone adduct ions at m/z 97, 155, 213 and the sum of the acetone adduct ion intensities.



Partial pressure of acetone (torr)

Figure 5.11 Comparison of acetone adduct ion peak intensity to potassium isotope peak intensity at m/z 41 for the grided and gridless ion source. A factor of 15 improvement is adduct formation is gained by using a grid in the ion source.

volume. The effect of pressure on the extent of conversion was studied using palmitic acid as the analyte and triethylamine as the steady state background pressure (Triethylamine was conveniently available in the sample vial used for mass calibration). A more appropriate collision gas would be one that does not react with the potassium ions, but only serves to absorb excess energy from excited K+ adduct ions.

Table 5.3 lists the results obtained at two different pressures of triethylamine for the analysis of the same amount of palmitic acid. The peak intensity for the MK+ of palmitic acid at m/z 295 is tabulated with the

peak intensity for the potassium isotope at m/z 39. The extent of conversion of $K^+ + M \rightarrow MK^+$ is calculated by the following equation:

$$\frac{\sum MK^+}{\sum (K^+ + MK^+)}$$

The number in parentheses in Table 5.3 is the percent of adduct ion formed relative to potassium ions available. Note that at higher pressures there is a "cooling" effect of the potassium bead due to the collision of the triethylamine with the potassium bead causing fewer potassium ions to be formed. An improvement by a factor of 6 in the extent of conversion results at the higher pressure.

Table 5.3 Extent of conversion of palmitic acid versus background pressure of triethylamine.

Table 5.3						
Peak intensity for MK+ of palmitic acid vs triethylamine partial pressure						
Triethylamine partial pressure (torr)	Peak intensity for K+ at m/z 39	Peak intensity for MK+ at m/z 295				
1.0e-04	12998	87(0.7%)				
1.5e-04	3170	131(4.1%)				

B. K+IDS spectra

During the course of these studies, the use of potassium carbonate as the source of K+ was investigated. Upon heating, potassium carbonate decomposes into K₂O and CO₂. On a hot wire, the K₂O produces K⁺. The reasoning for the use of K2CO3 is that the formation of K+ and CO2 will provide both the formation of potassium adduct ions and also a collision gas to stabilize the adduct ions. Potassium carbonate was dissolved in water and a 1µl drop of this solution placed on a bare rhenium wire (in place of the rhenium wire with the potassium bead) and allowed to dry. Rapid heating of the rhenium wire produces a large flux of potassium ions along with an increase in the ion source pressure to 5 x 10-4 torr for approximately 2 to 3 seconds. A steady state of K+ exists for several minutes after the initial "burst" of K+ at approximately the same abundance as that from a potassium glass. It was difficult to quantitate the improvement in the sensitivity afforded from the use of K₂CO₃ compared to use of a potassium bead due to the relatively large sample sizes needed for a K+IDS analysis on the BDTOF mass spectrometer. The sensitivity did, however, appear to be improved with the use of K_2CO_3 .

1. Polyethylene Glycol (PEG) 600

Polyethylene glycols are liquid and solid polymers of the general formula $H(OCH_2CH_2)_nOH$. Polyethylene glycol 600 (PEG 600) has an average value of n between 12.5 - 13.9, and a molecular weight range of 570 - 630 u. PEG 600 was analyzed by placing 1 μ l of neat PEG 600 on the wire sample holder and 1 μ l of a K_2CO_3 solution in H_2O on the rhenium filament wire and the H_2O allowed to evaporate. The current in the rhenium wire was set to 2.7 A and the data collected at 10 mass spectra/second from 250 to

930 u. The desorption profiles for the oligomers with n = 5,8,11,13,16,and 19 are shown in Figure 5.12. The desorption of PEG 600 is complete in approximately 6 seconds with increasing desorption times with increasing size of the oligomer. The 10 mass spectra/second acquisition rate allows an accurate reconstruction of the desorption profiles for the MK+ ions representing each of the oligomers in the mixture and provides a data base that contains mass spectra during the early and late stages of the desorption process. Figure 5.13 shows the mass spectrum resulting from the sum (scans 40 to 50) of the mass spectra early in the analysis; Figures 5.14 and 5.15 are the mass spectra that result from the sum of the mass spectra in scans 50 to 60 and scans 70 to 80, respectively. The mass spectrum in Figure 5.16 is the sum of all scans represented in Figures 5.13-13 (scans 40 to 80).

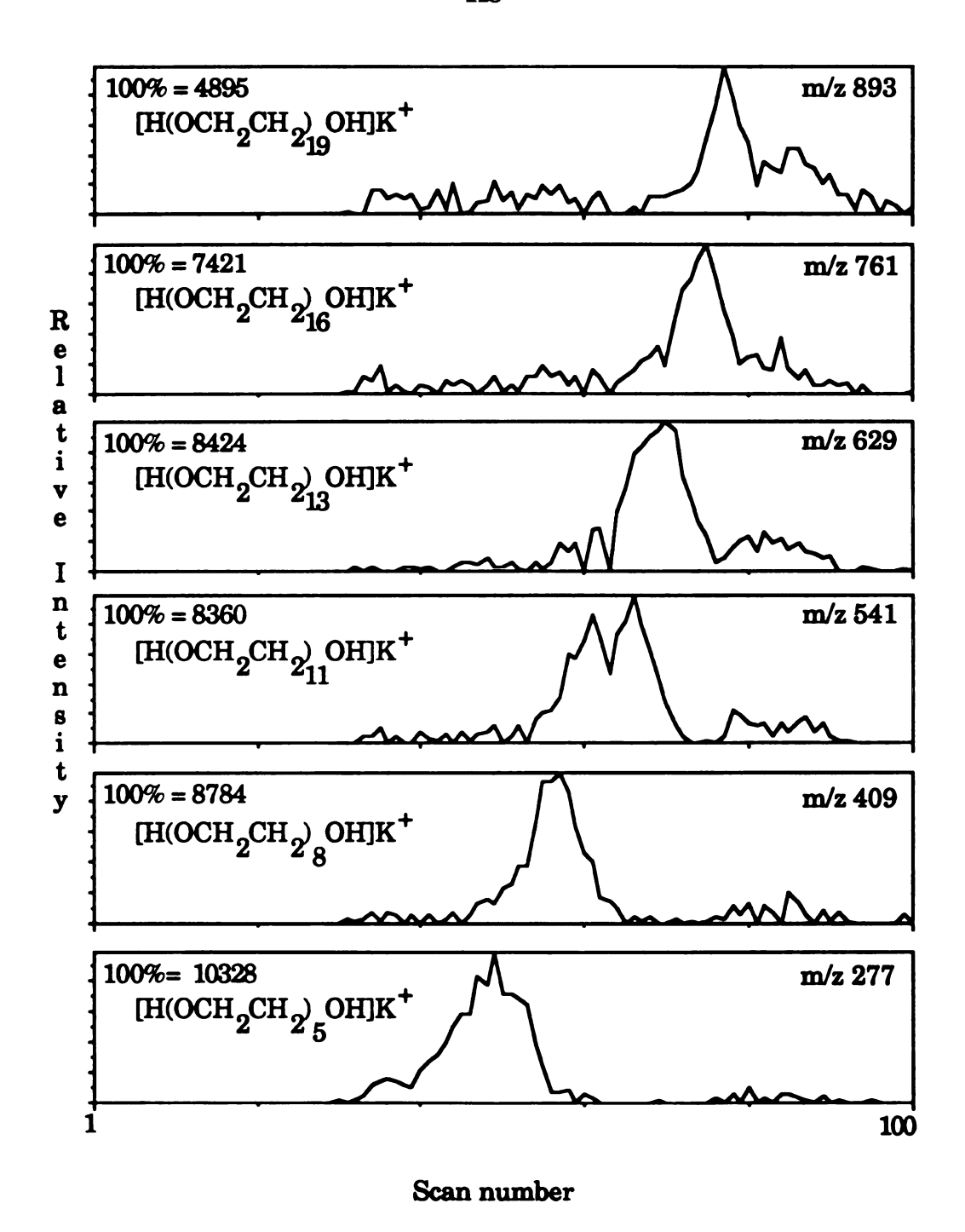
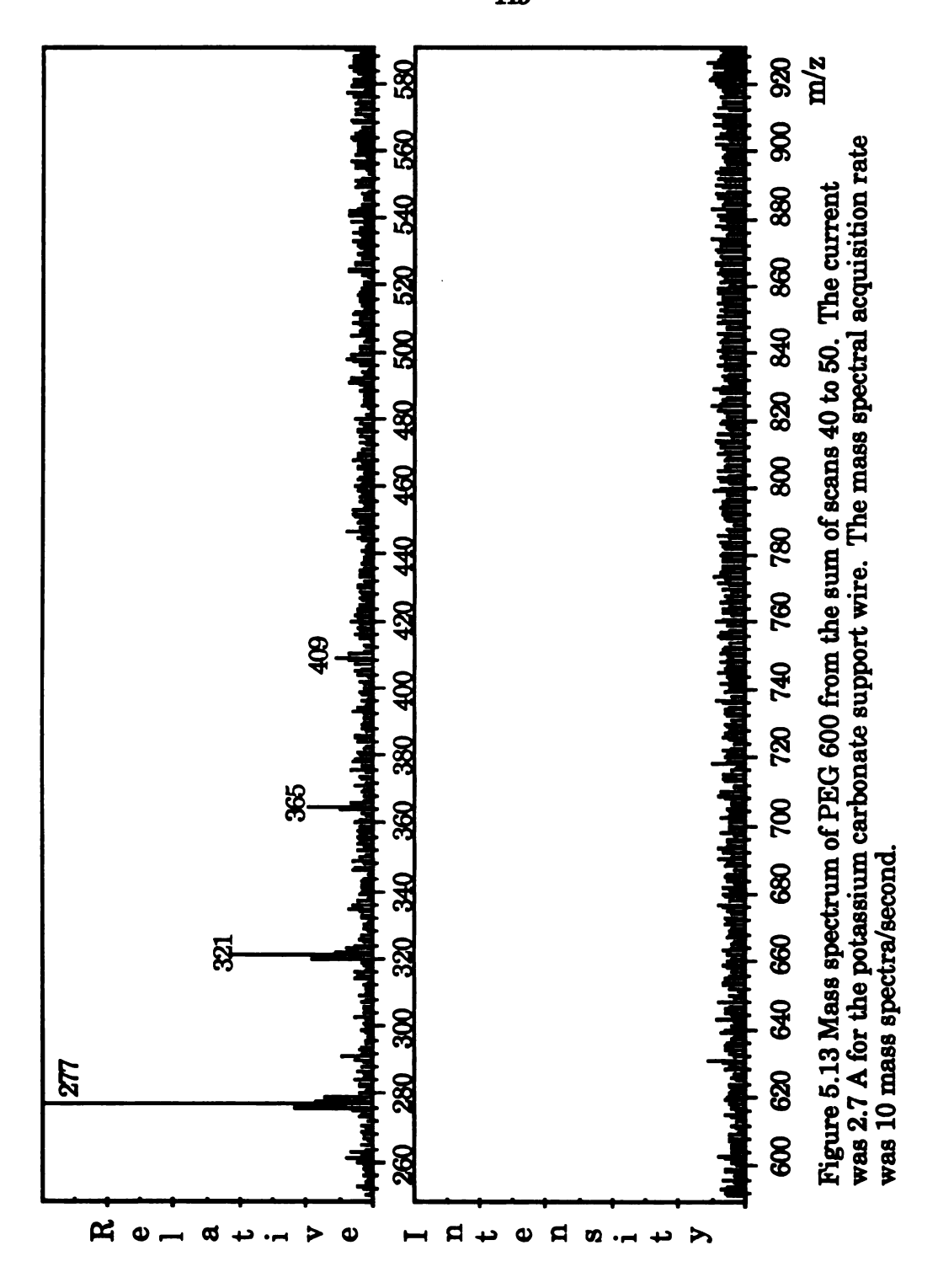
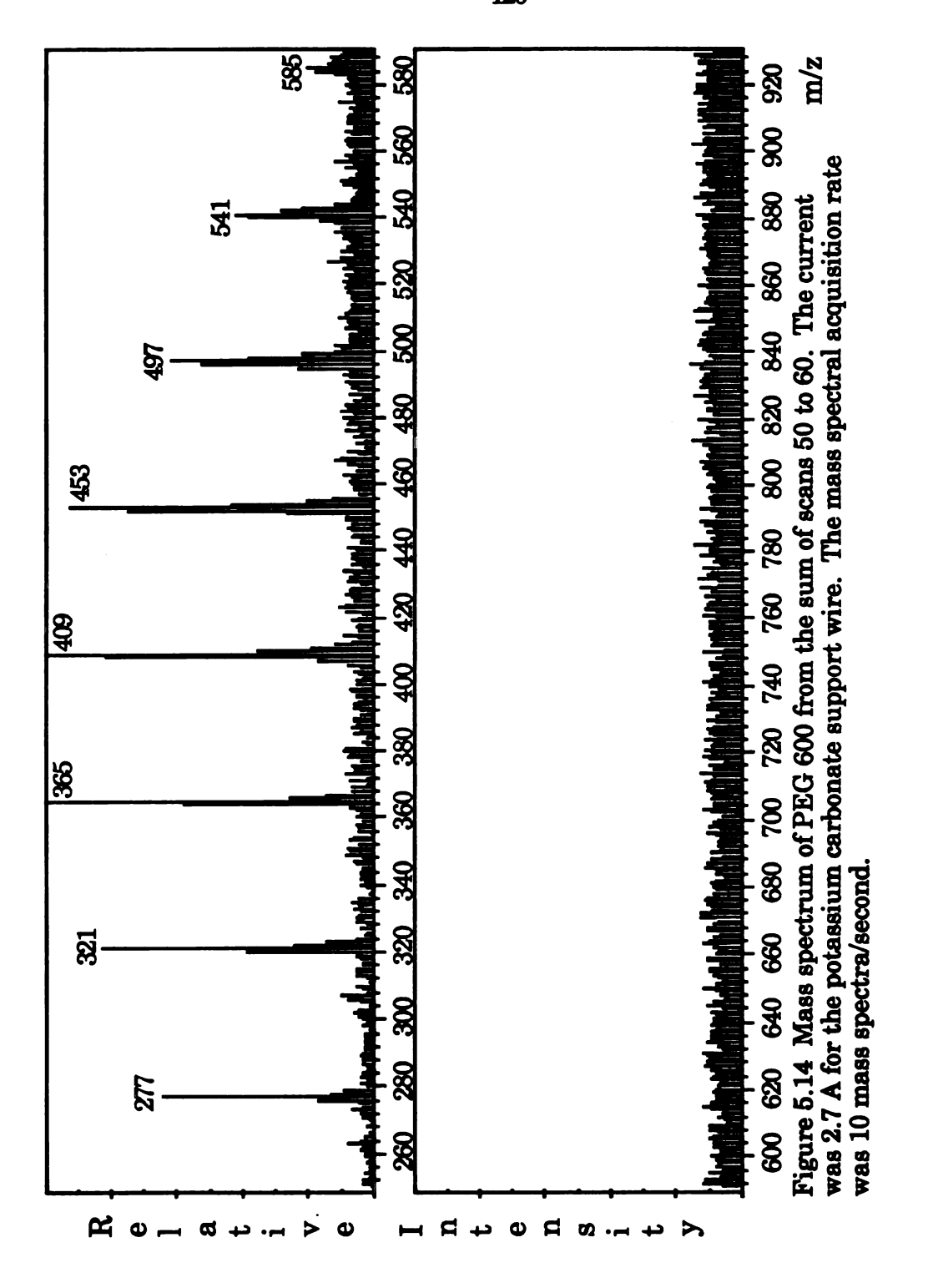
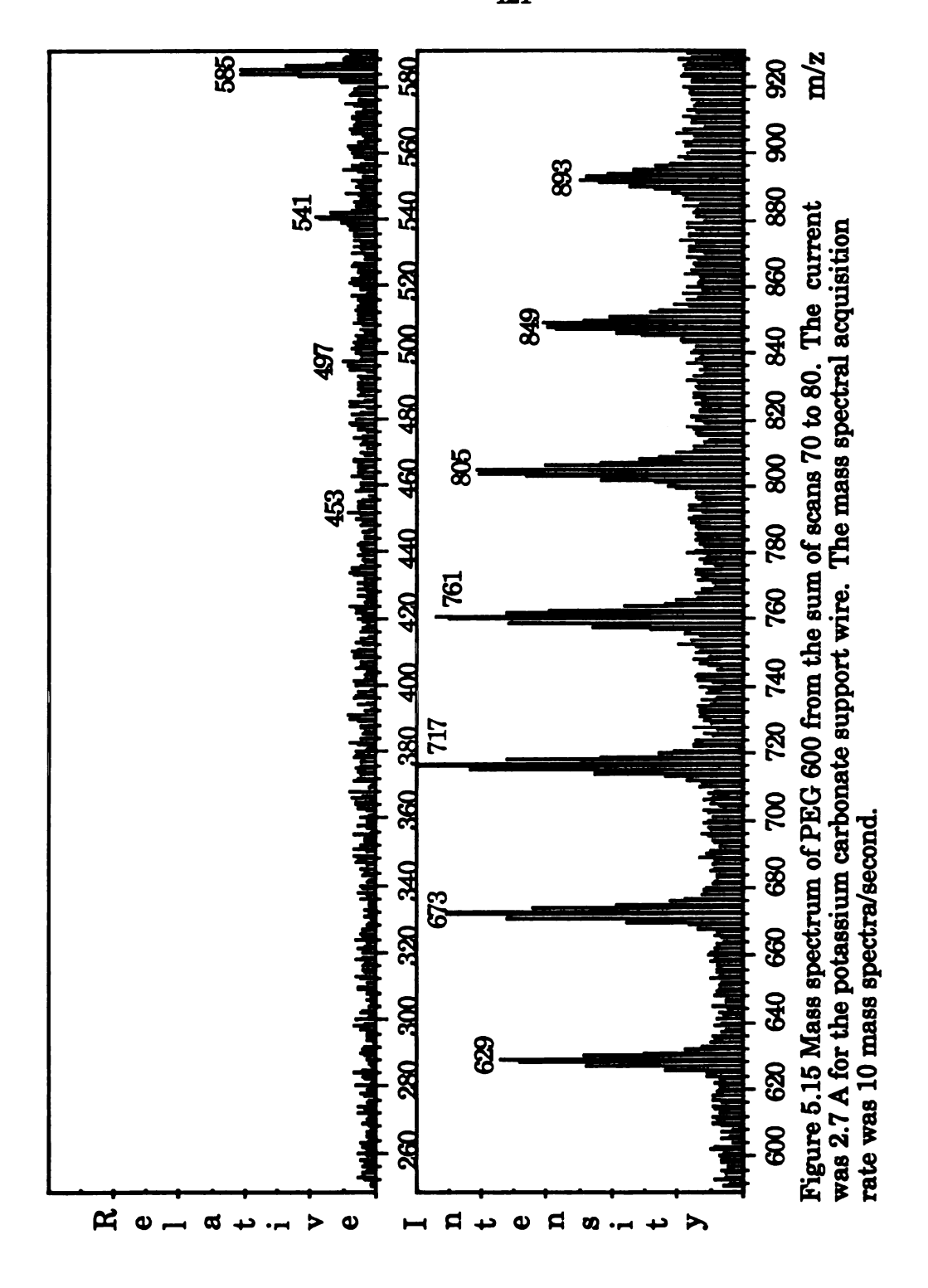


Figure 5.12 Desorption profiles for oligomers with n=5,8,11,13,16,and 19 for PEG 600. A potassium bead current of 2.7 A and mass spectral acquisition rate of 10 mass spectra/second were used.







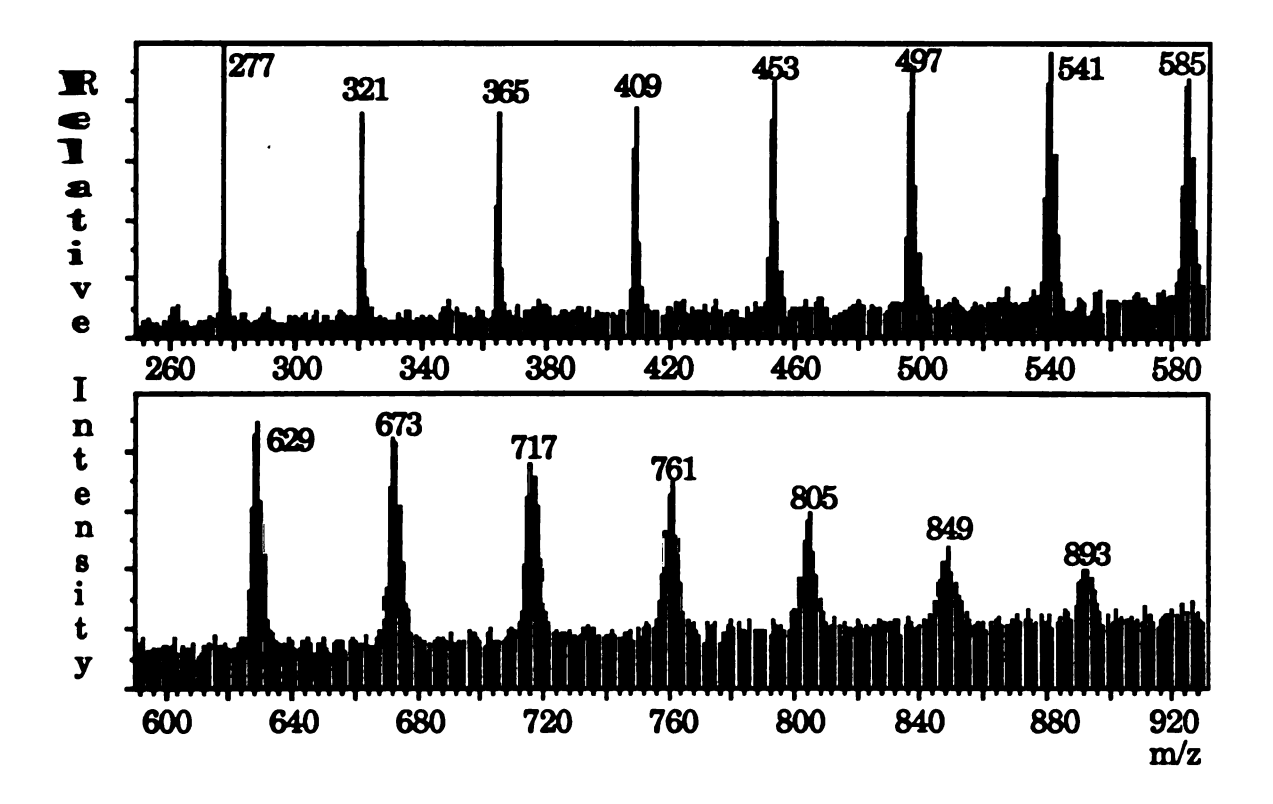


Figure 5.16 Mass spectrum of PEG 600 from the sum of scans 40 to 80. The current was 2.7 A for the potassium carbonate support wire. The mass spectral acquisition rate was 10 mass spectra/second.

Figure 5.16 shows the distribution of the oligomers in PEG 600 and can be used to provide information on the number-average molecular weight and weight-average molecular weight for this polymer.⁷² The number-average molecular weight, M_n , is defined by $M_n = \sum N_i M_i / \sum N_i$ where N_i is approximated by the peak intensity for each oligomer of molecular weight M_i . The weight-average molecular weight, M_w , is defined by $M_w = \sum N_i M_i^2 / \sum N_i M_i$. The peak intensity at each M_i was corrected by subtraction of the background intensity observed in Figure 5.16 at each m/z value. For this particular analysis, $M_n = 603$ and $M_w = 642$.

The analysis of PEG 600 by K+IDS can also provide structural information of the monomeric units of the polymer. The mechanism of fragmentation for K+IDS is believed to be a 1,2-elimination followed by K+ adduct formation of neutral species in the gas phase.²⁶ Figure 5.17 shows the mass spectrum of the low mass ions of PEG 600. Scheme I shows the fragmentation pathways and resulting ion series labeled as A,B,C, and D for PEG polymers. The four series of fragment ions observed in the mass spectra of PEG polymers are labeled in the mass spectrum in Figure 5.17. The fragmentation observed is sufficient to determine the structure of the polymer for this analysis.

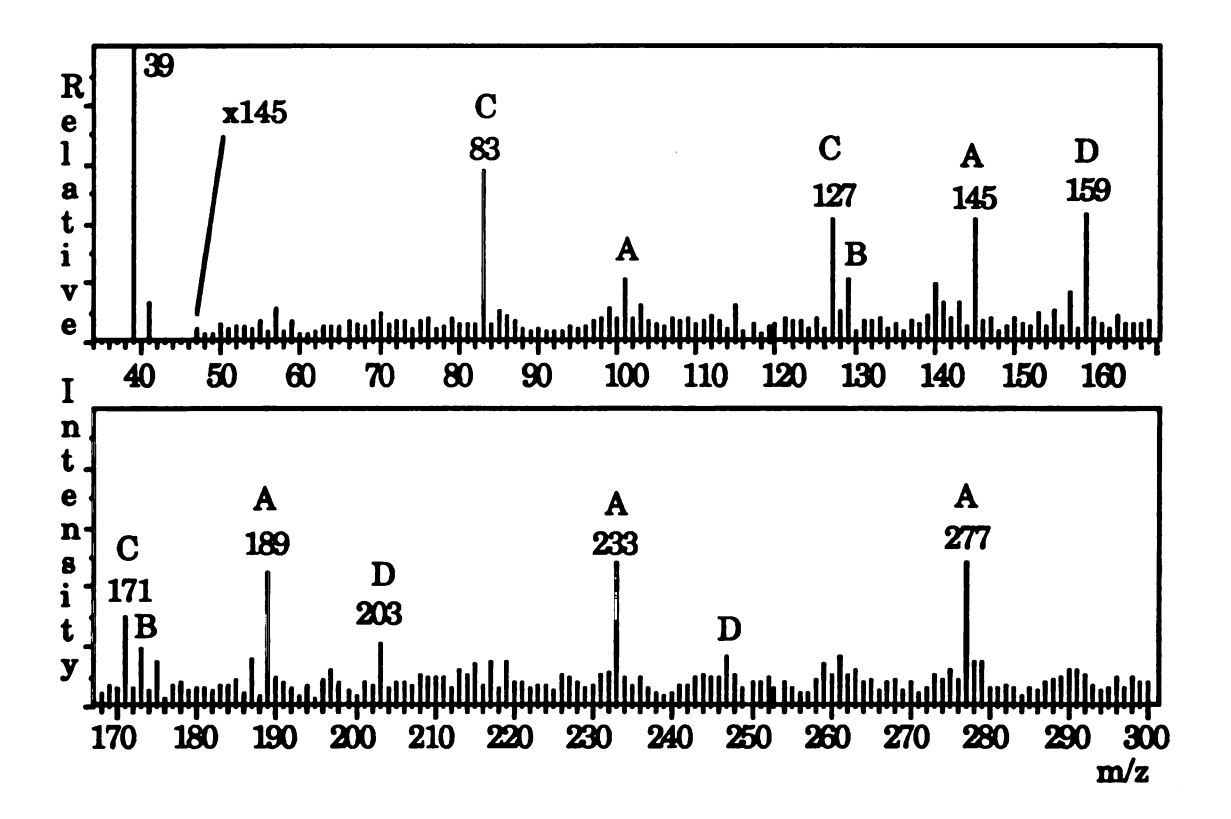


Figure 5.17 PEG 600 mass spectrum showing low mass ions. The scan rate is 10 mass spectra/second. Bead current is 2.6 A. Average of scans 20 to 100. Peaks are labeled based on Scheme I.

Scheme I

A [HOCH₂CH₂OCH₂CH₂(OCH₂CH₂)_nOH]K⁺

[HOCH₂CH
$$_{2}$$
O
 CH_{2} CH₂(OCH₂CH₂)_nOH]K⁺
 $-$ HOCH₂CH=O
 CH_{3} CH₂(OCH₂CH₂)_nOH]K⁺

В

D

CH₂=CHOCH₂CH₂(OCH₂CH₂)_nOHJK⁺

$$CH_2 = CHOCH_2CH_2(OCH_2CH_2)_nOHJK^+$$

$$\begin{array}{c} O \longrightarrow CH_2 \\ CH_2OCH_2CH_2(OCH_2CH_2)_nOH]K^+ \\ & \downarrow -CH_2=O \\ CH_3OCH_2CH_2(OCH_2CH_2)_nOH]K^+ \end{array}$$

The K+IDS analysis of PEG 600 with the BDTOF mass spectrometer does not induce as much fragmentation as that previously shown using the HP 5985 mass spectrometer. The BDTOF ion source was maintained at room temperature except for heating of the ion source by the potassium glass during each analysis by K+IDS. The mass spectra show fragment ions in the oligomers from n = 1 to 4 with little to no fragmentation in the larger oligomers. The temperature of the ion source used on the HP 5985 mass spectrometer is typically operated at 100°C and may contribute to the increased fragmentation and the duration of the adduct ion currents observed in K+IDS analyses using this instrument.

One observation from the mass spectrum of PEG 600 in Figure 5.16 is the broad increase in the width of each peak as the m/z increases. Figure 5.18 shows a region of the PEG 600 mass spectrum collected as raw data, with data points collected at 5 ns intervals. Peaks at m/z 581, m/z 585 and at m/z 590 are labeled in the figure. The mass resolution appears to be greatly reduced compared to that of the BDTOF mass spectrometer operated in the EI mode. This phenomenon is still under investigation, but is most likely due to the energy distribution in the ions upon formation. If this is so, installation of the electric sector between the ion source and the flight tube, as in the BEDER-TOF mass spectrometer, may improve the mass resolution.

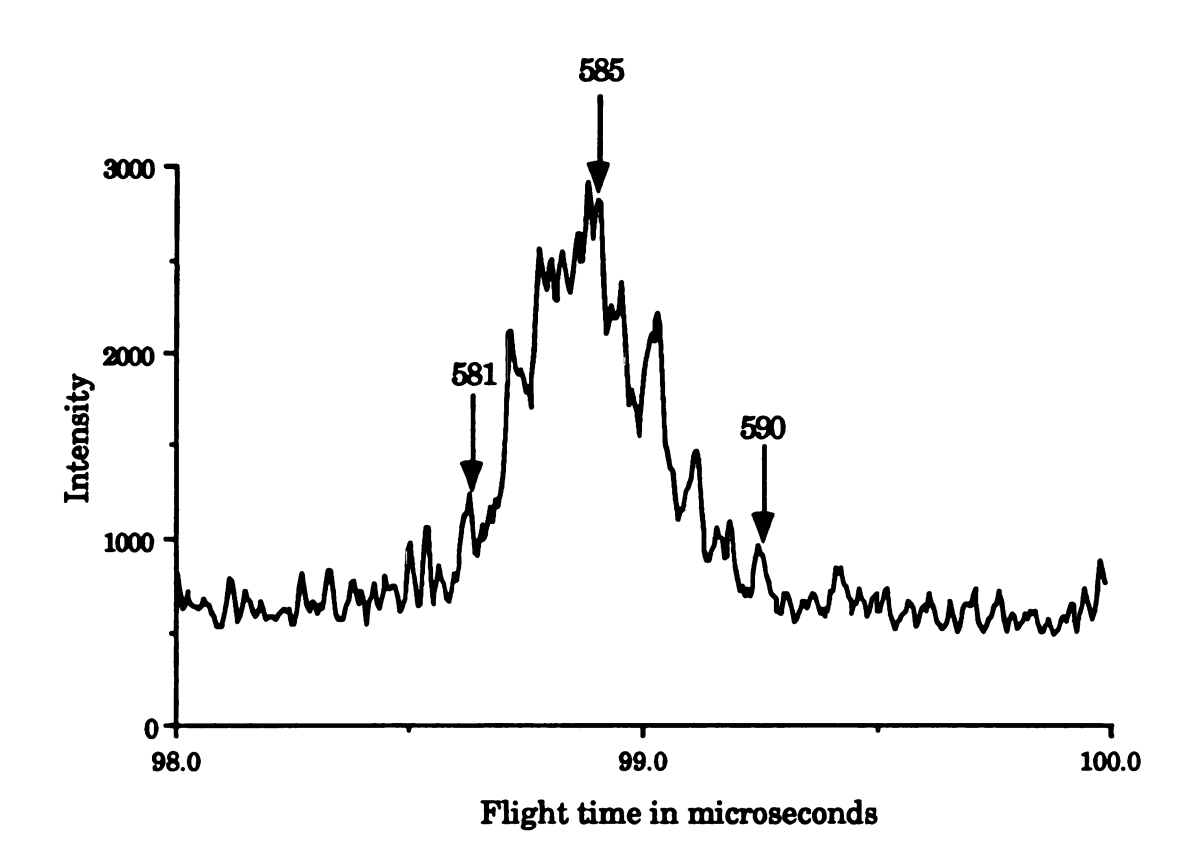


Figure 5.18 Raw data collected at 5ns time bins in flight time region of m/z 585 of PEG 600.

2. PEG 750

Figure 5.19 shows the K+IDS mass spectrum of PEG 750 with a potassium bead current of 2.6 A at a mass spectral acquisition rate of 10 mass spectra/second. A comparison of the mass spectra for PEG 600 (Figure 5.16) and PEG 750 show that the distribution of oligomers is shifted to a higher value of n as expected. Again, the distribution of the oligomers

in PEG 750 can be used to determine the number-average molecular weight, M_n , and the weight-average molecular weight, M_w . The peak intensity at each M_i was corrected by subtraction of the background intensity observed in Figure 5.19 at each m/z value. The experimental number-average and weight-average molecular weights are $M_n = 633$ and $M_w = 660$, respectively. The low values for M_n and M_w may result from approximating N_i by the peak intensity for each oligomer. The broad increase in peak widths at the higher m/z values may be responsible for the low peak intensities. Another factor that may contribute to the low values for M_n and M_w is the dependence of the detectors ion detection efficiency on m/z value. This dependence would be difficult to quantify.

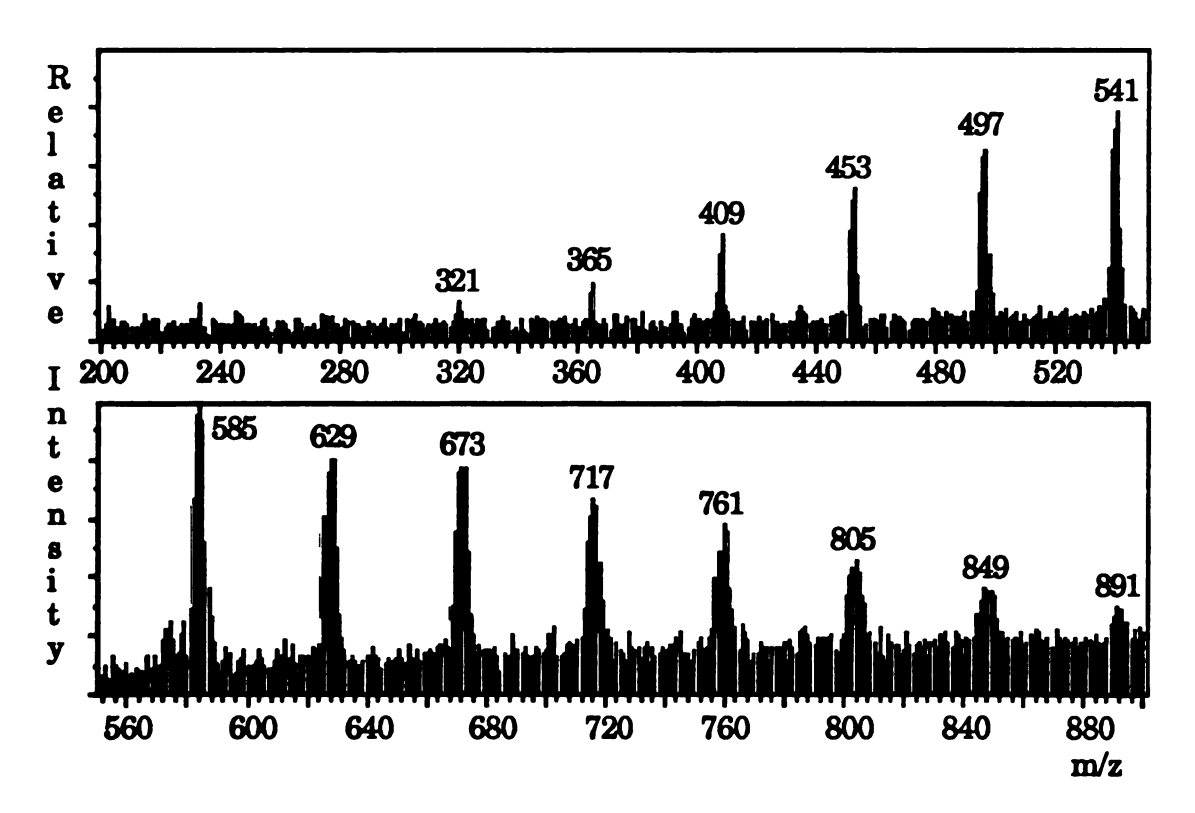


Figure 5.19 K+IDS mass spectrum of PEG 750 from average of scans 50 to 80. Bead current of 2.6 A was used at a mass spectral acquisition rate of 10 mass spectra/second.

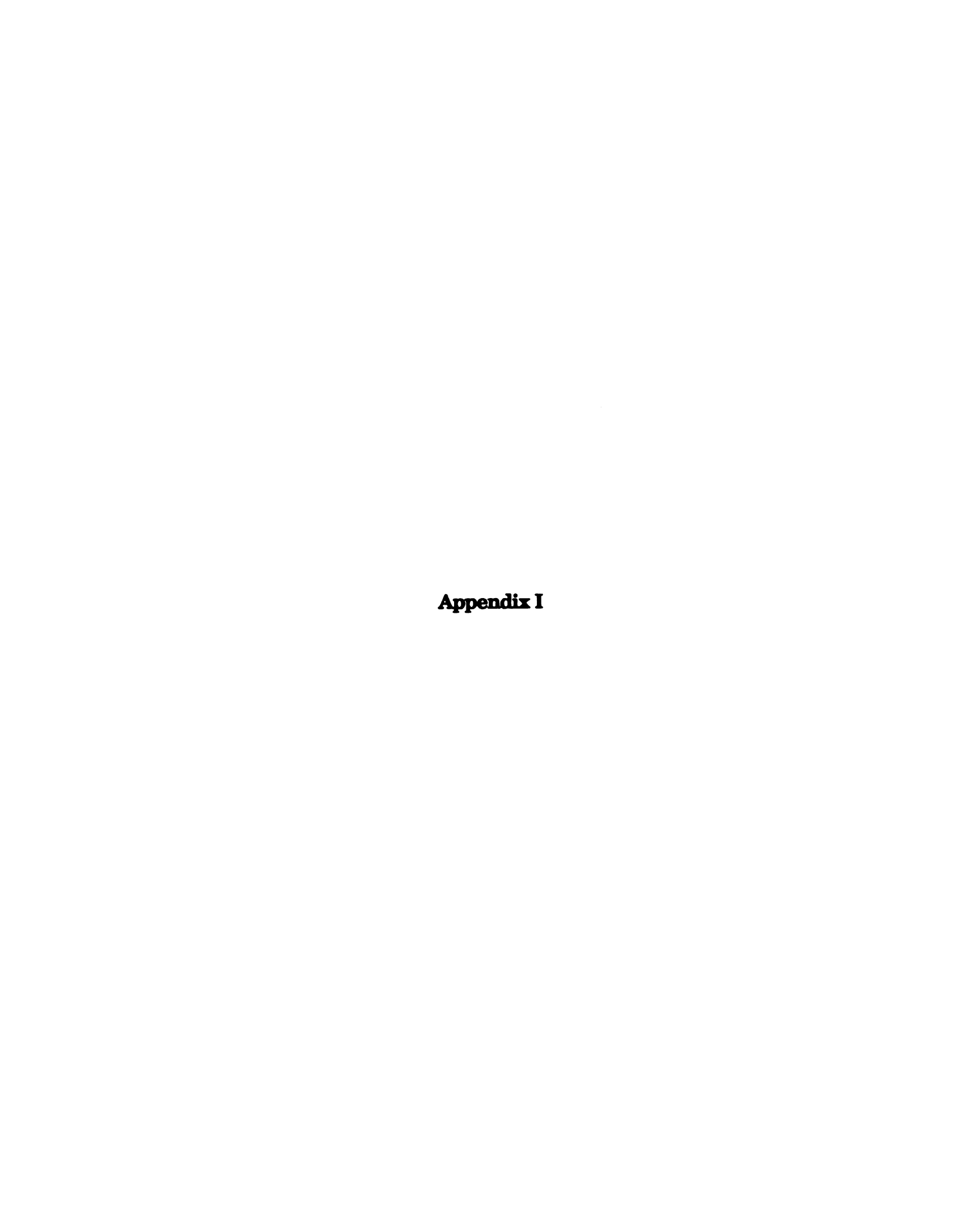
C. Current limitations of K+IDS by BDTOF-MS

There are a number of interesting conclusions that can be made from this work. The relative extent of conversion of the HP and BDTOF mass spectrometers are similar, if not the same, within experimental error. This means that whatever the sample size, both mass spectrometers produce the same relative amount of K+ adduct ions to potassium ions available. A limitation of the BDTOF mass spectrometer is the low ion current that is available for amplification compared to the HP 5985 quadrupole mass spectrometer. Also, the ion transmission efficiency of a quadrupole with wide apertures is much higher than that of a TOF mass spectrometer with narrow slits and beam deflection.

The comparison study of the HP 5985 and BDTOF mass spectrometers for the K+IDS analysis of acetone under K+ CI conditions determined that the HP 5985 mass spectrometer had similar detector output currents for the 4700 series CEM operating voltage of 1.2kV compared to the FTD-2003 operating at 2000 V. The Galileo FTD-2003 detector used in the BDTOF mass spectrometer is always operated at its maximum gain setting of 106 due to the low ion transmission efficiency of this instrument. The electron gain for the 4700 series CEM at an operating voltage of 1.2kV is 1 x 104.73 Therefore, it appears that the available ion current for detection is a factor of 100 higher for the HP 5985 compared to that in the BDTOF mass spectrometer. With a maximum electron gain of 4 x 106 possible for the 4700 series channeltron detector, it is apparent that improvements in the ion transmission efficiency or detector gain response is necessary for the

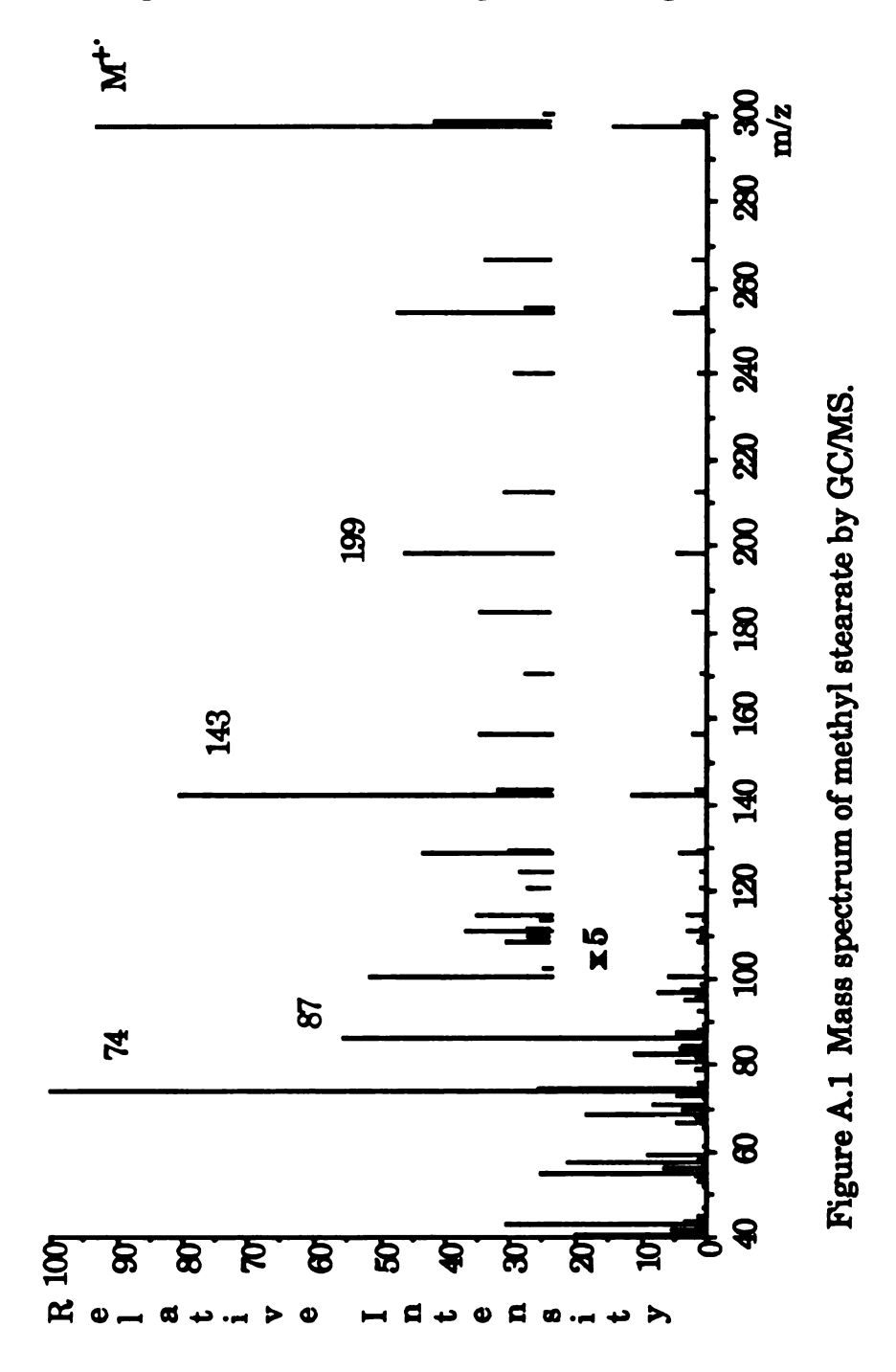
BDTOF mass spectrometer to utilize this instrument for further study of K+IDS.

The Becton-Dickinson MM-1-1SG may meet the gain requirements of the detector necessary for successful implementation of K+IDS on the BDTOF mass spectrometer. This detector can provide an electron gain up to 10⁹ when new or reactivated by the manufacturer. The detector gain for this type of detector (Cu-Be discrete dynodes) diminishes over time due to exposure to high currents and contamination due to exposure to the atmosphere. This detector was used for some of the K+IDS studies, but was not operating with its maximum gain characteristics because it was installed in the instrument after many years of exposure to the atmosphere.



Appendix I

Mass spectra of selected compounds using the BDTOF mass spectrometer



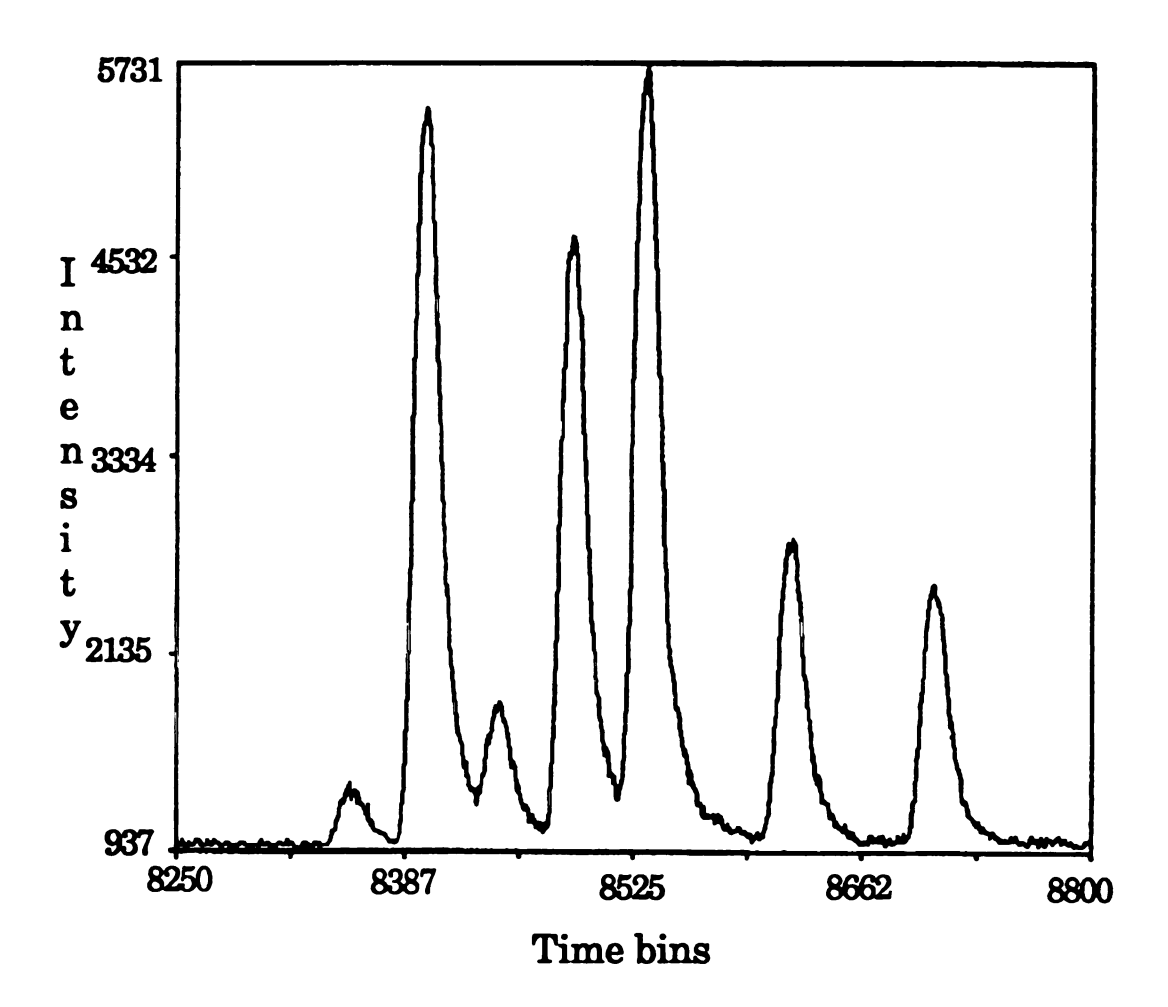


Figure A.2 EI mass spectrum of xenon with V_A of 1000 V. Beam deflection d spacing is 25 mm with no detector slit assembly.

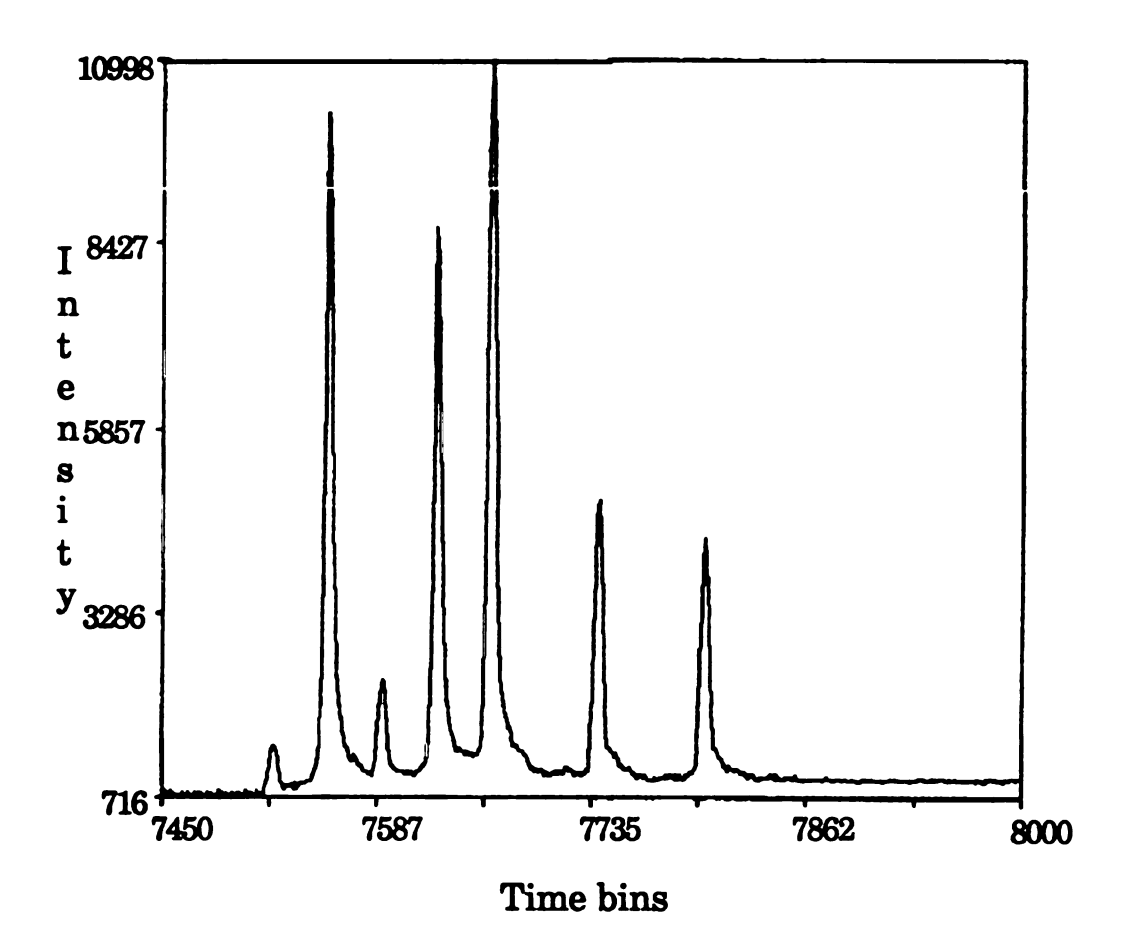


Figure A.3 EI mass spectrum of xenon with V_A of 1500 V. Beam deflection d spacing is 25 mm with no detector slit assembly.

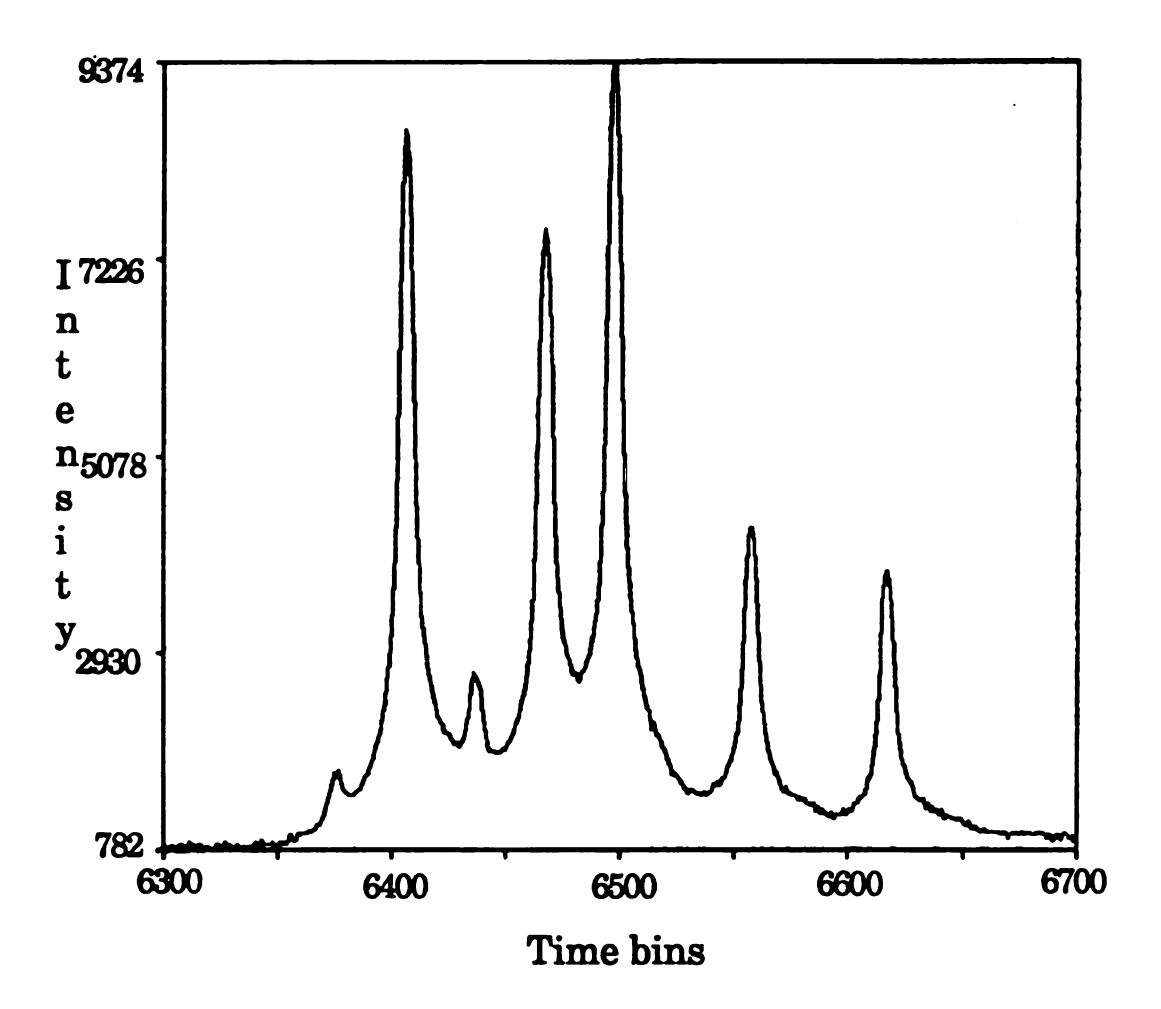


Figure A.4 EI mass spectrum of xenon with V_A of 2200 V. Beam deflection d spacing is 25 mm with no detector slit assembly.

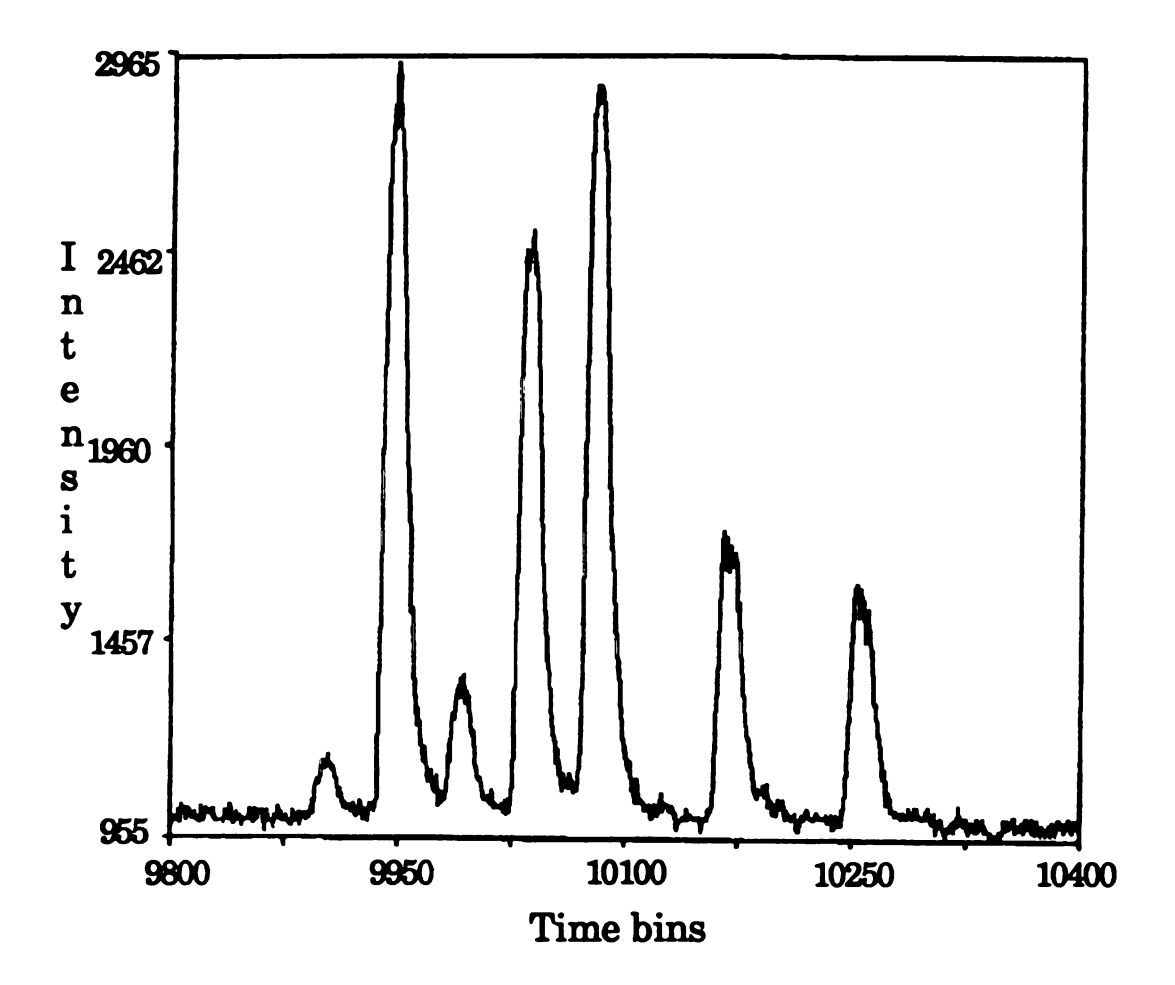


Figure A.5 EI mass spectrum of xenon with V_A of 1000 V. Beam deflection d spacing is 25 mm with the detector slit assembly adjusted to 5 mm.

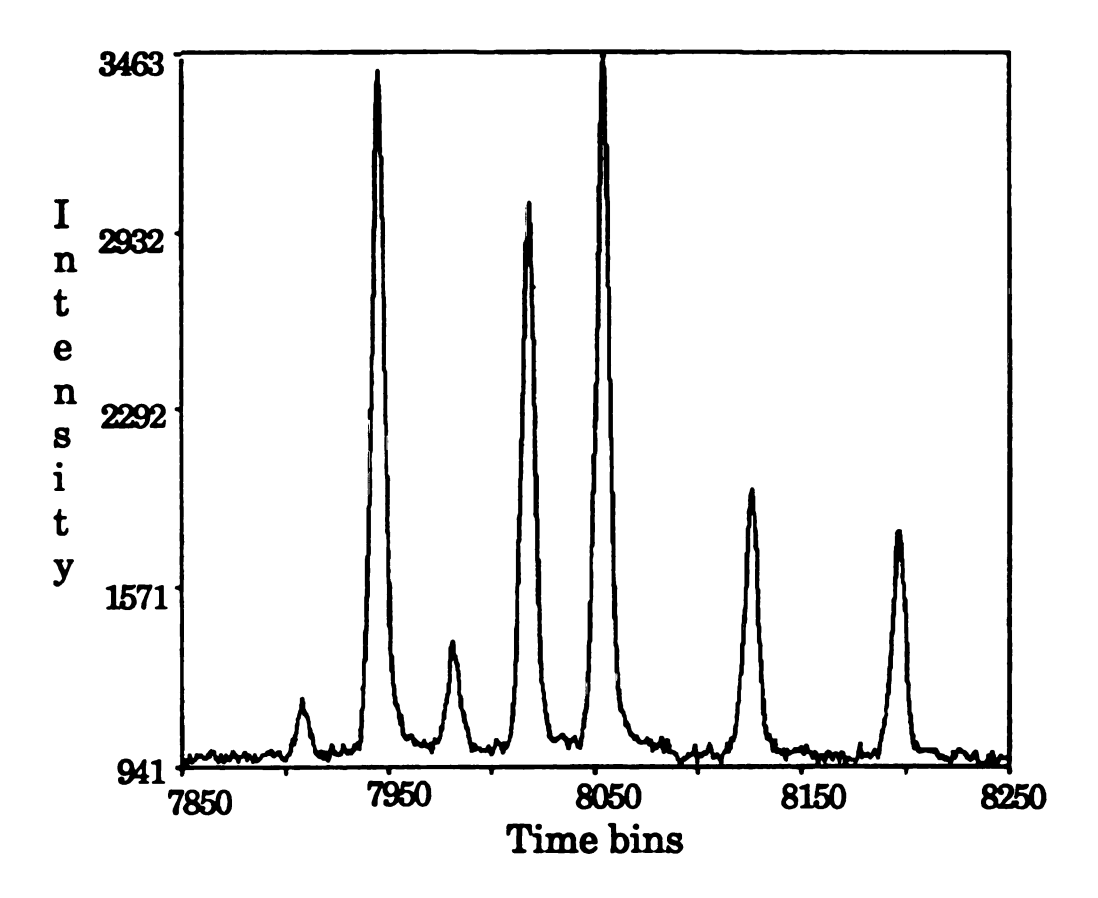


Figure A.6 EI mass spectrum of xenon with V_A of 1500 V. Beam deflection d spacing is 25 mm with the detector slit assembly adjusted to 5 mm.

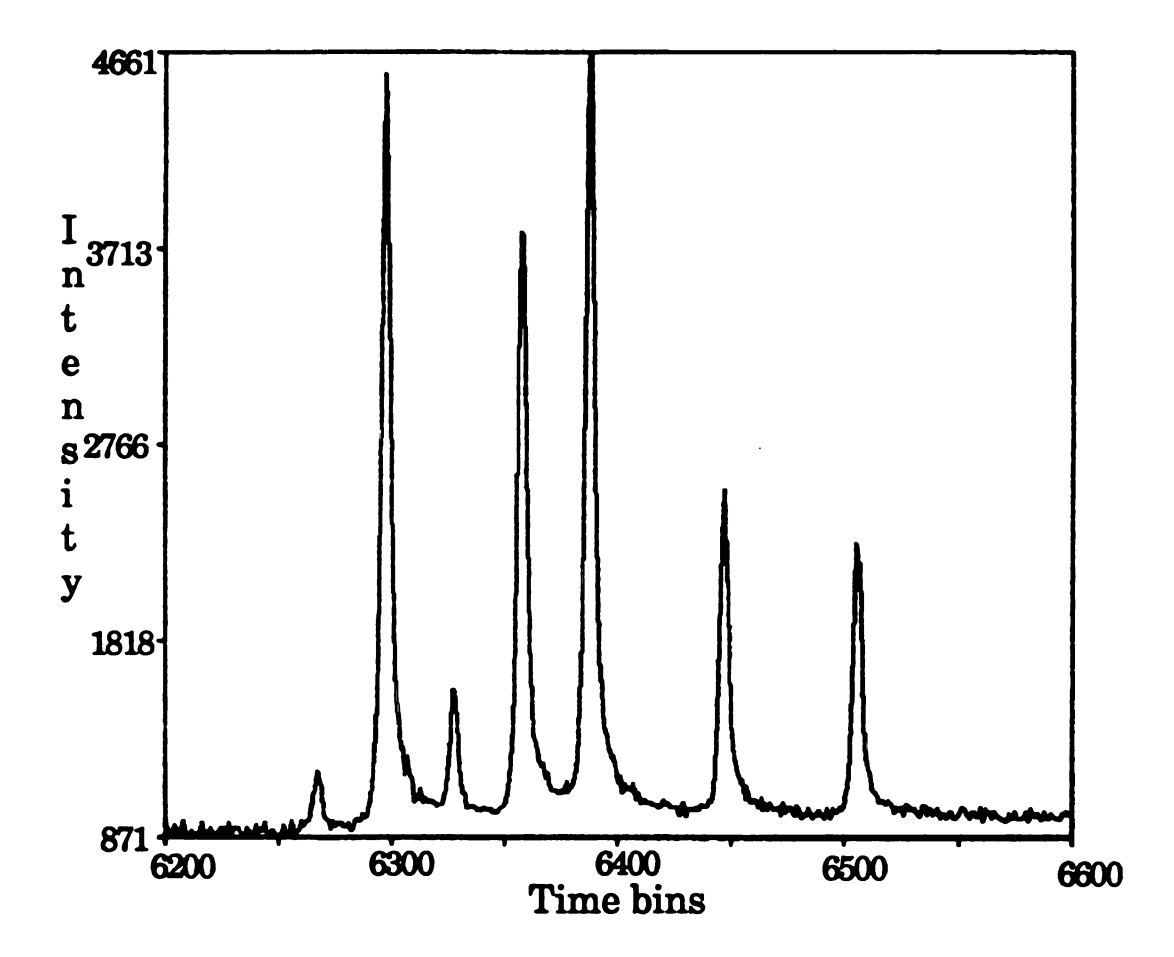


Figure A.7 EI mass spectrum of xenon with V_A of 2200 V. Beam deflection d spacing is 25 mm with the detector slit assembly adjusted to 5 mm.

vgvapg42.msu vgvapg 20ug 10sps sft0 grid em5000 5/2/91 Scans 42-52: 481 peaks; 100%= 39757, TII= 908061, Ret time =0.068

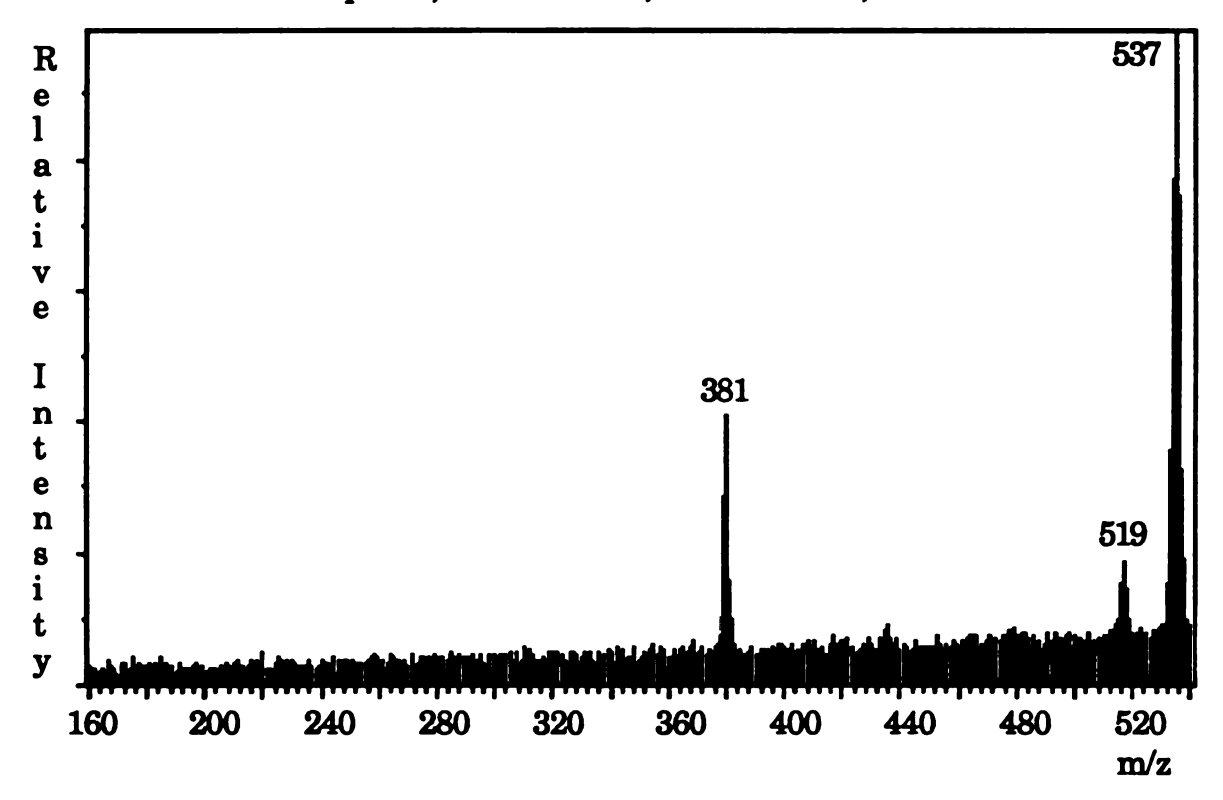


Figure A.8 K+IDS mass spectrum of the hexapeptide VGVAPG (MW = 498 u) at 10 mass spectra/second.



Beam Deflection for Temporal Encoding in Time-of-Flight Mass Spectrometry

G. E. Yefchak, G. A. Schultz, J. Allison, and C. G. Enke Department of Chemistry, Michigan State University, East Lansing, Michigan, USA

J. F. Holland

Department of Biochemistry, Michigan State University, East Lansing, Michigan, USA

The pulsed ion sources used in conventional time-of-flight mass spectrometry (TOFMS) generally do not provide adequate resolving power across the mass range required for applications such as gas chromatography combined with mass spectrometry (GCMS). Theoretical and experimental aspects of beam deflection techniques, which provide time encoding for TOFMS with continuous ions sources, are explored here. In this approach, ion source conditions do not affect resolving power, allowing for a greater variety of ionization modes to be used. Theoretical predictions for the resolving power attainable with beam deflection, which are satisfactory for GC/MS applications, agree well with experimentally determined values. The combination of GC-beam deflection-TOFMS with time-array detection is evaluated, and the capabilities of this system are compared to those of scanning mass spectrometers. (J Am Soc Mass Spectrom 1990, 1, 440–447)

Il varieties of time-of-flight (TOF) mass spectrometers share a need for synchronized ion packets from the ion source serves to indicate the starting times for ion velocity measurements, and the dimension of the ion packet determines mass resolving power. Although most TOF mass spectrometers make use of so-called pulsed ion sources (i.e., ion sources that generate ion packets directly), there are a number of circumstances in which it is desirable to use sources that produce ions continuously. Beams produced by these "continuous ion sources," which are similar to sources used in magnetic sector and quadrupole mass spectrometers, are spetially modulated as described below to create the desired ion packets for TOF mass analysis.

A theoretical treatment of beam modulation techniques in nuclear physics appeared in 1960 [1], and in 1973 many theoretical considerations for beam modulation in TOF mass spectrometry (TOFMS) were elegantly described by Bakker [2]. Shortly thereafter, Bakker reported the construction of a beam modulation TOF mass spectrometer and an experimental confirmation of the theory [3]. Various other TOF instruments incorporating beam modulation have since been reported, including those of Pinkston et al. [4], Glish and Goeringer [5], and Eckenrode et al. [6]. A beam modulation ion source was also developed for the early Bendix TOF spectrometers by Futrell and coworkers [7, 8]. In addition, a similar technique has

been used in a tandem TOF mass spectrometer to select parent ions prior to a second stage of mass analysis [9]. The "orthogonal-acceleration" TOFMS instrument recently described by Dawson and Guilhaus [10] incorporates beam-deflection in the broadest sense, but the operating principle of orthogonal acceleration differs sufficiently from conventional beam-modulation techniques to exclude its discussion in this work.

Ion packet production by modulation of a continuous beam eliminates some of the difficulties encountered with more conventional pulsed-source techniques, particularly when gaseous samples such as those encountered in gas chromatography combined with mass spectrometry (GC/MS) are ionized. With pulsed ion sources, three patterns of ion behavior can lead to decreased mass resolving power [11, 12]. The distribution of initial positions of ions within the source, especially important for gaseous samples, and the distribution of initial ion velocities both lead to a spread in final kinetic energy. This spread in kinetic energy leads to a distribution of arrival times for isomass ions and hence to the loss of resolving power. Furthermore, the thermal motion of ions moving with equal speeds toward and away from the source exit prior to the application of the extraction field results in the "turn-around" separation between isomass ions ultimately having identical on-axis energies. The deterioration of resolving power due to this turn-around problem has normally been most severe. necessitating the use of high extraction field gradients that minimize the turn-around time in pulsed ion sources. Unfortunately, the use of large field gradients exacerbates the spatial problem; this incompatibility between space

Address reprine requests to C. G. Ente. Department of Chemistry, Michigan State University. Sant Lansing, MI 48634.

focusing and energy focusing with gaseous samples has been described in the literature [11, 13]. Production of ion packets by modulation of continuous beams eliminates the turn-around problem because all ions in the accelerated beam are moving in the same direction. Furthermore, this elimination of the turn-around effect permits low extraction gradients to be used, which significantly decrease the energy spread caused by the initial spatial distribution. For these reasons, studies of beam modulation have been undertaken in an effort to achieve adequate mass resolving power in GC/MS with TOF instrumentation. Both the theoretical and experimental results reported here demonstrate that beam deflection TOFMS is a viable technique for GC/MS when used in combination with time-array detection.

Methodology

The beam deflection TOFMS used for this study was constructed by adapting the electron impact ion source from a Dupont 21-491B double-focusing mass spectrometer to a Bendix 12-101 TOFMS flight tube having a 2.1 m length. The ion source was operated at an accerating potential of 3 kV in a continuous ion extraction mode. The ion beam enters the flight tube region where beam modulation takes place. The beam deflection assembly was constructed from copper-plated circuit boards and consists of two plates, 1.4 cm in length × 2.0 cm in height, separated by a distance of 1.3 cm. This assembly was placed about 2 cm past the source exit slit. A Galileo CEMA detector was used to collect the ion current. The overall geometry of the instrument is shown in Figure 1.

Two dynamic voltages are used in tandem to modulate the continuous ion beam. Initially, the voltage applied to one of the plates is held at +63 V, while the voltage applied to the other plate is 0 V. When beam modulation is desired, these voltage levels are switched, in approximately 10 ns, to 0 V and +63 V, respectively. This is equivalent to the case in which one plate is held at ground potential throughout the experiment while the other plate is swept from -63

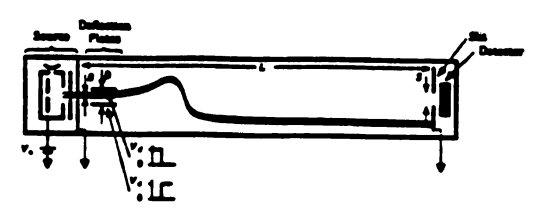


Figure 1. Schematic diagram of the beam-deflection TOFMS instrument. The parameters of interest include the beam width, B, the deflection plate separation. D, the flight-path length, L, and the detector aperture width, S. Ions are accelerated by the voltage V_a applied between the source block and the source exist slit. Beam deflection is accomplished by the voltage V_d applied to the upper and lower deflection plates as shown (see text).

V to +63 V (i.e., V_d = 63 V for the equations given below). The dual-voltage approach is used so that the magnitude of the field reversal can be twice as great, for the same rise time, as would be possible with only one pulsed voltage. The new voltage applied to each plate is maintained for 100 µs, which allows all of the ion packets to strike the detector surface before the next ion modulation occurs. This modulation generates a new set of ion packets, but the signal produced by these ions is ignored by the detection equipment so that only transients generated by every other modulation are collected. This process, which allows a 5kHz sampling rate, is used in order to avoid difficulties caused by asymmetry between the rising and falling edges of the deflection pulses. The beam modulation circuitry was designed in-house; schematic diagrams for the circuits may be obtained from the authors.

Computer programs used for the simulations were written in VAX-11 C and run on a Digital Equipment Corporation VAXstation 3200 computer (Mavnard, MA). The animation program was written in Microsoft QuickC (MicroSoft, Redmond, WA) and run on an IBM-AT compatible computer.

Theory

Models for Beam Modulation Techniques

The ideal desired behavior of all beam modulation techniques is illustrated in Figure 2; a packet having an arbitrarily short temporal width is "chopped" out of a continuous beam. Note that the packet retains the kinetic energy distribution present in the original beam and is finite in spatial and temporal width; these are the only nonidealities if the fringing rields near the ends of the deflection plates are ignored. All ions depicted in Figure 2 and throughout this work have the same mass-to-charge ratio. In actual operation. It course, an instrument would produce ions of various masses. Ion trajectories in a beam deflection inclument are independent of mass, though the velocines of the different isomass packets are mass-dependent.

Modulation techniques have so far all relied upon deflection of the beam by an electric field, generated by some voltage function V(t), applied across a pair of deflection plates between which the ions pass. Some portion of the beam is deflected across an aperture, causing an ion packet to emerge from the opposite side. Various V(t) functions may be used to generate ion packets via at least three modes of ion behavior. The ion behavior patterns corresponding to these modes

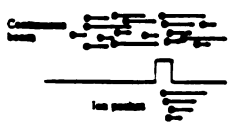
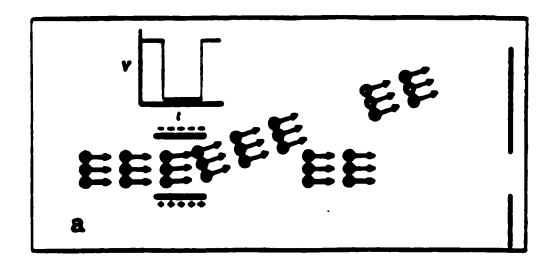
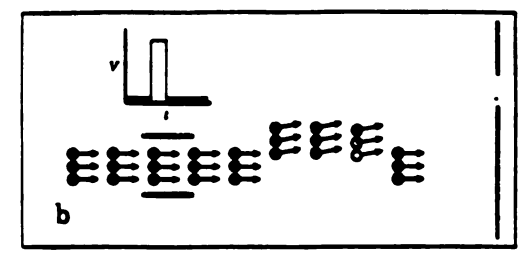


Figure 2. Ideal ion behavior in beam modulation: the process essentially yields a slice from the continuous beam. Arrow lengths indicate relative ion velocities; only isomass ions are considered.





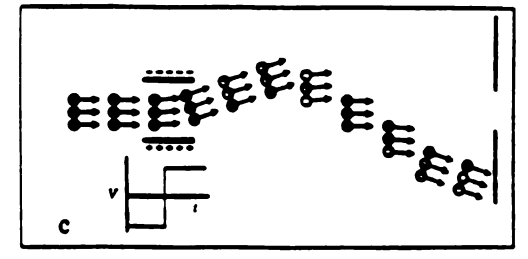


Figure 3. Three models for beam modulation techniques. Isomass ions are shown to pass through a pair of deflection places and move toward an aperture. Relative duration and polarity of the deflection voltage pulse is indicated for each case. The darker shading indicates ions that will pass through the aperture and form the ion packet. (a) Gate model: (b) Impulse Sweep model: (c) Differential Impulse Sweep model:

are illustrated in Figure 3. These include a pattern referred to here as the Gate mode, as well as the impulse Sweeping and Differential Impulse Sweeping modes that were identified by Fowler and Good [1]. In each of these modes, the "default" condition, which exists before and after application of the packet-forming voltage pulse, is the deflection of the ion beam away from the aperture. In the Gate mode (Figure 3a) the field changes to allow the beam to pass directly through the aperture for some period of time; at the end of this time the field returns to its original state. In this mode V(t) serves most closely as a "gate," either preventing or allowing passage of ions through the aperture. The Impulse Sweep mode (Figure 3b) is similar to the Gate mode in that the field is pulsed "on" for a period of time and then returned to its original value. In Impulse Sweeping, however, the deflection voltage pulse is short in duration, compared to the flight time through the plates. The pulse serves to add a velocity component perpendicular to the direction of ion motion; the resulting angular trajectories cause part of the beam to be swept into the aperture. Here the width of the emerging ion packet is related, but not equal, to the duration of the deflection pulse. The width and ion trajectories are also mass-dependent in this mode. Impulse Sweeping has been difficult to accomplish because it requires precise geometrical designs as well as a voltage impulse of precisely defined amplitude. Furthermore, it does not appear to have any advantage over the other two modes, so it will not be discussed further here. In the Differential Impulse Sweep mode (Figure 3c), the deflection voltage switches polarity, causing a "kink" to form in the beam. The portion of this kink that continues to move parallel to the original beam passes through the aperture to form the packet. A referee has noted that a type of Differential Impulse Sweeping could also be accomplished with unequal switching voltages.

The Gate mode is the simplest case. Here the width of the ion packet is essentially equal to the duration of the deflection pulse (neglecting the intermediate ion behavior that occurs when the voltage change takes place). Ions that pass through the plates while the deflection field is off continue onward and pass through the aperture; those that pass through before or after this pulse do not. In the description of this mode, the transient ion behavior caused by the voltage change itself is ignored; only the steady-state trajectories either through or away from the aperture are considered. Ion packets produced in the Gate mode are therefore always longer in duration than the flight time of the ions through the deflection plate region. This disadvantage may perhaps be offset by the fact that the Gate mode yields ion packets for which the temporal width is independent of mass.

The transient ion behavior that was ignored in the Gate mode is in fact responsible for packet formation in the Differential Impulse Sweep mode. This mode is therefore capable of producing much shorter ion packets. Consider ions that enter the deflection plate region just before the switch in the field direction. (The time under consideration here is somewhat earlier than that of the "snap shot" shown in Figure 3c.) These ions are deflected downward as they travel through the region. When the field changes polarity, however, they begin to experience an upward force. Those ions that have traveled half-way through the plate region when the pulse occurs will experience equal durations of downward and upward forces and thus exit the region moving parallel to their original trajectory. The aperture is assumed here to be located in line with the initial beam axis and the deflection plates. Some ions very near to the exact half-way point of the deflection plate region at the time of the field reversal will also obtain final trajectories that allow for their passage through the aperture. The extent to which this occurs contributes to the temporal width of the packet and will be discussed in the following section.

Ion Packet Quality

As derived by Bakker [2], the temporal base width of an ion packet resulting from the Differential Impulse Sweep process is given by the expression

$$w_t = \frac{(B+S)D}{LV_d} \sqrt{\frac{V_d m}{2e}}$$
 (1)

where B is the beam width, S is the aperture width, D is the deflection plate separation. L is the distance between the plates and the slit, and V_a and V_d are the acceleration and deflection voltages, respectively. (That is, the deflection voltage switches from $-V_A$ to $+V_A$.) The subscript in wi is meant to represent "ideal" because this is the width that would be obtained if the ion beam were ideal in terms of kinetic energy and angular dispersion. The principal assumptions for eq 1 are that the rise time for the voltage change is negligible and, more importantly, that the distance from the plates to the aperture, L, is much greater than the length of the plates. (Note, however, that the actual plate lengths do not appear in the expression.) This latter assumption implies that the aperture should not be placed near the deflection plates but rather at the detector. In fact, it is possible for the detector surface itself to serve as the aperture.

In addition to the ideal width w_l derived by Bakker, the packet is broadened by the kinetic energy distribution of ions within the packet. Two ions leaving an initial position x=0 simultaneously, but with differing kinetic energies U and $(1+\beta)U$, will arrive at a location x=L separated in time by $\Delta t \approx \beta L(2m/U)^{1/2}/4$. Thus, an ion packet having negligible initial width but with a normal kinetic energy distribution having standard deviation σ_U would be broadened, after traveling distance L, to have a half-width given approximately by

$$w_U = \sqrt{\frac{2m}{V_e e}} \frac{\beta L}{4} \tag{2}$$

where $\beta = 2.35 \sigma_U/U_0$.

A third cause for packet broadening was identified in this study for ion beams having nonzero angular divergence. Consider the two ions shown in Figure 4. The lower ion enters with no off-axis energy and is initially accelerated downward by the deflection field. As it reaches point a, half-way through the plate region, the field reverses and accelerates the ion in the upward direction. Since downward and upward force are experienced for equal periods of time, the ion leaves the region with no off-axis energy and thus is included in the final packet. The upper ion enters the region Δt seconds prior to the lower ion and at an angle from the beam axis. Due to its off-axis energy, this ion continues to move upward for a period of time but is eventually deflected downward by the electric field. This ion experiences the downward force longer than

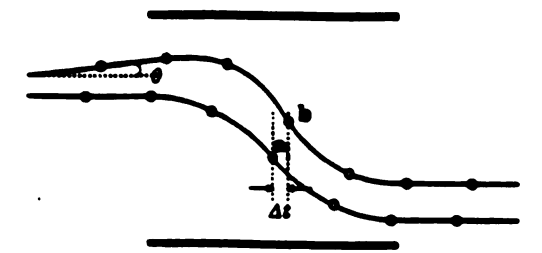


Figure 4. Two ions entering the deflection plate region with different trajectory angles. Field reversal occurs when the lower ion is at point a and the upper ion is at point b.

the lower ion does because the upper ion travels to point b before the field reverses. This longer duration of the applied downward force, followed by a shorter duration of upward force (experienced from point b to the end of the deflection region), compensates for the initial off-axis energy. The ion therefore leaves the region parallel to the beam axis and is included in the final packet, despite being offset from the ideal ion by a time Δt .

The value of Δt that satisfies these conditions may be related to off-axis angle, θ , as follows. Consider an "ideal" (i.e., initially on-axis) ion traveling with the most-probable velocity $v_0 = (2V_ue/m)^{1/2}$. An ion entering the deflection plate region with an off-axis angle θ will have a velocity vector perpendicular to the beam axis given by $v_v = v_0 \cos \theta$. When leaving the region, however, the perpendicular velocity v_v' is zero. If the ideal ion passes half-way through the plate region in time $t_{1/2}$, then the off-axis ion experiences downward and upward forces for times $t_{1/2} + \Delta t$ and $t_{1/2} - \Delta t$, respectively. The final perpendicular velocity of the off-axis ion is related to the initial value by the expression

$$v'_{1} = 0 = v_{0} \sin \theta - \frac{V_{d}e}{mD}(t_{1/2} + \Delta t) + \frac{V_{d}e}{mD}(t_{1/2} - \Delta t),$$

which rearranges to $\Delta t = \frac{mD}{2V_d e} v_0 \sin \theta$. This represents the broadening of the peak to lower flight times due to ions with trajectories that diverge in the upward direction. (Only two-dimensional motion in the plane of Figure 4 is considered here.) For a true beam having a divergence half-angle of θ , those ions having trajectory angles in the downward direction will cause similar broadening to higher flight times as well. Thus the quantity $2\Delta t$ could be used to approximate the base width of a packet broadened only by this angular effect, yielding

$$w_{\theta} = \frac{D}{V_{\theta}} \sqrt{\frac{2V_{\theta}m}{\epsilon}} \sin \theta \tag{3}$$

Equation 3 yields an underestimate of peak broadening due to the angular effect, however, because it is

not necessary for ions to be moving exactly parallel to the beam axis as they leave the deflection region in order to pass through the aperture. Consider, for example, an ion that enters the deflection region with the e trajectory as the upper ion discussed above but slightly ahead of it in time. This ion would experience even more net downward force than the upper ion pictured in Figure 4, and would thus leave the region with a small downward velocity component. This final trajectory could, however, still carry the ion through the aperture (at a position somewhat below the point at which the pictured ion passes through). lons acting in this way, as well as the analogous ions having initial downward motion, serve to further increase the final packet width. Though eq 3 cannot be used to obtain the complete magnitude of the peak broadening due to angular divergence, the digital simulation described below can be used to measure this effect.

The broadening caused by ions with positive and negative initial trajectory angles need not be symmetric because in both cases the forward velocity (in the direction of the beam axis) of these off-axis ions is reduced from the ideal velocity by a factor of $\cos\theta$ for ions having the same kinetic energy. The flight time for ions having an initial downward velocity component is increased over that of the ideal ion both by their lower velocity in the beam axis as well as the angular effect described above. For the ions having some initial upward motion, however, flight times tend to be decreased by the angular effect but increased by their reduced velocity. The net result of this is that the peak is skewed toward higher flight times.

It is difficult to combine the expressions for w_l , w_{ll} , and w_{ll} directly to obtain an expression for true peak width, but any of the expressions can be used alone to approximate peak widths for cases in which one effect (geometry, energy distribution, or angular divergence) predominates. The combination of the three effects was explored by means of digital simulations as described below: the individual expressions were useful for checking the validity of these simulations as well.

Simulations

In order to explore the combination of the energy spread and angular divergence effects with the ideal packet width given by eq 1, computer programs were developed to model ion packet behavior. First, an animation program was developed that illustrates ion behavior in beam modulation by moving colored dots, representing individual ions, across the screen of an IBM AT-compatible computer. (This program was used to ascertain the pattern of ion motion shown in Figure 4.) Then a simulation program was written to generate peak shapes for beam modulation TOFMS. The method used for this simulation will be explained with the aid of Figure 5. The program models the motion of various ions, chosen systematically from the region in-

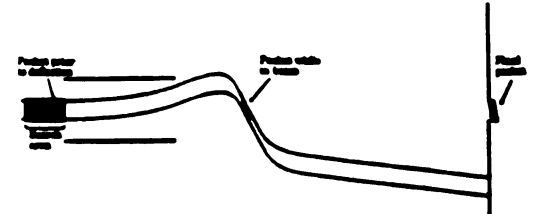


Figure S. Illustration of ion behavior modeled by the simulation program (see text).

dicated, by means of Runge-Kutta integration through the deflection plate region and onward to the aperture. Flight times for those ions found to pass through the aperture are tabulated in the form of a histogram to generate the peak shape. The three solid regions in Figure 5 are meant to indicate the locus of points occupied by these ions at three instants in time: prior to entering the deflection region, part-way along the flight path, and just after passage through the aperture. (See ref 2 for a complete description of the shapes of these regions.)

An example of the output from this program is given in Figure 6 for the parameters shown in Table 1. The peak widths obtained by this simulation method may be approximated by means of eqs 1–3 by using calculated values of w_l , w_{ll} , and w_l to obtain estimates of peak variances. The variance of the overall peak is then given by the sum of the contributing variances. Examples of this process and comparisons with the simulated peaks are summarized in Table 2. Values for variances shown in parentheses were calculated as the difference between the other simulated values under the additivity-of-variances assumption. The peak

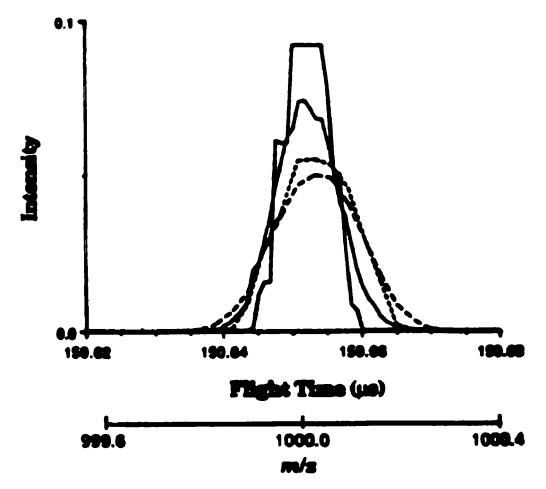


Figure 6. Simulated peak shape for m/z 1000. —— = Bakker effect only; · · · · · = Bakker effect with energy dispersion; · · · · · = Bakker effect with angular dispersion; · · · · · = all effects combined.

Table 1. Parameters used for simulated beam deflection peak shape

1	1000 u
	500. V
	100. V
	1.500 m
	0.005 m
	0. 005 m
	0. 003 m
	0.1*
$-(k_0T/2) =$	0.0215 eV

shape obtained by the Bakker effect alone may be approximated as a triangle. (This was found to yield more accurate results than a rectangular peak shape.) The variance of an isosceles triangle having a base width w_l is given by $w_1^2/24$. Similarly, the variance contributed by the angular effect may be approximated by $w_0^2/12$; a rectangular peak shape is assumed here to model cases in which all values of θ within the limits given are equally likely. If the peak shape corresponding to the energy effect is assumed to be normal with a standard deviation of $w_{ij}/2.35$, the variance contributed by the energy effect is then $(w_{ij}/2.35)^2$. The accuracy of the simulated peak variances cannot be well characterized without, for example, detailed Monte Carlo analysis, but these widths are believed to fall within a few percent of the true values. Note that the prediction of peak widths from variance calculations is unreliable, in particular for the angular divergence effect. This is due to the variety of peak shapes (nearly rectangular to nearly Gaussian) that can occur as the various parameters are altered. For cases in which the angular divergence is very small (e.g., $\theta < 0.01^{\circ}$), the predictions can be quite accurate; this was the case in the experimental study described below.

Experimental Results

A spectrum of perfluorotributylamine (PFTBA), obtained by direct inlet introduction with an ion source temperature of 150 °C, is shown in Figure 7. These data result from the integration of 5000 transients col-

lected in 1 s and summed by the integrating transient recorder (ITR) [14]. A comparison of peak basewidths for major ions in this spectrum to those produced by digital simulation is shown in Table 3. For the simulated data, parameters matching the physical dimensions and voltages of the instrument were used, namely L = 2.1 m, S = 6.35 mm, B = 0.13mm, D = 13 mm, $V_a = 3000$ V, and $V_d = 63$ V. The standard deviation of the kinetic energy distribution, σ_U , was approximated as 0.5 eV based on the potential distribution within the source; the angular divergence of the beam was neglected. The slope of base-width vs. $\sqrt{m/z}$ for the experimental values is calculated to be 3.7 ± 0.2 ns. and that for the simulated data is 4.0 ± 0.1 ns, demonstrating that the instrument performance follows the theory described above. An expected" slope can be obtained by summing eqs 1 and 2, then factoring out m. This procedure yields a value of 3.9 ns if β is assigned a value of 6σu/U₀ to represent base-widths. This simple method is not appropriate when the angular divergence is large, but it is quite adequate for this case.

Practical Considerations

Mass Resolving Power

The PFTBA spectrum shown above was obtained with unit or better mass resolution up to at least m/z 502. An estimate of the upper mass limit for unit mass resolving power with this instrument can be found as follows. The flight time separation between ions of two adjacent m/z values is given by

$$\Delta t = \frac{Lu}{\sqrt{2U}}(\sqrt{m/z+1} - \sqrt{m/z}) \tag{4}$$

where u is the atomic mass unit. Equation 4 may be approximated by the first term of the Taylor series as

$$\Delta t \approx \frac{L\sqrt{u}}{2\sqrt{2Um/z}} \tag{5}$$

In the previous section, the peak base width was found to be given approximately by $3.9\sqrt{m/z}$ ns. (Either the experimental slope or the value found via simulation

Table 2. Comparison of peak variances obtained from calculation using eqs 1-3 and from digital peak shape simulation

Source of pook broadening	Calculated base width × 10 ⁻⁹ s ²	Calculated vanence × 10 ⁻¹⁰ s ²	Simulation variance × 10 ⁻¹⁶ s ²
Bakker offect	13.6	8	9
Energy	7.7	11	(11)
Angle	8.9	7	(16)
Bakker + energy	-	19	20
Sakker + angle	-	15	25
Bakker + energy + angle	_	26	35

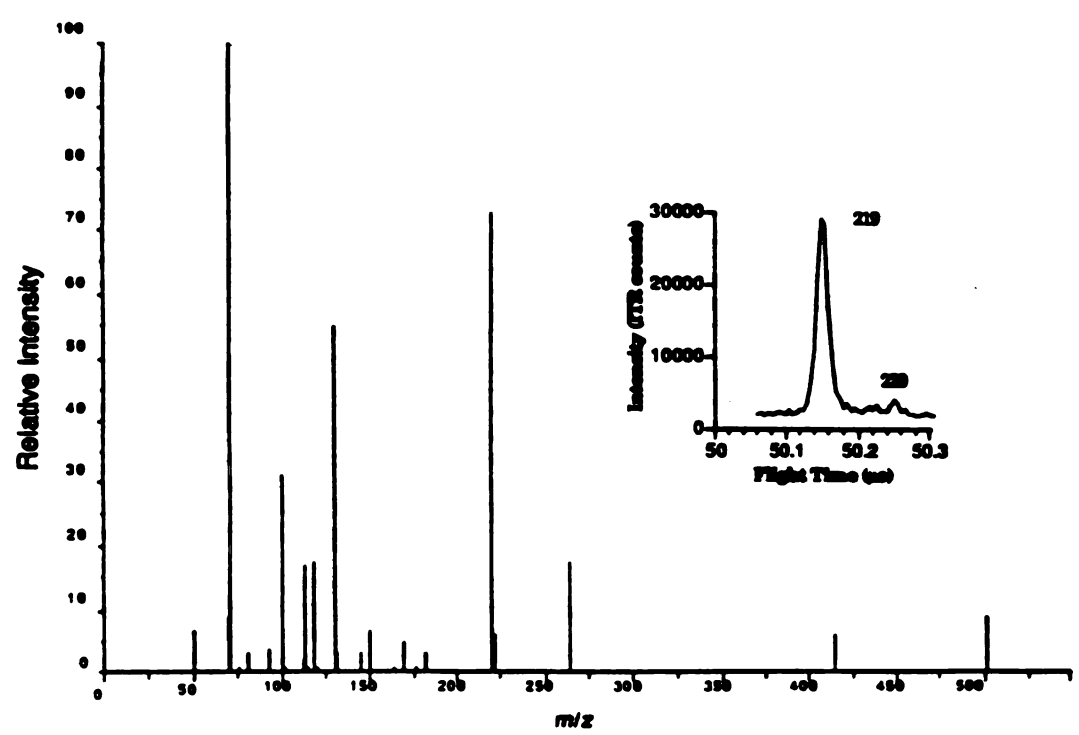


Figure 7. Mass spectrum of PFTBA collected by beam-deflection TOFMS. Typical peak shapes are shown in the inset for m/z 219 and m/z 220.

could also be used.) For simplicity, the width at halfheight (seconds) may be approximated as half of this value, thus

$$w_{1/2} \approx 2.0 \times 10^{-4} \sqrt{m/z}$$
 (6)

Setting $\Delta t \approx w_{1/2}$ yields the m/z value at which peak separation just equals peak width at half-height, and hence the approximate upper m/z limit for unit mass resolving power. For the parameters in this example, this upper limit is an m/z value of 710.

An improvement could be made if an ion mirror were incorporated into the instrument. The ion mirror would remove the effect of the energy dispersion and, in addition, increase the effective flight path length

Table 3. Comparison of measured and simulated peak base widths

m/z	Messured (± 5 ns)	Simulated (±3 ne)
69	40.	30.
100	36.	42.
131	52 .	46.
219	64.	61.
264	67 .	69.
502	88.	92.

by a factor of four. (The decreased flight time in the mirror contributes a factor of two, while the travel in the forward and reverse directions through the flight path contributes another factor of two.) In this case, the expected slope is obtained from eq 1 alone and has the value $2.5\sqrt{m/z}$ ns. Using this value, and replacing L by 4L in eq 5, the upper m/z limit increases to 4400. This is certainly adequate for most GC/MS applications.

Signal-to-Noise Considerations

It would appear that beam modulation in TOFMS would experience greatly reduced detectability and sensitivity due to the very small portion of the ion beam that is selected for detection. In addition, it would appear that the beam dimensions required for beam deflection, which are much smaller than those in conventional TOFMS, would further contribute to poor ion statistics. It is important to realize, however, that during the time an ion packet is striking the detector, the measured ion flux is the same as that seen from a continuous beam. The advantage of the continuous beam lies in the possibility of averaging the ion intensity measurements over a longer period of time. This advantage results in an improvement in signal-to-noise ratio (S/N) equal to the square-root of the ratio of the measurement times. A TOF instrument with a packet

width of 10 ns and an extraction repetition rate of 10 kHz would have an S/N 100 times worse than a continuous beam scanning instrument when used to monitor a single m/z value. In practice, scanning sector mass spectrometers generally have much lower ion transmission efficiencies than TOF instruments due to the smaller apertures required throughout the flight path. In quadrupole mass spectrometers ion transmission is also limited by the acceptance angle and apertures required. Because scanning mass spectrometers act as mass-selective filters, the ion transmission generally decreases as the mass resolving power is increased. On the other hand, a TOFMS system that focuses (rather than filters) the ions can intensify the peak current rather than just reducing the peak width, as resolving power is increased. Because the ion mirror is a focusing device and, without grids, can be made with excellent (ca. 90%) transmittance [15], the peak current in a mirror TOF instrument can be higher than the average instantaneous beam current for the same mass. These factors tend to counteract, to some degree, the decrease in S/N predicted from the duty cycle consideration alone.

In the previous paragraph, the ion intensity at the peak arrival time for an ion of a particular m/z in a TOF instrument is compared with the peak ion intensity for that same m/z in a mass scanning instrument that is fixed at the optimum setting for the m/z being monitored (selected-ion-monitoring, or SIM, mode). To compare TOF and scanning instruments for modes in which full spectra are generated, other factors need to be considered. In scanning mode, the scanning instrument monitors a single m/z window at a time. The average time spent at each window is equal to the scan time divided by the number of mass values sampled, assuming no dead time between values. With TOFMS using boxcar integrator detection (sometimes called time-slice detection), the output signal also represents the intensity of only one arrival time window at a time. The delay time for the sample window of the boxcar integrator is stepped or scanned to obtain a mass spectrum just as in the scanning filter mass spectrometers. For this type of detection, the relative S/N for both scanning and TOF mass spectrometers would be equal to that discussed above for the SIM mode. The duty cycle disadvantages of TOF are offset, at least partially, however, by its transmittance and focusing advantages.

A very significant advantage can be seen for TOF, however, when time-array detection is performed using an ITR. The ITR acquires, for all time slices within the collection period, the same information the boxcar integrator does for only one. For an ITR that stores 8192 samples per transient, the effect is an S/N improvement of $\sqrt{8192} \approx 91$ times that of the scanning boxcar data collection system. Because the scanning boxcar data system has, at worst, a 100-times lower S/N than the scanning filter instrument, the TOF spectrometer with an ITR and mirror should have an S/N

at least equal to and potentially much better than a scanning filter instrument in scanning mode. The increased data rate available with TOFMS with ITR detection can be used to great advantage when spectra are to be collected under conditions of rapidly changing sample pressure in the source such as encountered with high-performance chromatography.

Conclusions

Beam deflection is becoming a common technique in TOFMS, yet beam deflection systems are often designed with the assumption that the ion behavior so produced will follow the Gate model. For optimum time-resolution, however, the more complex Differential Impulse Sweep mechanism is required. This study showed that accurate predictions of ion behavior under this model can be obtained either by simple inspection of the equations given or by digital simulation of ion motion. Such predictions can be of assistance in the design of beam deflection TOFMS instruments. The study also demonstrated that a beam deflection TOFMS instrument incorporating an ion mirror and an ITR would have mass resolution and sensitivity suitable for modern GC/MS applications.

Acknowledgments

This work was supported by a grant from the Biotechnology Research Program of the National Institutes of Health Division of Research Resources (DRR-00480-20). The authors would like to thank M. Rabb and R. Tocklenburg for their assistance.

References

- 1. Powler, T. K.; Good, W. M. Nucl. Instrum. Math. 1900, 7,
- 2. Bakker, J. M. B. J. Phys. E: Sci. Instrum. 1973, 6, 785.
- 3. Bakker, J. M. B. J. Phys. E: Sci. Instrum. 1974. 7, 364.
- 4. Pinkston, J. D.; Rabb, M.; Watson, J. T.; Allison, J. Rev. Sci. Instrum. 1986, 57, 583.
- 5. Glish, G. L.; Goeringer, D. E. Anal. Chem. 1984, 56, 2291.
 6. Eckenrode, B. A.; Watson, J. T.; Enke, C. G.; Holland, J. F. Int. J. Mass Spectrom. Ion Proc. 1988, 83, 177.
- 7. Patrell, J. H.; Tiernan, T. D.; Abrameon, F. P.; Miller, C. D. Rev. Sci. Instrum. 1968, 39, 340.
- 8. Miller, C. D.; Tiernan, T. D.; Patrell, J. H. Rev. Sci. Instrum. 1960, 40, 503,
- 9. Schey, K.; Cooks, R. G.; Grix, R.; Wollink, H. Int. J. Mass Spectrom. Ion Proc. 1987, 77, 49.
- 10. Dewson, J. H. J.; Guilhaus, M. Rapid Commun. Mass Spastram. 1989, 3, 155.
- Yeichak, G. E.; Enha, C. G.; Holland, J. F. Int. J. Mass Spectrum. Ion Proc. 1989, 87, 313.
- 12. Wiley, W. C.; McLaren, I. H. Rev. Sci. Instrum. 1988, 26, 1150.
- 13. Stein, R. Int. J. Mass Spectrum. Ion Phys. 1974. 14, 205. 14. Holland. J. F.; Newcome, B.; Tecklenburg, R. E. Jr.; Dev
- port, M.; Allison, J.; Watson, J. T.; Enke, C. G. in prepara-
- 15. Hermann Wollink, personal communication, 1968.



Journal of Chromatography, 518 (1990) 283-295 Elsevier Science Publishers B.V., Amsterdam

CHROM. 22 656

Renaissance of gas chromatography-time-of-flight mass spectrometry

Meeting the challenge of capillary columns with a beam deflection instrument and time array detection

J. T. WATSON®

Departments of Chemistry and Biochemistry, Michigan State University, East Lansing, MI 48824 (U.S.A.)
G. A. SCHULTZ

Department of Chemistry, Michigan State University, East Lansing, MI 48824 (U.S.A.)
R. E. TECKLENBURG, Jr.

Department of Biochemistry, Michigan State University, East Lansing, MI 48824 (U.S.A.) and

J. ALLISON

Department of Chemistry, Michigan State University, East Lansing, MI 48824 (U.S.A.) (First received November 5th, 1989; revised manuscript received June 26th, 1990)

ABSTRACT

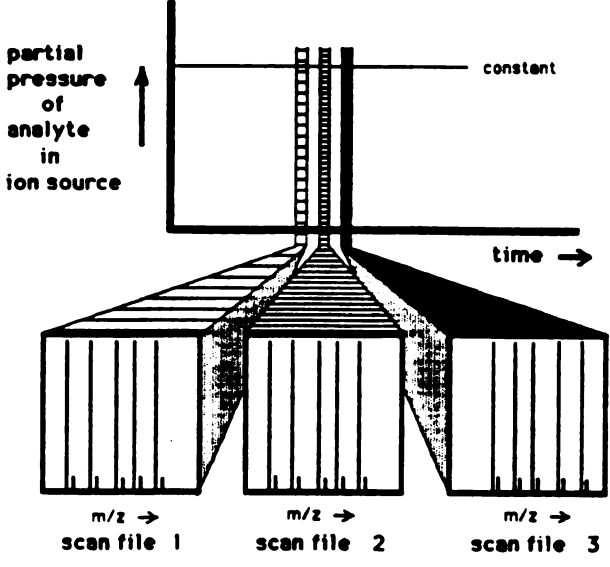
This report describes the use of a unique beam deflection time-of-flight mass spectrometer to address some of the demands made on mass spectrometry by new developments in high-resolution capillary column gas chromatography. An integrating transient recorder is used in combination with this beam deflection time-of-flight instrument to apply the concept of time array detection in capturing all of the mass spectral information available from the ion source, thereby greatly enhancing the signal-to-noise ratio quality of the mass spectral data. The applicability of the time array detection approach to gas chromatography-mass spectrometry is demonstrated in the context of an analysis of the standard Grob mixture for assessing performance of capillary column chromatography. During analysis of the Grob mixture by gas chromatography-mass spectrometry, mass spectra were recorded at a rate of 20 scan files per second. The data indicate that this rate of mass spectral scan file generation is adequate to provide a suitable data base for reconstruction of the chromatographic profile. In addition, the effective scan rate is high enough that there is no distortion in the relative peak intensities throughout the individual mass spectra of components regardless of the relatively high dynamic changes in partial pressure of the analyte as reflected by the sharp peaks in the chromatographic profile. The experimental results indicate that the beam deflection time-offlight mass spectrometer can provide mass spectra at a scan file generation rate much higher than that possible with the conventional quadrupole or magnetic sector mass spectrometer, but at comparable detection limits.

INTRODUCTION

Gas chromatography (GC)-mass spectrometry (MS) is a powerful technique because it combines a separation technique with an identification technique. The separation power of modern high-performance gas-liquid chromatography helps

CASE A

Sample introduced from reservoir



CASE B

Sample introduction by gas chromatograph

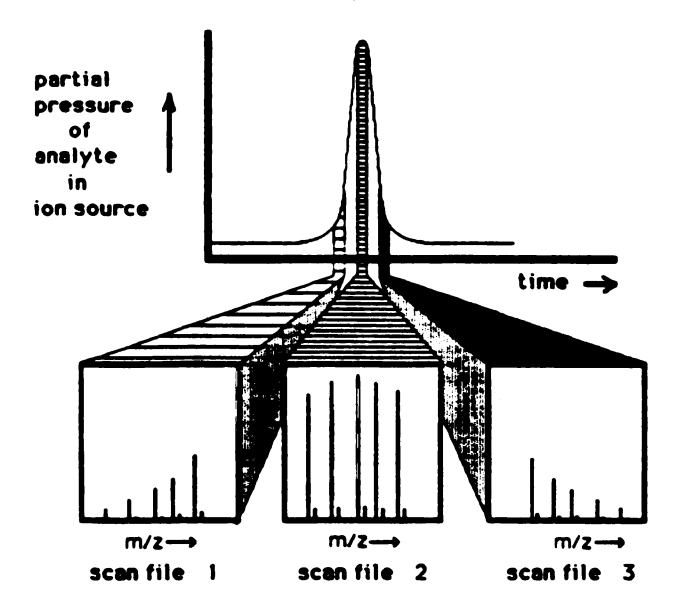


Fig. 1. Graphical illustration of the influence of analyte partial pressure in the ion source of a mass spectrometer on the resulting bar graph mass spectra. Case A: When analyte partial pressure is constant, spectra in scans 1, 2 and 3 are identical in the relative intensities of the peaks representing this hypothetical compound. Case B: When the partial pressure of the hypothetical compound changes in the ion source during scans 1, 2 and 3, the spectra are skewed as described in the text.

make available at least partially purified mixture components for analysis by mass spectrometry for identification purposes. Paradoxically, the dynamic nature of sample concentrations at the outlet of a gas chromatograph, especially in capillary column chromatography, tends to violate one of the cardinal rules in MS[1]. That is, it is important for the partial pressure of the analyte in the ionization chamber to remain constant during the time interval in which the mass spectrometer is scanned to acquire a mass spectrum; this condition ensures that the relative peak intensities represented in the mass spectrum are related to structural features of the molecule, and not distorted due to changes in partial pressure of the analyte during acquisition of that mass spectrum.

The influence of a dynamic partial pressure of an analyte in a mass spectrometer's ion source on the appearance of the acquired mass spectra is illustrated in Fig. 1. Case A in Fig. 1 represents the acquisition of three mass spectra of a hypothetical analyte maintained at constant pressure in the ion source. Case B in Fig. 1 represents analysis of the same hypothetical analyte when introduced to the mass spectrometer ion source via a gas chromatograph. The partial pressure of analyte in the ion source of the mass spectrometer rises and then falls as the analyte emerges from the gas chromatographic column. Scans 1 and 3 were acquired as the analyte concentration (partial pressure) was changing most rapidly in the ion source during mass spectral acquisition, and these mass spectra show a distortion or skewing of relative peak intensities. The relative peak intensities in each mass spectrum are indicative of the partial pressure of the analyte in the ion source, as well as the inherent fragmentation pattern of the compound. This situation complicates mass spectral interpretation, and limits compound identification based on mass spectral matching approaches.

Problems in capilary GC-MS

Problem 1: The acquisition of true mass spectra. The very definition of a gas chromatogram is, in fact, the temporal profile of partial pressures of analytes as they emerge from the chromatographic column. Improvements in the resolving power of capillary columns during the last decade, as reflected by the very sharp peaks (2-3 s in duration) in the chromatograms [2,3], have placed severe demands on the mass spectrometer to scan quickly enough to avoid distorting the mass spectra without sacrificing other important mass spectral features such as resolving power and the signalto-noise ratio associated with the data. This problem is exacerbated during the common occurrence of poorly resolved components; in this case, the ion source may contain the vapor of one component or the other for only a few milliseconds, and it is imperative to capture an undistorted "pure" spectrum during this brief interval. An assessment [4] of the capacity for various mass analyzers to scan rapidly during analyses by GC-MS indicates that present demands for high scan rates (approaching ten scans per second over the mass range 50 to 500 daltons) made by high-resolution GC has forced many of the common mass analyzers to their very limit of performance as established by the physics underlying their operating principles. On the other hand, the time-of-flight mass spectrometer, by virtue of its rapid cycle time, has the capacity for generating complete mass spectra at a rate even higher than that presently demanded by GC-MS instruments that utilize the most efficient high-resolution GC capillary columns.

286 J. T. WATSON et al.

Problem 2: The satisfactory reconstruction of the chromatographic profile from mass spectral data. The problem resulting from the great disparity between the rate of change in sample partial pressure in capillary GC and the data acquisition rate of complete mass spectra is illustrated in Fig. 2. In each of the three panels in Fig. 2, the true chromatographic profile is illustrated by the dashed line; the solid line in each of the three panels is an attempt to reconstruct the chromatographic profile from data points available from a data base consisting of consecutively-recorded mass spectra. Each point represents the reconstructed total ion current (TIC) obtained by summing the measured intensities of all of the mass spectral peaks in one mass spectrum. In panels A and B, the rate of data acquisition yielded one scan file per second; thus, in these two panels there is available only one TIC point per second for purposes of reconstructing the chromatographic profile. The only difference between panels A and B is the synchrony between the repetitive scanning of the mass spectrometer and initialization of the chromatographic process. As can be seen in panels A and B, such utilization of mass spectral data for reconstruction of the true chromatographic profile is severely limited. However, as shown in panel C, if three points per second are available (due to scanning the mass spectrometer three times per second) from which to reconstruct the chromatographic profile as indicated by the solid line in panel C, the true chromatographic profile is more correctly described.

Problem 3: Limitations of "scanning" mass analyzers. Another major problem in GC-MS is the sacrifice of considerable ion counting statistical information when the technique of scanning of the mass spectrometer is used. As in most spectroscopic

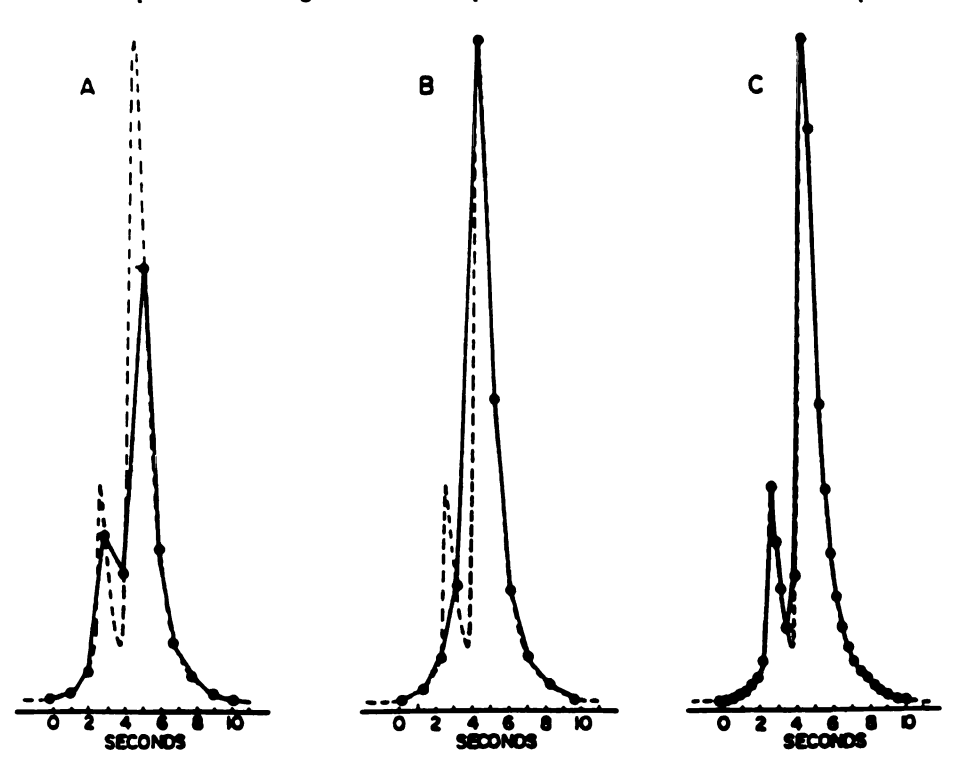


Fig. 2. Comparison of the true chromatographic profile (---) and attempts to reconstruct the chromatographic profile (---) from 10 data points for cases A and B, and 30 data points for case C, as described in the text (adapted from ref. 4 with permission of the American Chemical Society).

instruments which use the exclusive process of scanning, considerable information is lost as some parameter is varied to allow resolution elements of the mass spectrum to consecutively pass across the detector slits. Sweeley et al. [5], Hammar et al. [6] and other pioneers as reviewed by Falkner [7] solved this problem with selected-ion monitoring (SIM) which dedicates the instrument to monitoring ion current at only a selected resolution element (m/z value). Whereas the excellent sensitivity of SIM (femtomoles) is achieved by integrating all of the ion current from the ion source at a particular resolution element or m/z value of the mass spectrum, such good sensitivity could be achieved, in principle, while acquiring complete mass spectra if it were possible to integrate all ion current at all resolution elements or all m/z values across the mass spectrum all of the time. Such a process is possible only through array detection which measures all ion currents over a range of m/z values simultaneously. It would be desirable to acquire the complete mass spectrum in consecutive scans at the same high sensitivity otherwise available only by selected-ion monitoring. The key features of repetitive scanning and its advantages and disadvantages are presented in Fig. 3 in parallel with the key features of SIM together with its advantages and disadvantages.

A solution

As indicated in the conclusion of Fig. 3, the beneficial aspects of repetitive acquisition of mass spectra in the generation of a complete data field for a GC-MS

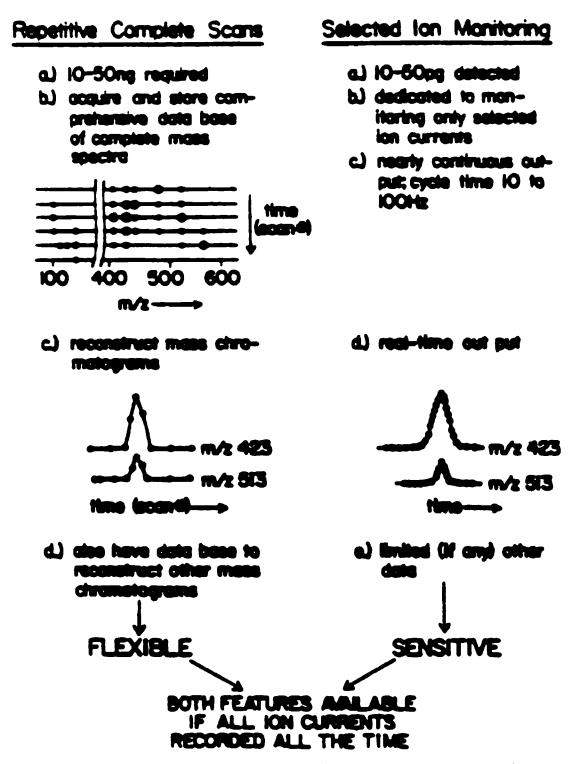


Fig. 3. Summary of operational features and mutually exclusive advantages of the technique of repetitive scanning and selected ion monitoring (reprinted from ref. 1 with permission from Raven Press).

288 J. T. WATSON et al.

analysis can be combined with the high sensitivity of SIM only if array detection is used to record the mass spectrum. The approach of using array detectors in mass spectrometry was pioneered by Giffen et al. [8] at the Jet Propulsion Laboratory in the 1970s. This resulted in the development of a device called an electro-optical ion detector which was evaluated subsequently in GC-MS by Hedfjall and Ryhage [9]. The technique of Fourier transform (FT) MS also provides array detection in that all ions present in the device are detected simultaneously [10], although the application of this instrument in GC-MS has not been extensively pursued to date. While FT-MS can obtain an impressive number of mass spectra per second, there are acquisition rate/resolution trade-offs. To avoid problems with limited dynamic range and other potential mechanical difficulties with these and other approaches to array detection, the research effort in the Michigan State University (MSU) Mass Spectrometry Facility has pursued developments in time-of-flight MS to conduct array detection in time.

Time-of-flight (TOF) MS, because of its pulsed nature and the very short time required for producing any given transient mass spectrum, i.e., an ion sampling time ranging from 3 to 100 µs, makes this technique an ideal method for sampling rapidly changing partial pressures of analytes in the ion source. As explained in early reports on this work [4,11], time array detection is achieved in TOF-MS by digitizing the output from the detector such that all information in all resolution elements of the transient time-of-flight mass spectrum are collected following each extraction pulse from the ion source. For this purpose, an integrating transient recorder (ITR) has been designed and implemented, as described elsewhere [12]. Briefly the ITR digitizes the ion detector output at 200 MHz, is capable of producing up to 50 complete mass spectra per second, and can sustain high data collection rates continuously for up to one hour without loss of data. Another major requirement for proper utilization of time array detection is the necessity of providing optimum ion focus for ions of all m/zvalues from each ion packet so that each of the 5000-10 000 transient mass spectra reaching the detector per second have properly resolved mass spectral peaks. Conventional techniques in TOF-MS such as time-lag focusing are mass-dependent and are not generally useful in conjunction with time array detection, although we have obtained preliminary results [13] using time array detection with mass collection over narrow mass ranges which fall within the limits of acceptable focus by a fixed value of the time-lag parameter. The MSU group also has pursued techniques of beam deflection TOF-MS for purposes of achieving mass-independent ion focus and for improving the resolving power, in general, of TOF-MS by eliminating the aberration in resolution caused by the "turn around time" problem [14]. The technical details of a most recent version of a beam deflection TOF-MS system will be described elsewhere [15]. This report provides a preliminary assessment of the beam deflection TOF-MS system developed at MSU with time array detection for purposes of gathering complete mass spectra from a standard test mixture introduced via capillary column GC.

EXPERIMENTAL

Preliminary results from the GC-TOF-MS system based on beam deflection as represented schematically in Fig. 4 are presented here. In brief, the gas chromatograph used is a Hitachi 663-30, fitted with an 18 m (DB-1, 0.18 mm I.D.) capillary column; the test sample described herein is the Grob mixture (Supelco catalog No.

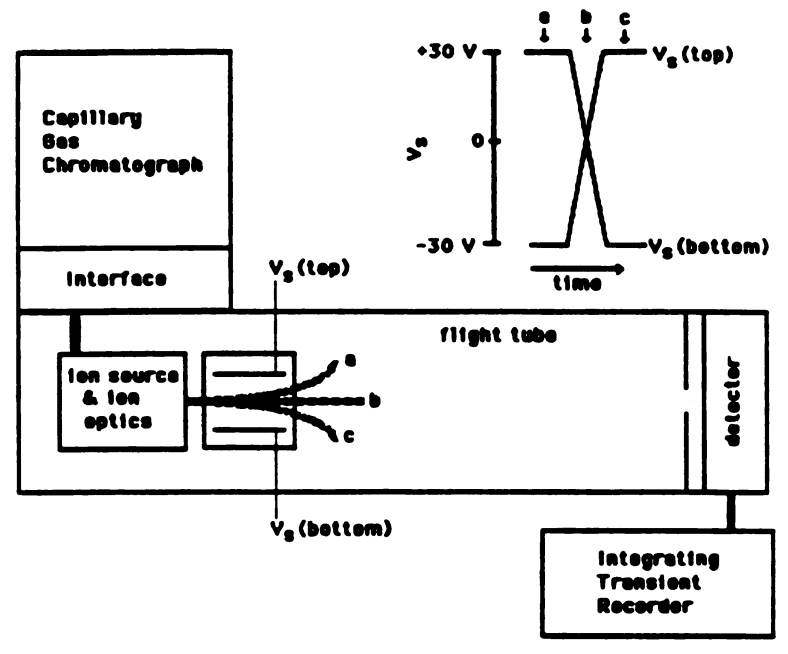


Fig. 4. Schematic diagram of the beam deflection TOF-MS system showing the gas chromatograph, continuous ion source, beam deflection assembly, CEMA detector, and ITR.

4-7304). The GC-MS interface is a heated block design from JEOL. The time-offlight mass spectrometer is a highly modified Bendix 12-101 instrument. The source and source housing from a double-focusing mass spectrometer, a DuPont 21-491, is used to provide a continuous, narrow, focussed beam of ions produced by electron or chemical ionization. Ions formed in the source are accelerated to a kinetic energy of approximately 3000 eV. Ion packets are formed by beam deflection [14]. To obtain a rapidly changing electric field in the beam deflector for good mass spectral resolution, dynamic voltages ("pulses") of equal magnitude, but of opposite sign (designated as V_{\bullet} in Fig. 4), are applied to each deflection plate yielding temporally narrow ion packets. The time-dependent voltages used are generated from pulsing circuitry that was developed in-house. Typically, the voltages V, applied are modulated between +30 V and -30 V. The circuitry provides a rise time of <10 ns and a fall time of <20ns. Ion packets traverse a 2.0-m flight tube, and transient mass spectra are generated at a rate of 5000 s⁻¹. This beam deflection TOF-MS system provides better than unit resolution for all ions in the m/z 2-1000 range, with all ions in optimal focus for each ion packet. A resolving power of > 1400 has been demonstrated for this instrument [15].

An in-house designed and built integrating transient recorder [12] was used to continuously collect full mass range, mass spectra throughout the entire duration of the GC-MS run (20 min). Data collection with the ITR is accomplished by a 200 MHz flash analog-to-digital converter. The digitized data are passed to 16 high speed ECL (emitter coupled logic) summer cards where 5 to 5000 transients are summed to form a mass spectral scan file. If 5000 transients are produced each second by the

290 J. T. WATSON et al.

TOF-MS system, summation of 5 to 5000 transients corresponds to mass spectral generation rates of 1000 scan files per second to 1 scan file per second, respectively. The integrated scan files are passed across a VME bus to three Motorola 68020 parallel processors whereby time/mass calibration, and/or conversion to reconstructed mass chromatograms and/or real-time conversion to mass, intensity pairs occurs. Finally, the processed scan files are written to a 300 Mbyte Priam disk drive (typical scan file sizes = 500-2000 bytes).

RESULTS AND DISCUSSION

The principal goals of this paper are to demonstrate that beam deflection TOF-MS is capable of producing good quality mass spectra and that these mass spectra are well focussed and resolved over the complete mass range so that time array detection can be implemented by means of an ITR. The importance of acquiring complete mass spectra at a rate of 20 scan files per second in deconvoluting unresolved chromatographic components is illustrated in the analysis of a capillary column test mixture. As described elsewhere, the ITR is capable of generating up to 1000 complete summed spectra per second [4,11,12]. This scan file generation rate would provide 1000 data points per second from which a chromatographic profile could be reconstructed from a data base of consecutively-recorded mass spectra. However, such a high frequency of scan file generation is not necessary to reconstruct the profiles available from most high-resolution gas chromatographs at this time. In the preliminary assessment of time array detection described here, a scan file generation rate of 20 scan files per second has been found adequate to provide 20 data points per second from which to reconstruct chromatographic profiles having peak widths on the order of two seconds.

Representation of the chromatographic profile

Fig. 5 shows the reconstructed total ion current (RTIC) chromatogram of a standard test mixture [16] analyzed using GC-beam deflection TOF-MS-ITR, repre-

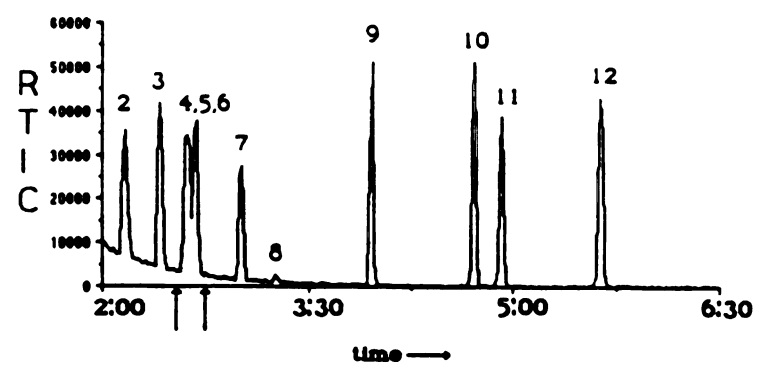


Fig. 5. Reconstructed TIC chromatogram (RTIC) of standard Grob test mixture as separated on a 20 m \times 0.18 mm I.D. column containing DB-1, 0-0.4 μ m film thickness at a flow-rate of 1.5 ml/min with a temperature program of 20°C.min from 120 to 200°C. Components (approx. 50 ng each) in the mixture: 1 = 2,3-butanediol; 2 = decane; 3 = 1-octanol; 4 = nonanal; 5 = 2,6-dimethylphenol; 6 = undecane; 7 = 2,6-dimethylaniline; 8 = 2-ethylhexanoic acid; 9 = C_{10} acid methyl ester; 10 = C_{11} acid methyl ester; 11 = dicyclohexylamine; 12 = C_{12} acid methyl ester. Time in min:s.

senting approximately 50 ng of each component. A scan file generation rate of one scan file per second offers one TIC point per second to reconstruct the chromatographic profile. Generation of one TIC point per second is typical of most available GC-MS instruments (e.g., quadrupoles and magnetic sector instruments) in use today.

Several questions must be addressed concerning the results in Fig. 5. Does the RTIC, reconstructed from the one-scan-file-per-second data base, adequately represent the chromatography? Also, it was known that the mixture contained 12 components, but only 10 peaks are shown in the RTIC. The portion of the chromatogram containing the solvent peak and 2,3-butanediol is not shown here (Fig. 5), so there should be 11 components represented by the RTIC. To answer these questions, another aliquot of the test mixture was analyzed by GC-beam deflection TOF-MS-ITR, summing every 250 transient mass spectra, thereby generating 20 scan files per second. The RTIC chromatogram, resulting from the 20-scan-files-per-second data base at approximately 2.5 min into the run, is shown in Fig. 6b; for comparison, the corresponding segment of the RTIC in Fig. 5 (between the vertical arrows), obtained from the one-scan-file-per-second data base is reproduced as Fig. 6a. There are two obvious advantages to the greater scan file generation rate that can be seen upon comparing Fig. 6a and b. Because the 20-scan-files-per-second data base offers 20 points per second to reconstruct the waveform (Fig. 6b), the chromatographic profile is more accurately represented in terms of peak shapes, relative heights, and relative

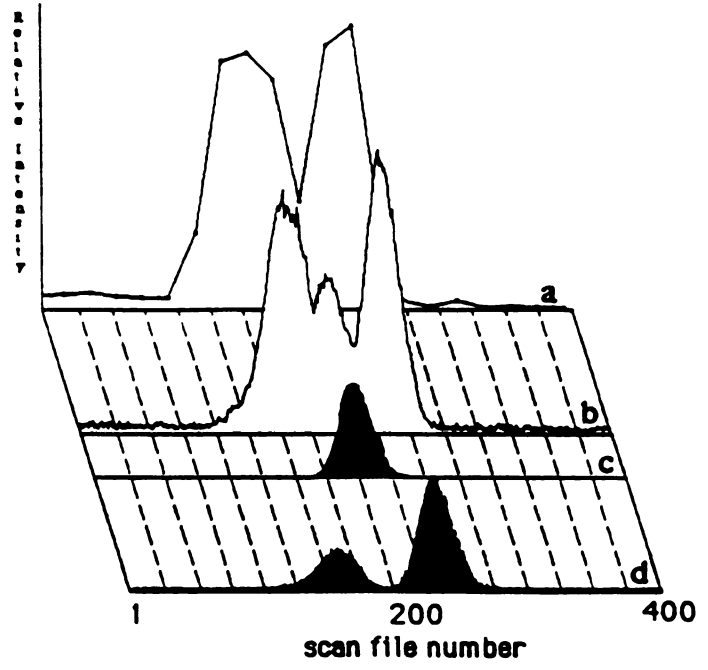


Fig. 6. (a-d) Data over a region of the chromatogram representing coeluting components. (a) RTIC obtained from spectra collected at 1 scan file/s; it only shows evidence for two components. (b) RTIC obtained from spectra collected at 20 scan files/s; it shows evidence for three components. (c) Mass chromatogram at m/z 122 representing the molecular ion of 2.6-dimethylphenol. (d) Mass chromatogram at m/z 57 representing an alkyl cation, a characteristic ion of both nonanal and undecane.

292 J. T. WATSON et al.

areas. This feature of the data provides better quantification of the components in the mixture. The other advantage is that the RTIC generated from higher scan file generation rates more accurately represents the true chromatographic profile. It is obvious from the RTIC presented in Fig. 6b that this region of the chromatogram contains three components.

Chester and Cram [17] have investigated the relationship between the number of data points required to represent the profile of a given chromatographic peak and the characteristic features of that peak shape as described by σ , where σ^2 is the variance that can be related to the mathematical function describing the profile. It has been previously estimated that 10 data points (scan files) per standard deviation unit are necessary to obtain an accurate representation of the chromatographic peak height, area, and position assuming a Gaussian peak [18]. The minimum number of data points which can accurately represent this profile is 10 scan files per second. Most scanning mass analyzers would not be able to represent the chromatography in this situation due to their scan file generation rate limitations.

The high scan file generation rates allow the presence of three components to be recognized in this unresolved region of the reconstructed chromatogram in Fig. 6b. Can the three components be identified from the mass spectral data base even though the components are coeluting? Because the components in the test mixture are known, as well as the type of column used for analysis, we were able to determine which components were expected to be in this region of the chromatogram. One of the expected components is 2,6-dimethylphenol. Instead of searching through the 200 scan files which contain mass spectral data for a match of the data to a library mass spectrum of this compound, we can display the mass chromatogram of one of the dominant ions in the mass spectrum of 2.6-dimethylphenol. A mass chromatogram is a graphic display of the peak intensity at a specified mass-to-charge value versus scan file number [19]. The library mass spectrum of 2.6-dimethylphenol indicates that the molecular ion is represented by the base peak at miz 122. Fig. 6c is the mass chromatogram of m/z 122 and identifies the middle component as 2.6-dimethylphenol. Another component expected to be in this region of the RTIC is undecane: the alkyl cation $C_4H_0^+$, m_{12} 57, was selected as a designate ion for this hydrocarbon. The mass chromatogram at m/z 57 displayed in Fig. 6d shows that the mass spectra of both of the other two components contain this alkyl cation. The mass chromatograms at m/z 57 and 122 (Fig. 6d and c, respectively) provide information on the chromatographic peak shapes of the three components. By choosing a scan file which does not contain both m/z 122 and m/z 57, one can obtain a pure mass spectrum for each of the three components represented here. A visual inspection of the mass chromatogram represented in Fig. 6d shows a region (scan files 190–200) where the ion current at m/z 57 is minimal. Because the mass spectra of the other two components have an intense peak at m/z 57, this is a region of the data base that should provide a reasonably pure mass spectrum of the middle component. The mass spectrum contained in scan file 192 is shown in Fig. 7a. A similar procedure was used to obtain pure mass spectra of the other two components by choosing scan files which do not contain ion current at m/z122. Ion current at m/z 122 is observed in scan files 160-232. Fig. 7b shows the mass spectrum in scan file 159 which is identical with the library spectrum of nonanal. Fig. 7c shows the mass spectrum in scan file 240 which is identical with that of undecane.

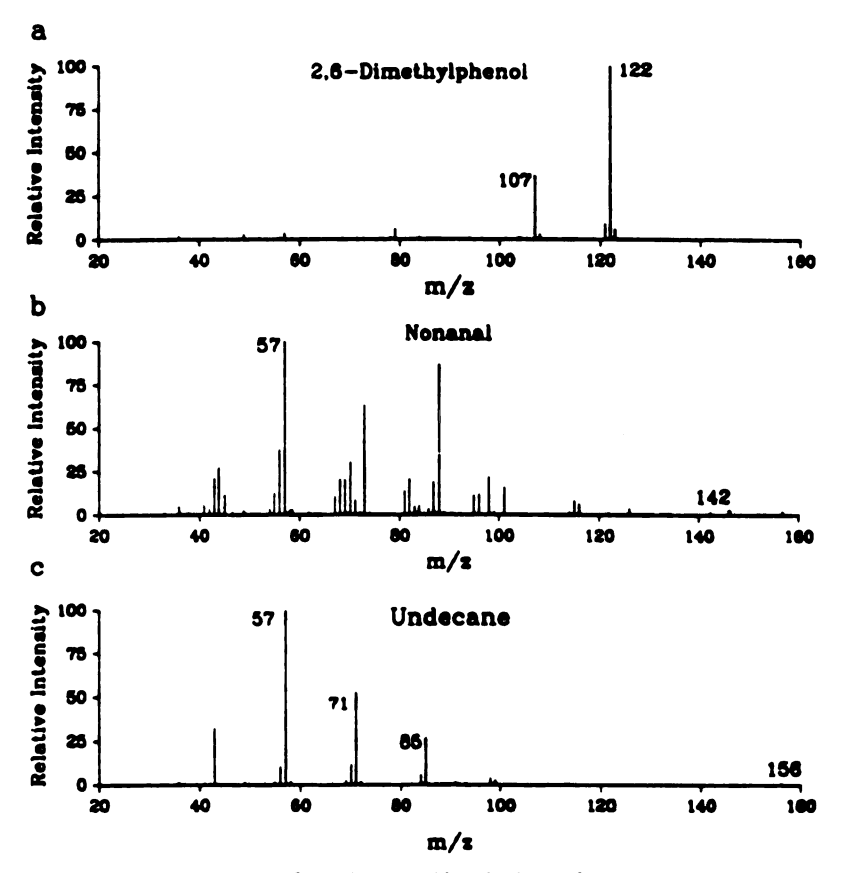


Fig. 7. Mass spectra selected from the several hundred scan files collected at 20 scan files/s as represented in Figs. 5 and 6. (a) Mass spectrum of 2.6-dimethylphenol obtained from scan file 192. (b) Mass spectrum of nonanal obtained from scan file 159. (c) Mass spectrum of undecane obtained from scan file 240. These spectra represent components 5, 4 and 6 in Fig. 5.

Limits of detection

The detection limit of the GC-beam deflection TOF-MS-ITR at 20 scan files per second was compared to that of the JEOL JMS-AX505H MS system which is a commercially available double-focusing sector instrument routinely used for GC-MS analyses. The fastest scan rate available with the JEOL instrument is 0.9 s per decade (e.g., m/z 50-500) which generates 1.1 scan files per second.

Complete mass spectra were collected during the analysis of the standard test mixture at various concentrations at the scan file generation rate described above for each mass spectrometer. Mass chromatograms were reconstructed from the corresponding data bases. The area of the peak in the mass chromatogram at m/z 122 (corresponding to the base peak in the mass spectrum of 2,6-dimethylphenol) was plotted versus the amount of analyte injected. The limit of detection was calculated using the method of regression analysis [20] on each data set. The y-intercept of each regression line was used as an estimate of the blank signal, y_b . The signal, $y = y_b + 3s_b$, determines the limit of detection. The limit of detection calculated for both the

294 J. T. WATSON et al.

JEOL instrument and the GC-beam deflection TOF-MS-ITR system was 0.6 ± 0.2 ng of 2,6-dimethylphenol.

Quality of mass spectra

An important feature of the data obtained with GC-beam deflection TOF-MS-ITR is the absence of mass spectral skew, due to the high sampling rate (5000 s⁻¹) of the continuous ion beam. Thus, the mass spectra of individual components obtained at different scan file generation rates are identical, each having the same relative peak intensities throughout the mass range. This feature of the data would have allowed identification of the three components by use of available mass spectral deconvolution routines [21] to distinguish the coeluting components based on their characteristic contributions to peak intensities among the adjacent scan files.

CONCLUSIONS

We have shown that the GC-beam deflection TOF-MS-ITR combination is capable of providing good-quality GC-MS data. The GC-beam deflection TOF-MS-ITR system can generate data files at a rate greater than those commonly available from quadrupole and magnetic sector instruments. The importance of the high scan file generation rate was illustrated by comparison of reconstructed total ion current chromatograms from data bases collected at 20 scan files per second and at one scan file per second, the latter being representative of the performance of most magnetic or quadrupole instruments (even though, in principle, these instruments can generate data at higher rates, but at the expense of performance and data quality). Here we have shown an example where one scan file per second is insufficient to reproduce the chromatographic profile; in this case, we reanalyzed the mixture by GC-MS generating 20 scan files per second. Each mass spectral transient is free of any skewing due to the changing partial pressure of the analyte in the ion source, thus the summed spectra are free of the types of skew that would be imposed by other scanning instruments.

This report describes one approach by which the MSU research group is attempting to respond to the fact that developments (e.g., scan speeds) in MS have not progressed in a timely fashion commensurate with improvements in GC resolving power. Chromatograms are now being reported with peak widths on the order of tens of milliseconds [2]; further improvements in GC could make contemporary MS of little use as a GC detector. While these preliminary results with the GC-beam c election TOF-MS-ITR system are not competitive from the standpoint of sensitivity (because the source is designed for a magnetic sector instrument), they do illustrate that developments in TOF-MS and its use with the ITR provide a mass spectrometer that can "keep up" with the demands imposed by high-resolution GC on MS. These developments provide the basis for sustaining the use of MS as a GC detector, the data from which can be used to both adequately represent the chromatography and identify eluting components of complex mixtures.

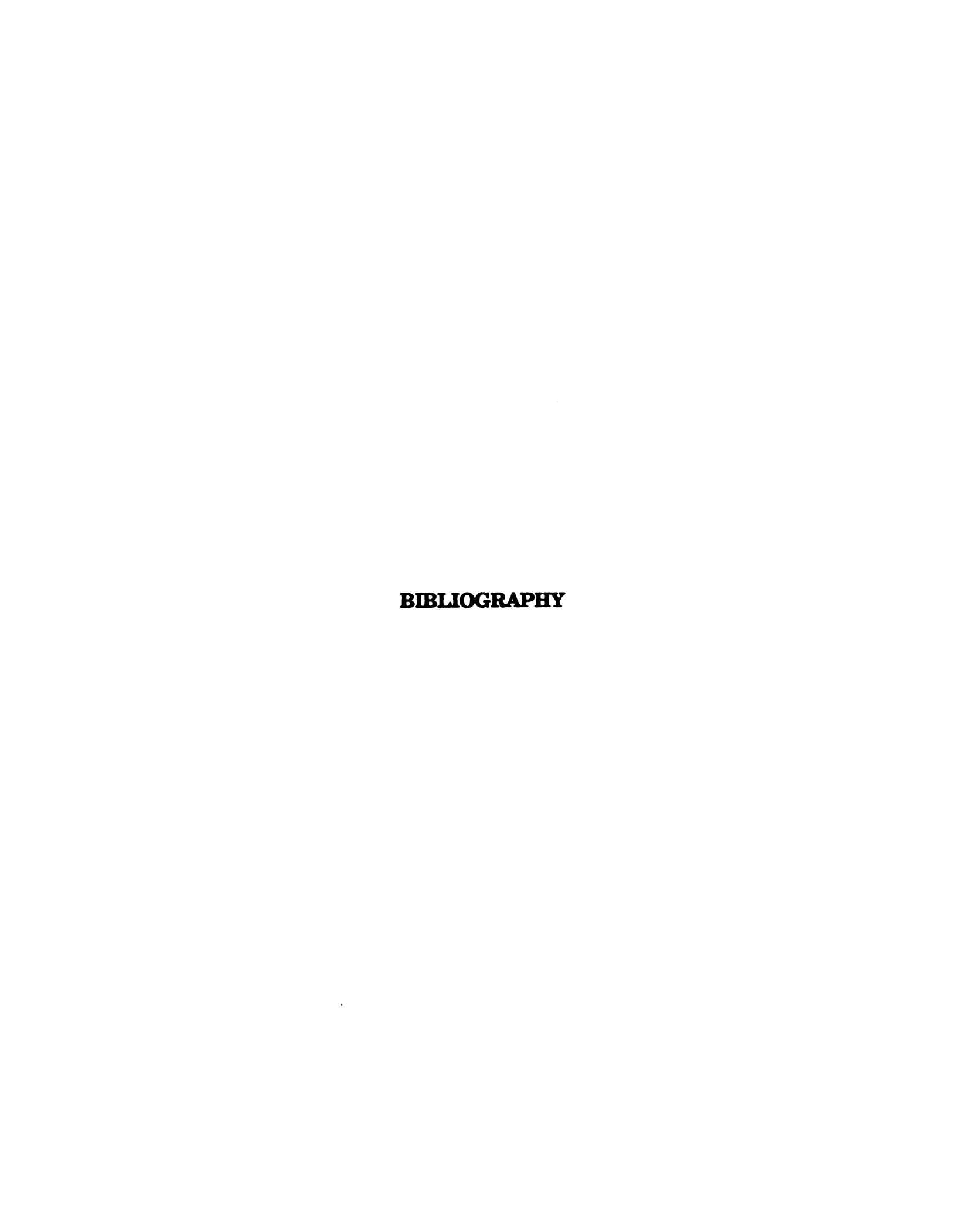
RENAISSANCE OF GC-TIME-OF-FLIGHT MS

ACKNOWLEDGEMENT

This work was funded through a Biomedical Research Technology Program grant (NIH-DRR-00480) from The National Institutes of Health.

REFERENCES

- 1 J. T. Watson, Introduction to Mass Spectrometry, Raven Press, New York, 2nd ed., 1985.
- 2 L. A. Lanning, R. D. Sacks, R. F. Mouradian, S. P. Levine and J. A. Foulke, Anal. Chem., 60 (1988) 194-196
- 3 P. A. Leclercq and C. A. Cramers, J. High Resolut. Chromatogr. Chromatogr. Commun., 11 (1988) 845-848.
- 4 J. F. Holland, C. G. Enke, J. T. Stults, J. D. Pinkston, B. Newcome, J. Allison and J. T. Watson, Anal. Chem., 55 (1983) 997A.
- 5 C. C. Sweeley, W. H. Elliott, I. Fries and R. Ryhage, Anal. Chem., 38 (1966) 1549-1553.
- 6 C.-G. Hammar, B. Holmstedt and R. Ryhage, Anal. Biochem., 25 (1968) 532-548.
- 7 F. C. Falkner, Biomed. Mass Spectrom., 4 (1977) 66-67.
- 8 C. E. Giffen, H. G. Boettger and D. D. Norris, Int. J. Mass Spectrom. Ion Phys., 15 (1974) 437-449.
- 9 B. Hedfjall and R. Ryhage, Anal. Chem., 53 (1981) 1641-1644.
- 10 M. L. Gross and D. L. Rempel. Science (Washington, D.C.). 226 (1984) 261.
- 11 J. Allison, J. F. Holland, C. G. Enke and J. T. Watson, Anal. Instr., 16 (1987) 207.
- 12 R. Tecklenburg, B. Newcome and J. F. Holland, Rev. Sci. Instrum., (1990) in press.
- 13 E. Erickson, G. C. Enke, J. F. Holland and J. T. Watson, Anal. Chem., 62 (1990) 1079-1084.
- 14 J. D. Pinkston, M. Rabb, J. T. Watson, and J. Allison, Rev. Sci. Instrum., 57 (1986) 583.
- 15 G. E. Yefchak, G. A. Schultz, J. Allison and C. G. Enke, J. Am. Soc. Mass Spectrom., (1990) in press.
- 16 K. Grob, Jr., G. Grob and K. Grob, J. Chromatogr., 156 (1978) 1-20.
- 17 S. N. Chesler and S. P. Cram. Anal. Chem., 43 (1971) 1922.
- 18 C. G. Enke, J. T. Watson, J. Allison and J. F. Holland, presented at the 37th ASMS Conference on Mass Spectrometry and Allied Topics, Miami Beach, FL, May 1989, Abstract No. MOA 1130, p. 32.
- 19 R. A. Hites and K. Biemann, Anal. Chem., 42 (1970) 855-860.
- 20 J. C. Miller and J. N. Miller, Statistics for Analytical Chemistry, Wiley, New York, 1984.
- 21 J. W. Biller and K. Biemann, Anal. Lett., 7 (1974) 515-528.



BIBLIOGRAPHY

- 1. Gohlke, R. S., Anal. Chem. 31, 535 (1959).
- 2. Holland, J. F., Enke, C. G., Allison, J., Stults, J. T., Pinkston, J. D., Newcome, B., and Watson, J. T., Anal. Chem., 55, 997A (1983).
- 3. V G Analytical Ltd., Manchester, UK.
- 4. Hewlett-Packard HP 5970B GC/MSD, product literature, Hewlett-Packard, Palo Alto, CA 94304.
- 5. Varian Associates, Inc., 220 Humboldt Court, Sunnyvale, CA 94089.
- 6. Varian Application Note Number 5, Varian Associates, Inc., 220 Humboldt Court, Sunnyvale, CA 94089.
- 7. Holland, J. F., Newcome, B., Tecklenburg, R. E. Jr., Davenport, M., Allison, J., Watson, J. T. and Enke, C. G., Rev. Sci. Instrum., 62, 69 (1991).
- 8. Erickson, E. D., Yefchak, G. E. and Enke, C. G., Int. J. of Mass Spectrom. Ion Proc., 97, 87 (1990).
- 9. Bakker, J. M. B., J. Phys. E: Sci. Instrum., 6, 785 (1973).
- 10. Bakker, J. M. B., J. Phys. E: Sci. Instrum., 7, 364 (1974).
- 11. Bakker, J. M. B., J. Phys. E: Sci. Instrum., 6, 457 (1973).
- 12. Pinkston, J. D., Rabb, M., Watson, J. T., and Allison, J., Rev. Sci. Instrum., 57(4), 583 (1986).
- 13. Pinkston, J. D., Doctoral Dissertation, Michigan State University, 1985.
- 14. Stults, J. T., Enke, C. G. and Holland, J. F., Anal. Chem., 55, 1323 (1983).
- 15. Eckenrode, B. A., Watson, J. T., Enke, C. G., and Holland, J. F., Int. J. Mass spectrom. Ion Proc. 83, 177 (1988).

- 16. Enke, C. G., Stults, J. T., Holland, J. F., Pinkston, J. D., Allison, J. and Watson, J. T., Int. J. Mass Spectrom. Ion Proc. 46, 229 (1983).
- 17. Stults, J. T., Holland, J. F., Watson, J. T. and Enke, C. G., Int. J. Mass Spectrom. Ion Proc., 71, 169 (1986).
- 18. Eckenrode, B. A., Watson, J. T., Holland, J. F. and Enke, C. G., *Anal. Chem.*, **62**, 1362 (1990).
- 19. Yefchak, G. E., Schultz, G. A., Allison, J., Holland, J. F., and Enke, C. G., J. Am. Soc. Mass Spectrom., 1, 440 (1990).
- 20. Watson, J. T., Schultz, G. A., Tecklenburg, R. E., Jr., and Allison, J., J. Chromatogr., 518, 283 (1990).
- 21. Barber, M., Bordoli, R. S., Sedgwick, R. D. and Tyler, A. N., *Nature*, 293 270 (1981).
- 22. Barber, M., Boldoli, R. S., Sedgwick, R. D. and Tyler, A. N., J. Chem. Soc. Chem. Comm., p. 325 (1981).
- 23. Busch, K. L., Unger, S. E., Vincze, A., Cooks, R. G. and Keough, T., J. Am. Chem. Soc., 104 1507 (1982).
- 24. Barofsky, D. F., Giessmann, U. and Barofsky, E., Int. J. of Mass Spectrom. Ion Proc., 53, 319 (1983).
- 25. Musselman, B. D., Stults, J. T. and Holland, J. F., <u>Proc. 35th ASMS Conf. Mass Spectrom. Allied Topics</u>, 302 (1987).
- 26. Bombick, D. D., Doctoral Dissertation, Michigan State University, 1986.
- 27. Blewett, J. P. and Jones, e. J., J. Phys. Rev., 50, 464 (1936).
- 28. Stephens, W. E., *Phys. Rev.*, **69**, 691 (1946).
- 29. Cameron, A. E. and Eggers Jr., D. F., Rev. of Sci. Instrum., 19, 605 (1948).
- 30. Wolff, M. M. and Stephens, W. E., Rev. Sci. Instrum., 19, 605 (1948).
- 31. Katzenstein, H. S. and Friedland, S. S., Rev. Sci. Instrum., 26, 324 (1955).
- 32. Wiley, W. C. and McLaren, I. H., Rev. Sci. Instrum, 26, 1150 (1955).
- 33. Stein, R., Int. J. of Mass Spectrom. Ion Proc., 14, 205 (1974).

- 34. Bakker, J. M. B., Dynamic Mass Spectrometry, 4, 25 (1976).
- 35. Mamyrin, B. A., Karataev, V. I., Shmikk, D. V., Sov. Phys. Tech. Phys., 16, 1177 (1972).
- 36. Poschenrieder, W. P., Int. J. of Mass Spectrom. Ion Proc., 6, 413 (1971).
- 37. Poschenrieder, W. P., Int. J. of Mass Spectrom. Ion Proc., 9, 357 (1972).
- 38. Sakurai, T., Matsuo, T., and Matsuda, H., Int. J. of Mass Spectrom. Ion Proc., 63, 273 (1985).
- 39. Wollnick, H. and Przewloka, M., Int. J. of Mass Spectrom. Ion Proc., 96, 267 (1990).
- 40. Marable, N. L. and Sanzone, G., Int. J. of Mass Spectrom. Ion Proc., 13, 185 (1974).
- 41. Muga, M. L., Anal. Instrum., 16, 31 (1987).
- 42. Yefchak, G. Y. and Enke, C. G., Int. J. of Mass Spectrom. Ion Proc., 87, 313 (1989).
- 43. Kinsel, G. R. and Johnston, M. V., Int. J. of Mass Spectrom. Ion Proc., 91, 57 (1989).
- 44. Turner, C. M. and Bloom, S. D., Rev. Sci. Instrum., 29, 480 (1958).
- 45. Chudleigh, P. W., Rev. Sci. Instrum., 39, 356 (1968).
- 46. Anderson, J. H. and Swann, D., Nucl. Instrum. Meth., 30, 1 (1964).
- 47. Fowler, T. K. and Good, W. M., Nucl. Instrum. Meth., 7, 245 (1960).
- 48. Cowen, K. A. and Coe, J. V., Rev. Sci. Instrum., 61, 2601 (1990).
- 49. Knorr, F. J., Ajami, M., and Chatfield, D. A., Anal. Chem., 58, 690 (1986).
- 50. Dawson, J. H. J. and Guilhaus, M., Rapid Commun. Mass Spectrom., 3, 155 (1989).
- 51. Schagen, P., <u>Advances in Image Pick-up and Display</u>, Vol. 1, Academic Press, New York, 1974.
- 52. Gilbert, J. R., Doctoral Dissertation, Michigan State University, 1991.

- 53. Grob, K., Jr., Grob, G., and Grob, K., J. Chromatogr., 156, 1 (1978).
- 54 Holland, J. F., Leary, J. J., and Sweeley, C. C., J. Chromatogr., 3, 379 (1986).
- 55. Chamberlin, B. A. and Sweeley, C. C., Clin. Chem., 33/4, 572 (1987).
- 56. Sweeley, C. C. and Chamberlin, B. A., Department of Biochemistry, Michigan State University.
- 57. Enke, C. G., Watson, J. T., Allison, J. and Holland, J. F., <u>Proc. 37th ASMS Conf. Mass Spectrom. Allied Topics</u>, Abstract No. MOA 1130, p. 32 (1989).
- 58. Chesler, S. N. and Cram, S. P. Anal. Chem., 43, 1922 (1971).
- 59. Enke, C. G., Watson, J. T., Allison, J. and Holland, J. F., <u>Proc. 37th ASMS Conf. Mass Spectrom. Allied Topics</u>, Abstract No. MOA 1130, p. 32 (1989).
- 60. R. Reimendal, and J. Sjovall, Anal. Chem., 44 (1972) 21.
- 61. Blewett, J. P. and Jones, E. J., J. Phys. Rev., 50, 464 (1936).
- 62. Kassel, D., Doctoral Dissertation, Michigan State University, 1989.
- 63. Bombick, D., Pinkston, J. D. and Allison, J., Anal. Chem., 56, 396 (1984).
- 64. Simonsick, W. J., Jr., <u>Proc. 37th ASMS Conf. Mass Spectrom. Allied Topics</u>, p. 291 (1989).
- 65. Kassel, D. B. and Allison, J., Biomed. Environ. Mass Spectrom. 17, 221 (1988).
- 66. Bombick, D. D. and Allison, J. Anal. Chem., 59, 458 (1987).
- 67. Simonsick, W. J., Jr.and Volpe, T. P., <u>Proc. 36th ASMS Conf. Mass Spectrom. Allied Topics</u>, p. 470 (1988).
- 68. Williams, B. W., Irsa, A. P., Zmora, H., and Beuhler, R. J., J. Phys. Chem., 87, 2185 (1983).
- 69. Light, K. J., Doctoral Dissertation, Michigan State University, 1990.
- 70. Dahl, D. A., Delmore, J. E. and Appelhans, A. D., *Rev Sci. Instrum.*, **61**, 607 (1990).

- 71. Laszlo, P. and Simonsick, W. J., Jr., <u>Proc. 38th ASMS Conf. Mass Spectrom. Allied Topics</u>, p. 251 (1990).
- 72. Channeltron Electron Multiplier Handbook for Mass Spectrometry Applications, Galileo Electro-Optics Corporation, Galileo Park, P.O. Box 550, Sturbridge, MA 01566.

